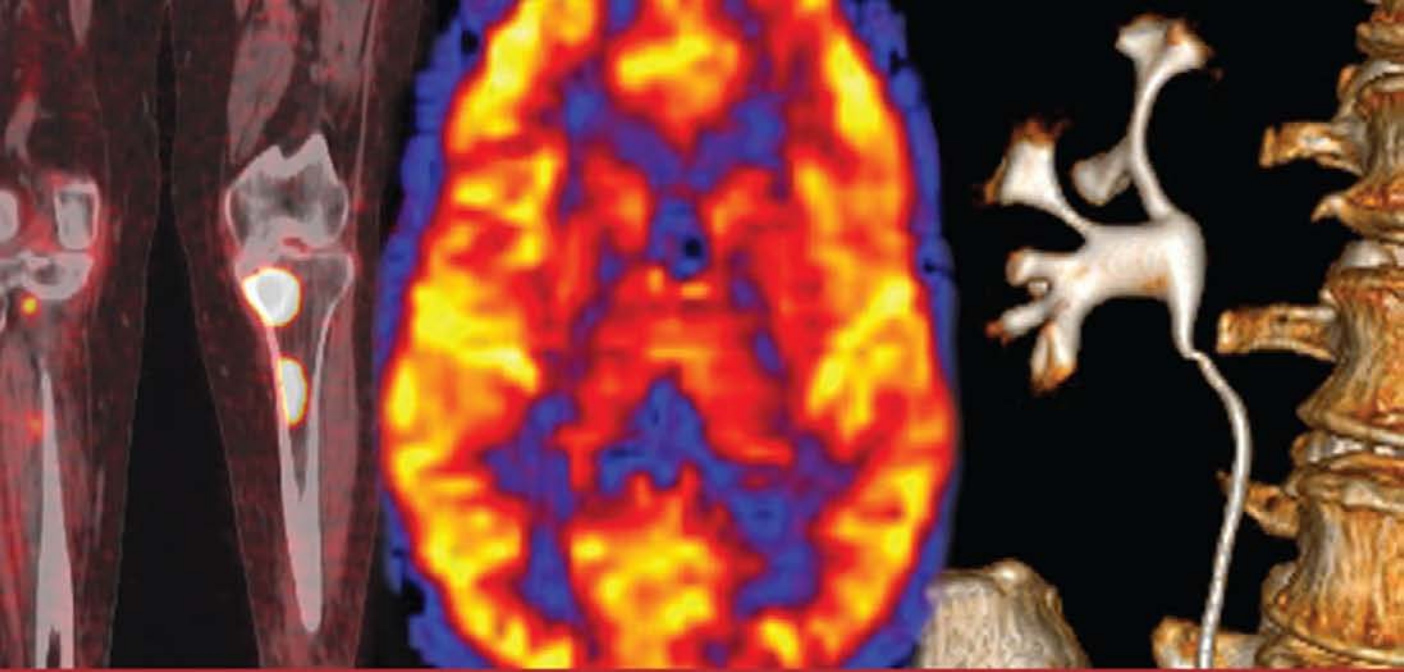

second edition

BASIC RADIOLOGY

Michael Y. M. Chen • Thomas L. Pope • David J. Ott

LANGE

a LANGE medical book

BASIC RADIOLOGY

2ND EDITION

Editors

Michael Y. M. Chen, MD
Associate Professor of Radiology
Department of Radiology
Wake Forest University School of Medicine
Winston-Salem, North Carolina

Thomas L. Pope, MD
Professor of Radiology
Department of Radiology and Radiologic Science
Medical University of South Carolina
Charleston, South Carolina

David J. Ott, MD
Professor of Radiology
Department of Radiology
Wake Forest University School of Medicine
Winston-Salem, North Carolina

Mc Graw Hill Medical

New York Chicago San Francisco Lisbon London Madrid Mexico City
Milan New Delhi San Juan Seoul Singapore Sydney Toronto

The McGraw-Hill Companies

ISBN: 978-0-07-176664-7

MHID: 0-07-176664-2

The material in this eBook also appears in the print version of this title: ISBN: 978-0-07-162708-5,
MHID: 0-07-162708-1.

Notice

Medicine is an ever-changing science. As new research and clinical experience broaden our knowledge, changes in treatment and drug therapy are required. The authors and the publisher of this work have checked with sources believed to be reliable in their efforts to provide information that is complete and generally in accord with the standards accepted at the time of publication. However, in view of the possibility of human error or changes in medical sciences, neither the authors nor the publisher nor any other party who has been involved in the preparation or publication of this work warrants that the information contained herein is in every respect accurate or complete, and they disclaim all responsibility for any errors or omissions or for the results obtained from use of the information contained in this work. Readers are encouraged to confirm the information contained herein with other sources. For example and in particular, readers are advised to check the product information sheet included in the package of each drug they plan to administer to be certain that the information contained in this work is accurate and that changes have not been made in the recommended dose or in the contraindications for administration. This recommendation is of particular importance in connection with new or infrequently used drugs.

To the memory of my mother
M.Y.M.C.
To Susan, Stephen, and the memory of my parents and father-in-law
D.J.O

Contents

This page intentionally left blank

Contributors

Joseph S. Ayoub, MD
Fellow, Department of Radiology, Baylor College of Medicine, Houston, Texas

Robert E. Bechtold, MD
Professor, Department of Radiology, Wake Forest University School of Medicine, Winston-Salem, North Carolina

Michelle S. Bradbury, MD, PhD
Assistant Attending Radiologist, Molecular Imaging & Neuroradiology Sections Department of Radiology, Memorial Sloan Kettering Cancer Center
Assistant Professor of Radiology, Weill Medical College of Cornell University, New York, New York

Melanie P. Caserta, MD
Assistant Professor, Department of Radiology, Wake Forest University School of Medicine, Winston-Salem, North Carolina

Fakhra Chaudhry, MD
Mecklenburg Radiology Associates, Charlotte, North Carolina

Michael Y. M. Chen, MD
Associate Professor, Department of Radiology, Wake Forest University School of Medicine, Winston-Salem, North Carolina

Caroline Chiles, MD
Professor, Department of Radiology, Wake Forest University School of Medicine, Winston-Salem, North Carolina

Robert L. Dixon, PhD
Professor, Department of Radiology, Wake Forest University School of Medicine, Winston-Salem, North Carolina

Rita I. Freimanis, MD
Associate Professor, Department of Radiology, Wake Forest University School of Medicine, Winston-Salem, North Carolina

Jud R. Gash, MD
Professor, Department of Radiology, University of Tennessee at Knoxville, Knoxville, Tennessee

Lawrence E. Ginsberg, MD
Professor of Radiology and Head and Neck Surgery, Department of Radiology, University of Texas, M. D. Anderson Cancer Center—Houston, Texas

Nandita Guha-Thakurta, MD
Assistant Professor, Diagnostic Radiology, Department of Radiology University of Texas, M. D. Anderson Cancer Center, Houston, Texas

Shannon M. Gulla, MD
Mid-South Imaging and Therapeutics, Memphis, Tennessee

Tamara Miner Haygood, MD, PhD
Assistant Professor, Department of Diagnostic Radiology, University of Texas, M. D. Anderson Cancer Center, Houston, Texas

Jacob Noe, MD
Chief Resident, Department of Radiology, University of Tennessee at Knoxville, Knoxville, Tennessee

David J. Ott, MD
Professor, Department of Radiology, Wake Forest University School of Medicine, Winston-Salem, North Carolina

Thomas L. Pope, MD
Professor, Department of Radiology and Radiologic Science, Medical University of South Carolina, Charleston, South Carolina

James G. Ravenel, MD
Professor, Chief of Thoracic Imaging, Department of Radiology and Radiologic Science, Medical University of South Carolina, Charleston, South Carolina

Mohamed M. H. Sayyouh, MD
Assistant Lecturer, Department of Radiology, National Cancer Institute, Cairo University, Egypt

Paul L. Wasserman, DO
Assistant Professor, Department of Radiology, Wake Forest University School of Medicine, Winston-Salem, North Carolina

Christopher T. Whitlow, MD, PhD
Fellow, Department of Radiology, Wake Forest University School of Medicine, Winston-Salem, North Carolina

Daniel W. Williams III, MD
Professor, Department of Radiology, Wake Forest University School of Medicine, Winston-Salem, North Carolina

Michael E. Zapadka, DO
Assistant Professor, Department of Radiology, Wake Forest University School of Medicine, Winston-Salem, North Carolina

Preface

The primary goal of this book was to create a concise text on current radiologic imaging for medical students and residents not specializing in radiology. After the first two introductory chapters, subsequent chapters employ an organ-system approach. Imaging techniques pertinent to the organ system, including their appropriate indications and use, are presented. Question-oriented exercises highlight the most commonly encountered diseases for each organ system.

The first chapter describes the various diagnostic imaging techniques that are available: conventional radiography, nuclear medicine, ultrasonography, computed tomography (CT), and magnetic resonance (MR) imaging. In recent years, many new techniques, such as CT angiography, CT colonography, MR angiography, MR cholangiopancreatography, and positron emission tomography (PET)/CT have emerged with new generations of CT and MR equipment. The second chapter gives an overview of the physics of radiation and its related biological effects, ultrasound, and magnetic resonance imaging. The remaining chapters focus on the individual organ systems of the heart, lungs, breast, bones, joints, abdomen, urinary tract, gastrointestinal tract, liver, biliary system, pancreas, brain, and spine. The chapters have a similar format to provide a consistent presentation. Each chapter briefly describes recent developments in the radiologic imaging of these organ systems. This is followed by a description of the normal anatomy and a discussion of the most appropriate and rational imaging techniques for evaluating each organ system. Each chapter stresses the proper selection of each imaging examination based on clinical presentation, need for patient preparation, and potential conflicts between techniques. Finally, all chapters end with questions and imaging exercises to enhance and reinforce the principles of each chapter. All exercises include numerous images and specific questions focusing on common diseases or symptoms. One question per case is used in all exercises, and the case and question numbers are matched for clarity. A short list of suggested readings and general references is included at the end of each chapter.

We hope that this book will help medical students and residents not specializing in radiology to better comprehend the basics of each imaging technique. Ideally, this book will also aid them in selecting and requesting the most appropriate imaging modality for each patient's presenting symptoms. Our further hope is that the interactive exercises presented will familiarize readers with the more common diseases that current radiologic imaging can best evaluate.

We wish to thank Allen D. Elster, MD, Director of the Division of Radiologic Sciences and Professor and Chairman of the Department of Radiology of the Wake Forest University School of Medicine, and C. Douglas Maynard, MD, now retired former Director of Division of Radiologic Sciences and Professor and Chairman of the Department of Radiology of the Wake Forest University School of Medicine, who have provided us with the supportive environment needed to complete this endeavor. This book would not have been possible without the able support of Michael Weitz, Karen Edmonson, Laura Libretti, and their fine associates at Lange Medical Books/McGraw-Hill.

This page intentionally left blank

Scope of Diagnostic Imaging

1

Michael Y. M. Chen, MD
Christopher T. Whitlow, MD, PhD

For almost half a century following the discovery of x-rays by Roentgen in 1895, radiologic imaging was mainly based on plain and contrast-enhanced radiography. Those images were created by exposing film to an x-ray beam attenuated after penetrating the body. The production of x-rays and radiographic images is described in the next chapter. In the recent half century, diagnostic radiology has undergone dramatic changes and developments. Conventional angiography, nuclear medicine, ultrasonography, and computed tomography (CT) were developed between 1950 and 1970. Magnetic resonance (MR) imaging, interventional radiology, and positron emission tomography (PET) were developed later. Conventional radiology, including contrast-enhanced radiography and CT, uses ionizing radiation created from x-ray equipment. Nuclear medicine uses ionizing radiation that is emitted from injected or ingested radioactive pharmaceuticals in various parts of the body. Ultrasonography and MR imaging modalities use sound waves and magnetism, respectively, rather than ionizing radiation.

Radiologic subspecialties have been developed based on organ systems, modalities, and specific fields. Organ-oriented subspecialties of radiology include musculoskeletal, breast, neurologic, abdominal, thoracic, cardiac, gastrointestinal, and genitourinary imaging. Modality-oriented subspecialties comprise nuclear medicine, interventional, ultrasonography, and MR imaging. Specific field subspecialties include pediatric and women's imaging. Functional and metabolic imaging methods are now being used clinically, with genetic and molecular marker imaging expected in the future.

This chapter is intended to provide an overview of a variety of modalities in diagnostic radiology and basic knowledge regarding radiologic image-based diagnosis. Specific modality settings in each field and diagnostic interpretation for the use of these modalities in evaluating various organ systems are described in subsequent chapters.

CONVENTIONAL RADIOGRAPHY

Conventional radiography refers to plain radiographs that are generated when x-ray film is exposed to ionizing radiation and developed by photochemical process. During development, the metallic silver on the x-ray film is precipitated, rendering the latent image black. The amount of blackening on the film is proportional to the amount of x-ray radiation exposure. Plain radiography relies on natural and physical contrast based on the density of material through which the x-ray radiation must pass. Thus, gas, fat, soft tissue, and bone produce black, gray-black, gray, and white radiographic images, respectively, on film (Figure 1-1).

Although other image modalities such as CT, ultrasonography, and MR imaging are being used with increasing frequency to replace plain radiographs, conventional radiography remains a major modality in the evaluation of chest, breast, bone, and abdominal diseases.

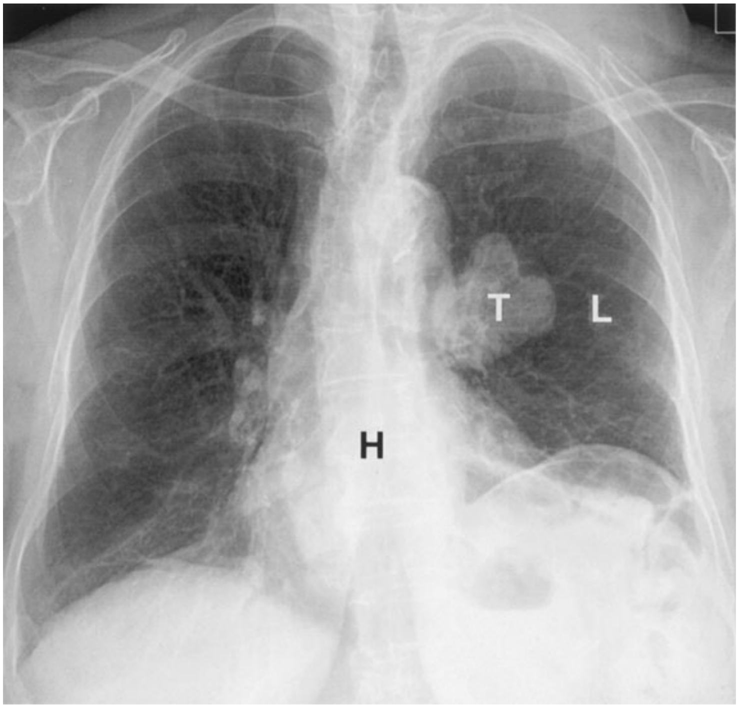

▲ **Figure 1-1.** Standard posteroanterior chest radiograph demonstrated the striking contrast between the heart (H) and lungs (L). A tumor (T) is seen at the left hilum.

Computed radiography (CR) or digital radiography is presently replacing conventional screen-film combination techniques. The most common CR technique, photostimulable phosphor computed radiography (PPCR), uses a phosphor-coated plate to replace the film-screen combination. When a cassette containing the phosphor-coated plate is exposed to x-rays, the phosphor stores the absorbed x-ray energy. The exposed cassette is then placed in a PPCR reader that uses a laser to stimulate release of electrons, resulting in the emission of short-wavelength blue light. The brightness of the blue light is dependent on the amount of absorbed x-ray photon energy. This luminescence generates an electrical signal that is reconstructed into a gray-scale image, which may be displayed on a monitor or printed as a hard copy. Digital images generated from PPCR are capable of being transmitted through a picture archiving and communications system (PACS), similar to other digital images acquired from CT or MR facilities. PPCR is better than plain radiography in linear response to a wide range of x-ray exposure. However, PPCR provides less spatial resolution than plain radiography. Another CR technique that is being developed uses an amorphous selenium-coated plate, which directly converts x-ray photons into electrical charges.

Fluoroscopy uses a fluorescent screen instead of radiographic film to view real-time images generated when an x-ray beam penetrates through a certain part of the body. An image intensifier absorbs x-ray photons and produces a quantity of light on the monitor. The brightness of the image is proportional to the number of incident photons received. Fluoroscopy is a major modality used to examine the gastrointestinal tract. For example, fluoroscopy can be used to follow the course of contrast materials through the gastrointestinal tract, allowing the evaluation of both structure and function. Spot filming or video recording may be used synchronously with fluoroscopy to optimally demonstrate pathology. Fluoroscopy is also used to monitor catheter placement during angiography and to guide interventional procedures. In recent years, digital detectors (such as charge-coupled devices, CCDs) have begun to replace video cameras on fluoroscopy units.

Conventional tomography produces an image of one intended area by blurring structures superimposed on both sides of a focus plane. This technique, however, has been largely replaced by CT.

Mammography uses a film-screen combination technique to evaluate breast lesions for the early detection of breast carcinoma. A mammographic unit is installed with a special x-ray tube and a plastic breast-compression device. A standard mammogram obtains views in two projections, producing craniocaudal (CC) and mediolateral oblique (MLO) images of the breast. Additional images of the breast in other projections, such as mediolateral (ML) views, and using diagnostic techniques such as magnification and/or spot compression views may also be obtained to further characterize potential pathologic findings. Ultrasonography (US) is also used in breast imaging as a complementary modality to further characterize breast pathology. Several image-guided breast interventional procedures, such as preoperative needle placement for lesion localization and core needle biopsy using stereotactic ultrasound or MR guidance, are widely available.

Contrast Studies

Contrast materials are used to examine organs that do not have natural inherent contrast with surrounding tissues. Contrast media are commonly used to evaluate the gastrointestinal tract, the urinary tract, the vascular system, and solid organs. Contrast media used in MR imaging are described in the MR modality section.

Barium suspension is still used daily in the examination of the gastrointestinal tract. Barium suspension is a safe contrast media that provides high imaging density on upper gastrointestinal (UGI) series, small-bowel studies, and evaluation of the colon. Both single-contrast and double-contrast techniques may be used to evaluate the gastrointestinal tract (Figure 1-2). In the single-contrast study, barium suspension is administered alone. In the double-contrast study, both barium and air are introduced to delineate the details of the mucosal surface, which facilitates the identification of superficial lesions in the bowel lumen. In the UGI double-contrast study, air is introduced into the bowel lumen by administering oral effervescent agents. For double-contrast evaluation of the lower GI tract with barium enema, air is introduced into the bowel lumen via direct inflation with a small pump through a rectal catheter. Small-bowel contrast studies include peroral, enteroclysis, and retrograde techniques. The peroral small-bowel study is performed by feeding barium suspension to the patient and recording the progress of contrast through the small bowel. Enteroclysis is performed by placing a catheter in the proximal jejunum and infusing barium suspension through the catheter. Enteroclysis is preferred for evaluating focal small-bowel lesions or the cause of small-bowel obstructions. Retrograde small-bowel examination is performed by retrograde reflux of barium suspension into the small bowel during barium enema or via direct injection through an ileostomy.

Water-soluble contrast media are commonly used for angiography, interventional procedures, intravenous urography, and enhancement of CT. All water-soluble contrast media are iodinated agents that are classified as high or low osmolar, ionic or nonionic, and monomeric or dimeric in chemical nature. The iodine atoms in contrast medium absorb x-rays in proportion to the concentration in the body when radiographed. The most common water-soluble contrast

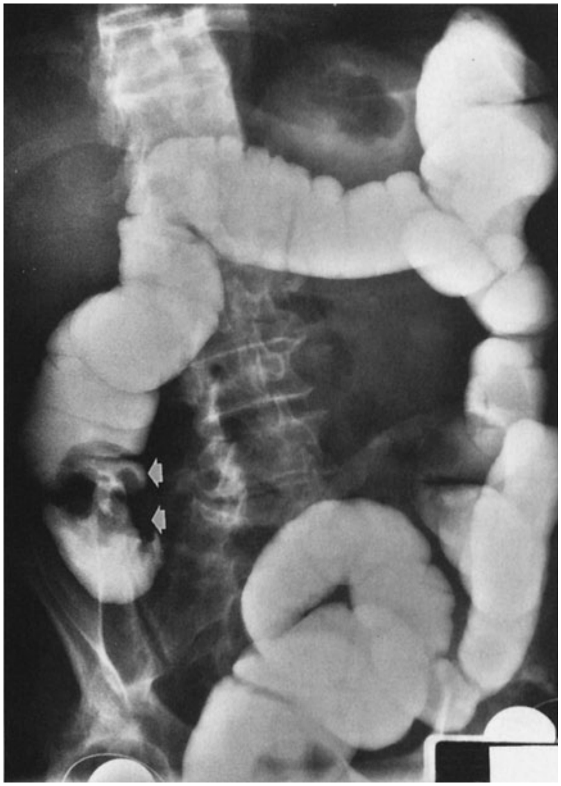

▲ **Figure 1-2.** A single-contrast retrograde colonic enema in the left posterior oblique view demonstrates an annular lesion representing a cecal carcinoma (arrows). Bilateral hip prostheses are an incidental observation.

media are the high osmolar ionic contrast agents (diatrizoate and its derivatives). Low osmolar contrast media include ionic (meglumine ioxaglate) and nonionic (iohexol, iopamidol, ioversol, iopromide) monomers, as well as nonionic dimers (iodixanol). Low osmolar contrast media have an overall lower incidence of adverse reactions, including nephrotoxicity and mortality, than high osmolar ionic agents; however, lower osmolar agents are also three to five times more expensive.

The occurrence and severity of adverse reactions after administration of iodinated contrast material are unpredictable. These reactions are categorized as mild, moderate, or severe based on degree of symptoms. Mild adverse reactions include nausea, vomiting, and urticaria that do not require treatment. The incidence of mild adverse reactions may be less if using a lower osmolality contrast agent. Moderate reactions include symptomatic urticaria, vasovagal events, mild bronchospasm, and/or tachycardia that requires treatment. Severe and life-threatening reactions, such as severe bronchospasm, laryngeal edema, seizure, severe hypotension, and/or cardiac arrest, are unpredictable and require prompt recognition and immediate treatment.

Contrast-induced nephropathy (CIN) is characterized by renal dysfunction after intravenous administration of iodinated contrast material. There is no standard definition of CIN. Findings with CIN include percent increasing serum creatinine from baseline (such as 20% to 50%) or increasing absolute serum creatinine above baseline (such as 0.5 to 2.0 mg/d) within 24 to 48 hours (or in 3 to 5 days). The incidence of CIN is variable. Patients with renal failure or underlying renal diseases are several times more likely to develop CIN than those with normal renal function following the administration of iodinated contrast material.

Water-soluble contrast agents are used in the gastrointestinal tract when barium suspension is contraindicated, when perforation is suspected, when surgery is likely to follow imaging, when confirmation of percutaneous catheter location is necessary, and when gastrointestinal opacification is required during abdominal CT evaluation. Unlike barium suspension, water-soluble contrast agents are readily absorbed by the peritoneum if extraluminal extravasation occurs, but provide less image density. High osmolar water-soluble contrast agents may cause severe pulmonary edema if aspirated. High osmolar contrast agents may also cause fluid to shift from the intravascular compartment into the bowel lumen, resulting in hypovolemia and hypotension, which is less likely to occur with low osmolar water-soluble contrast media.

Intravenous urography (IVU) uses ionic or nonionic water-soluble contrast agents to evaluate the urinary tract. Renal excretion/concentration of intravenously administered iodinated contrast material opacifies the kidneys, ureters, and bladder approximately 10 minutes postinjection. Intravenous urography has been largely replaced over the past decade by unenhanced helical CT evaluation. IVU, however, remains useful for the evaluation of subtle uroepithelial neoplasms and other diseases of the renal collecting system, and it can provide additional information that complements data from cross-sectional image modalities. Additional contrast-enhanced imaging examinations of the genitourinary system include cystography, voiding cystourethrography, and retrograde urethrography to evaluate the bladder and urethra.

Hysterosalpingography is primarily used to evaluate the patency of fallopian tubes and uterine abnormalities in patients with infertility. Hysterosalpingography is also used for postsurgical evaluation and to define anatomy for reanastomosis procedures.

Hysterosalpingography is performed by inserting a catheter into the uterus and subsequently injecting water-soluble contrast medium (some institutions prefer oil-based iodine contrast) to delineate the uterine cavity and the patency of the fallopian tubes. A fluoroscopic spot image is taken once contrast medium fills the uterus and fallopian tubes, but before spillage into the peritoneum. A second image is taken after fallopian tube spillage appears. A transcervical recanalization of obstructed fallopian tube has been introduced to improve the fertility rate.

Angiography is the study of blood vessels following intra-arterial or intravenous injection of water-soluble contrast agents. A series of rapid exposures is made to follow the course of the contrast medium through the examined blood vessels. Angiographic images are recorded by standard or digital imaging, and/or stored digitally.

Thoracic aortography is performed when there is suspicion of traumatic aortic injury, dissection (Figure 1-3), or atherosclerotic aneurysm, and to evaluate cerebral and upper extremity vascular disease. Multidetector CT has largely replaced conventional aortography as the initial modality to evaluate aortic trauma (Figure 1-4). Conventional aortography, however, remains important in specific settings, such as planning endovascular stent graft therapy and assessing small branch vessel injuries in stable patients. Abdominal aortography is used to evaluate vessel origins in vascular occlusive disease or prior to selective catheterization. Abdominal aortography is also used for vascular mapping prior to aneurysm repair or other intra-abdominal surgery. Coronary angiography is most commonly performed to evaluate coronary occlusion. Pulmonary angiography is used in patients who are suspected of having pulmonary embolus, especially in the setting of equivocal results on ventilation-perfusion imaging. Inferior venacavography is performed to evaluate for caval occlusion from venous thrombosis, obstruction or compression by retroperitoneal lymphadenopathy, or fibrosis. Inferior venacavography is also performed to evaluate the configuration of the inferior vena cava before filter placement. In recent years, conventional angiography has been replaced by CT angiography and MR angiography.

Less commonly used contrast studies include myelography (evaluating disk herniation and spinal cord compression), fistulography (sinus tracts for abscesses and cavities), sialography (evaluating the salivary glands for ductal obstruction or tumor), galactography (assessing the breast ductal system), and oral cholecystography, cholangiography (evaluating the biliary tree), and lymphangiography (assessing lymph nodes and lymph channels for malignancies).

Computed Tomography

Computed tomography, an axial tomographic technique, produces source images that are perpendicular to the long axis of the body (Figure 1-5). Attenuation values generated by CT reflect the density and atomic number of various tissues and are usually expressed as relative attenuation coefficients, or Hounsfield units (HUs). By definition, the HUs of water and air are zero and –1,000, respectively. The HUs of soft tissues range from 10 to 50, with fat demonstrating negative HU. Bone is at least 1,000 HU. The contrast resolution of vascular structures, organs, and pathology, such as

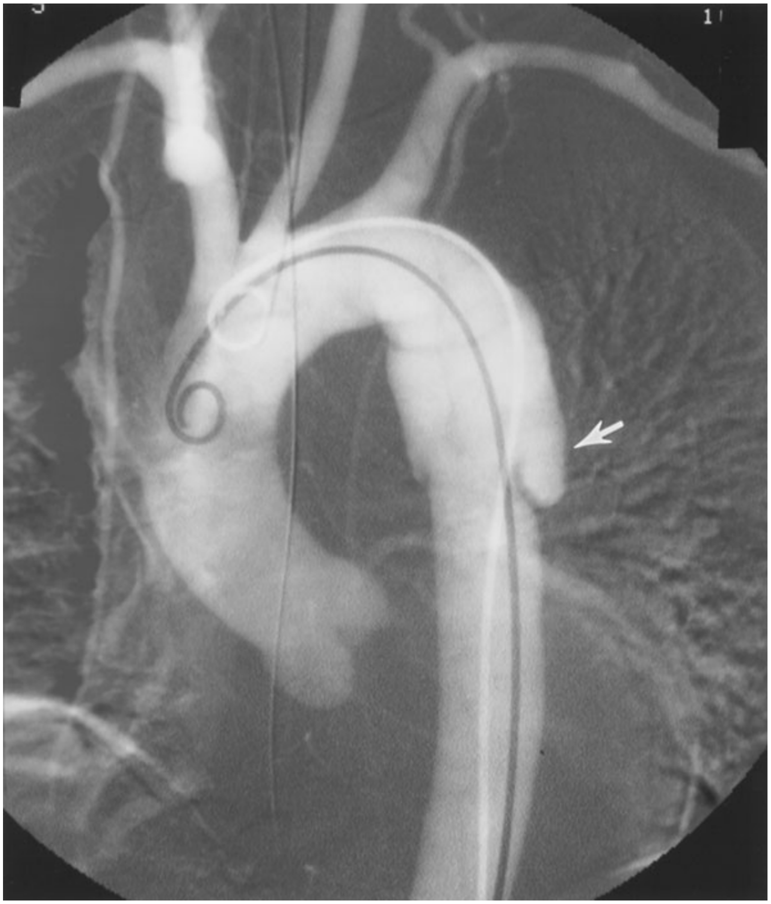

▲ **Figure 1-3.** An aortogram demonstrated transection (arrow) of the aortic arch at the aortic isthmus extending about 4 cm below.

hypervascular neoplasms, can be enhanced following intravenous infusion of water-soluble contrast media. The type, volume, and rate of administration as well as the scan delay time vary with specific study indication and protocol. Additionally, oral contrast material, namely, water-soluble agents or barium suspensions, can be administered for improved bowel visualization. Artifacts may be produced by patient motion or high-density foreign bodies, such as surgical clips.

Variety Scanners

Conventional CT scanners have traditionally operated in a step-and-shoot mode, defined by data acquisition and patient positioning phases. During the data acquisition phase, the x-ray tube rotates around the patient, who is maintained in a stationary position. A complete set of projections are acquired at a prescribed scanning location prior to the patient positioning phase. During this latter phase, the patient is transported to the next prescribed scanning location.

The first helical (spiral) CT scanner was introduced for clinical applications in the early 1990s. Helical CT is characterized by continuous patient transport through the gantry while a series of x-ray tube rotations simultaneously acquire volumetric data. These dynamic acquisitions are typically obtained during a single breath hold of about 20 to 30 seconds. Higher spatial resolution can be achieved with narrower collimations. The advantages of helical CT technology include reduced scan times, improved speeds at which the volume of interest can be adequately imaged, and increased ability to detect small lesions that may otherwise change position in non-breath-hold studies. In addition, gains in scan speed permit less contrast material to be administered for the same degree of vessel opacification.

The evolution of multidetector CT (MDCT) scanners has resulted from the combination of helical scanning with multislice data acquisition. In this CT system, a multiple-row detector array is employed. Current state-of-the-art models are capable of acquiring 64, 128, or 256 channels of helical data

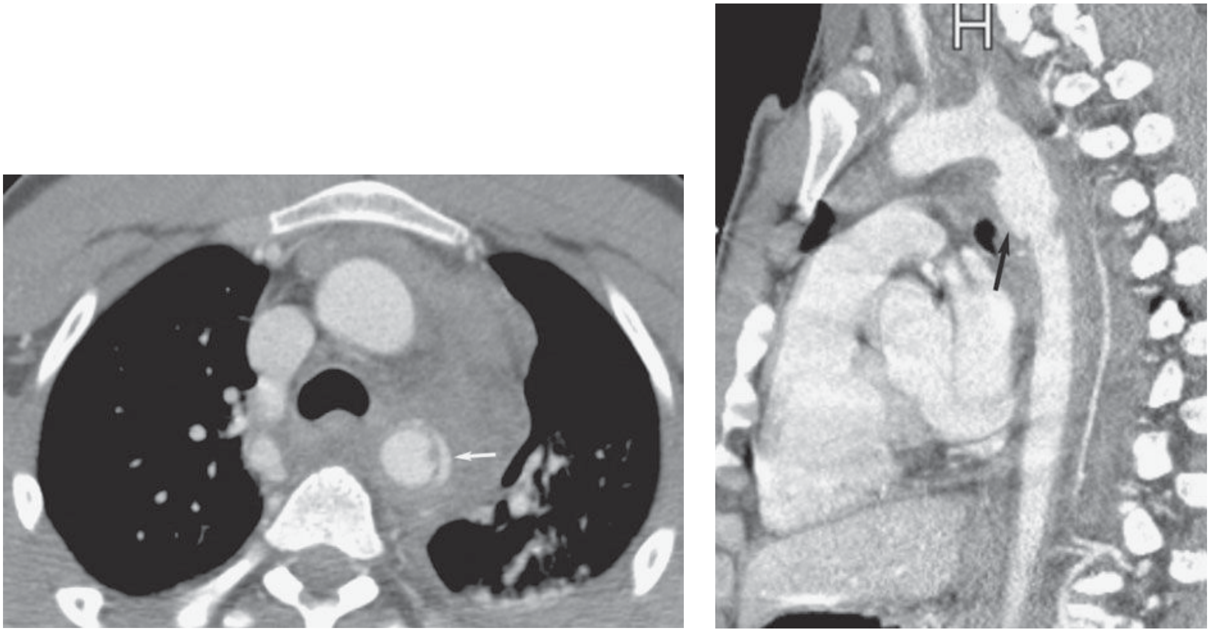

A B

▲ **Figure 1-4.** Axial (**A**) and sagittal (**B**) view of CT angiography (CTA) on a patient with a motor vehicle accident showing aortic transection (arrow) at the level of the ductus arteriosus with a surrounding mediastinal hematoma that extends superiorly along the aorta.

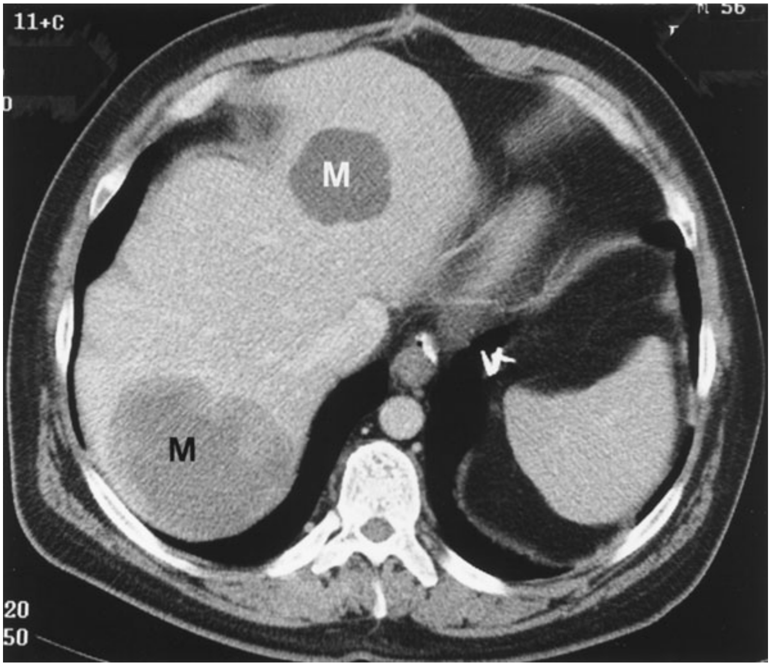

▲ **Figure 1-5.** Contrast-enhanced CT image of the upper abdomen demonstrated two low-attenuation areas (M) confirmed as multiple hepatic metastases from a gastrointestinal stromal tumor.

▲ **Figure 1-6.** 3D reformatted image from CT angiography of brain shows a 16-mm aneurysm (arrow) arising from the left lateral aspect of the mid basilar artery.

simultaneously. For a given length of anatomic coverage, multidetector CT can reduce scan time, permit imaging with thinner collimation, or both. The use of thinner collimation (0.4 mm to 2 mm) in conjunction with high-resolution reconstruction algorithms yields images of higher spatial resolution (high-resolution CT), a technique commonly used for evaluation of diffuse interstitial lung disease or the detection of pulmonary nodules. Multidetector CT offers additional advantages of decreased contrast load, reduced respiratory and cardiac motion artifact, and enhanced multiplanar reconstruction capabilities. These innovations have had a significant impact on the development of CT angiography (CTA). Multidetector CT has replaced conventional angiography as a primary modality in patients with acute aortic injuries.

CT Angiography

CT angiography protocols combine high-resolution volumetric helical CT acquisitions with intravenous bolus administration of iodinated contrast material. Using an MDCT scanner, images are acquired during a single breath hold, ensuring that data acquisition will commence during times of peak vascular opacification. This has permitted successful imaging of entire vascular distributions, in addition to minimizing motion artifact and increasing longitudinal spatial resolution, thus potentially lowering administered contrast doses. The time between the start of contrast injection and the commencement of scanning can be tailored in response to a particular clinical question, permitting image acquisition during the arterial, venous, and/or equilibrium phases. Exquisite anatomic detail of both intraluminal and extraluminal structures is revealed using this technique, including detection of intimal calcification and mural thrombosis. CT angiography has become an important tool for assessment of the abdominal and iliac arteries and their branches, the thoracic aorta, pulmonary arteries, and intracranial and extracranial carotid circulation (Figure 1-6).

CT Colonography

CT colonography (virtual colonoscopy), introduced in 1994, is a relatively new noninvasive method of imaging the colon in which thin-section helical CT data are used to generate two-dimensional or three-dimensional images of the colon. This technology has been used primarily in the detection and characterization of colonic polyps, rivaling the traditional colonoscopic approach and conventional barium enema examinations. These images display the mucosal surface of the colon and internal density of the detected lesions, as well as directly demonstrating the bowel wall and extracolonic abdominal/pelvic structures.

ULTRASONOGRAPHY

Diagnostic ultrasound is a noninvasive imaging technique that uses high-frequency sound waves greater than 20 kilohertz (kHz). A device known as a *transducer* is used to emit and to receive sound waves from various tissues in the body.

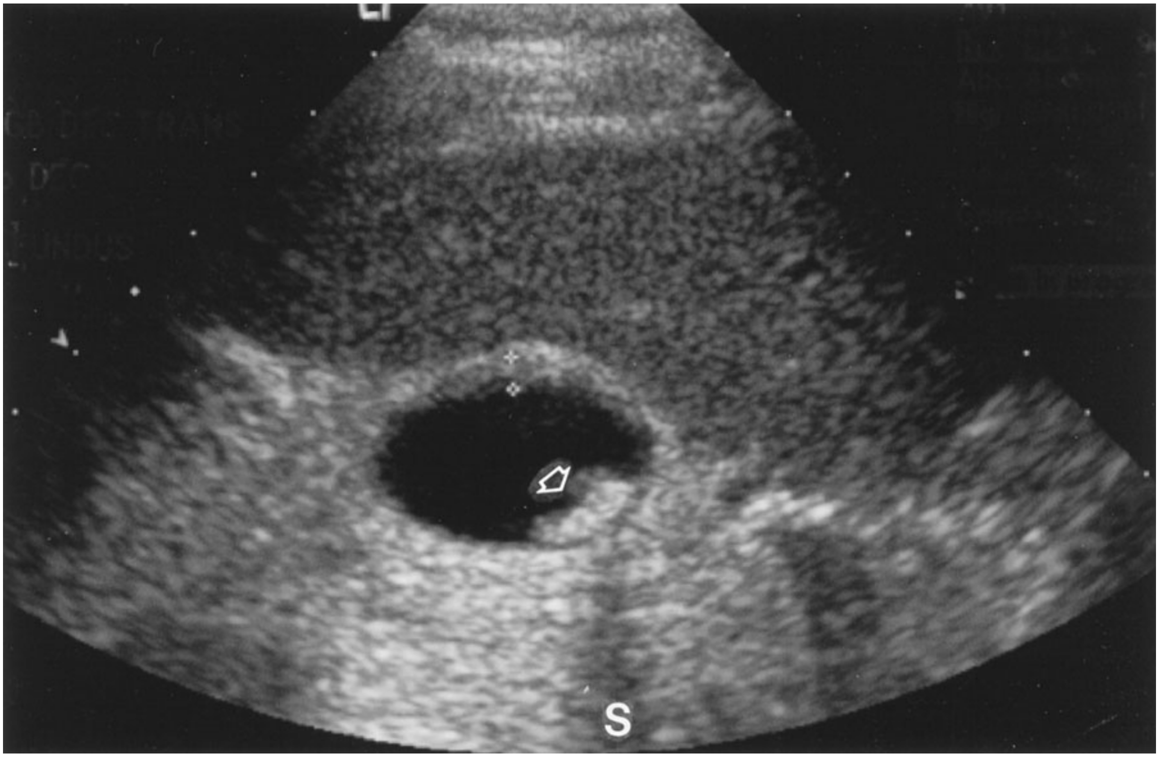

▲ **Figure 1-7.** A transverse ultrasound image of the gallbladder demonstrates a gallstone (arrow) with the characteristic distal acoustic shadowing (S) because sound waves cannot penetrate the gallstone.

The transducer is placed against the patient's skin with a thin layer of coupling gel. This gel displaces the air that would otherwise reflect virtually the entire incident ultrasound beam. As sound travels into the patient, wave fronts spread out, diminishing the overall beam intensity. Beam attenuation also occurs secondary to partial tissue absorption with associated heat conversion. At tissue interfaces, the beam is partially reflected and transmitted. The reflected sound waves, or echoes, travel back to the transducer and are converted into electric signals and amplified. The amplitude of the returning wave partially depends on the degree of beam absorption. A shade of gray is then assigned to each amplitude, with strong echoes being typically assigned a shade near the white end of the spectrum, and weak echoes assigned a shade near the black end of the spectrum. In addition, the depth of the reflecting tissue can be calculated from the known total beam travel time and the average sound velocity in human tissue (1,540 m/s). Limitations of this modality are primarily operator-dependent in nature. Additional limitations include variable visualization of midline abdominal organs (pancreas) and vasculature when obscured by overlying bowel gas, as well as inability of sound waves to penetrate gas or bone.

There are many common applications of ultrasonography, including imaging of the abdomen (liver, gallbladder, pancreas, kidneys) (Figure 1-7), pelvis (female reproductive organs), fetus (routine fetal surveys for detection of anomalies), vascular system (aneurysms, arterial-venous communications, deep venous thrombosis), testicles (tumor, torsion, infection), breasts, pediatric brain (hemorrhage, congenital malformations), and chest (size and location of pleural fluid collections). In addition, ultrasound-guided interventions are routinely used to facilitate lesion biopsy, abscess drainage, and radiofrequency ablation.

Doppler ultrasound is used primarily to evaluate vascular flow by detecting frequency shifts in the reflected beam, utilizing a principle termed the *Doppler effect*. This effect occurs when a sound emitter or reflector is moving relative to the stationary receiver of sound. Objects moving toward the detector appear to have a higher frequency and shorter wavelength, whereas objects moving away from the detector appear to have a lower frequency and longer wavelength. If the ultrasound beam strikes a reflector moving toward it, the reflected sound will have a higher frequency than the original beam. Alternatively, if the ultrasound beam strikes a reflector moving away from it, the reflected sound will have a lower frequency than the original beam. The Doppler shift is the frequency difference between the original beam frequency and the reflected beam frequency. Frequency differences are used to calculate the corresponding flow velocities, from which a Doppler waveform, or tracing, can be generated. This tracing depicts the relationship between velocity and time and is unique to the flow pattern within the vessel. Color flow Doppler assigns colors (blue and red) to structures according to their motion toward or away from transducers. This information can be superimposed on a gray-scale image. Endoluminal sonography uses a high-frequency catheter-based transducer (9 to 20 megahertz [MHz]) to image structures beyond the lumen of the hollow viscus. It is accurate in local staging of cancer and in detecting small lesions that may not be visualized with other imaging modalities. Limitations for optimal evaluation include inability to precisely position the transducer within an area of interest that may restrict full entry.

Diverse applications of ultrasonography are presented as follows. Gastrointestinal (GI) applications of endoluminal sonography include quantification of the size and wall thickness of esophageal carcinoma or to detect and characterize esophageal varices. Transrectal ultrasound is performed to evaluate the prostate gland. Transesophageal echocardiography is used for evaluating cardiovascular abnormalities. Genitourinary (GU) applications include guidance of collagen injections, examination of the severity and length of ureteral strictures, diagnosis of upper-tract neoplasms and urethral diverticula, identification of submucosal calculi, and visualization of crossing vessels prior to endopyelotomy. Evaluation of the uterus, adnexa, and fetus can be conducted using a transvaginal probe in the presence of an empty bladder. Sonohysterography, an ultrasound-guided procedure, requires instillation of a sterile saline solution into the uterine cavity following cannulation for evaluation of endometrial masses or other abnormalities. More recently, intravascular application of sonography has been promising for quantitating the degree of arterial stenosis, and for monitoring the therapeutic effects of angioplasty in both peripheral and coronary arteries. Intravascular ultrasound (IVUS) has been applied to modeling plaque morphology, blood flow, and the geometry of the vessel lumen. Three-dimensional ultrasound (3D-US) has been developed with advancements in computer processing power and has rapidly achieved widespread use for some clinical applications, including the evaluation of normal embryonic and/or fetal development, as well as cardiac morphology in specific congenital anomalies.

MAGNETIC RESONANCE IMAGING

In 1952, Felix Bloch and Edward Purcell were awarded the Nobel Prize for their independent discovery of the magnetic resonance phenomenon in 1946. Between 1950 and 1970, nuclear magnetic resonance (NMR) was developed and used for chemical and physical molecular analysis. In 1971, Raymond Damadian demonstrated that NMR had utility in cancer diagnosis, based on prolonged relaxation times in pathologic tissue. The first 2D proton NMR image of a water sample was generated in 1972 by Paul Lauterbur using a back-projection technique, similar to that used in CT. In 1975, Richard Ernst used phase and frequency encoding, as well as Fourier transform analysis, to form the basis of current magnetic resonance imaging (MRI) techniques. All of these experiments used defined, nonuniform magnetic fields or linear variations in field strength along all coordinate axes. The application of these nonuniform fields (magnetic field gradients) permitted discrimination of various signals from different spatial locations. In MR imaging, a pulsed radiofrequency (rf) beam is used in the presence of a strong main magnetic field to generate high-quality images of the body. These images can be acquired in virtually any plane, although sagittal, coronal, and axial images are commonly obtained.

Although a detailed explanation is beyond the scope of this chapter, substances (eg, fluid) that have a long Tl will appear dark on Tl-weighted images, whereas those with short Tl (fat) will display high signal intensity. On T2-weighted images, a long-T2 substance (fluid) will appear bright. Advantages of MR imaging include superb contrast resolution, high spatial resolution, and lack of ionizing radiation.

The most commonly used clinically approved contrast agents for MR imaging are gadolinium-based compounds that produce T1 shortening. Tissue relaxation results from interactions between the unpaired electron of gadolinium and tissue hydrogen protons, which significantly decrease the T1 of the blood relative to the surrounding tissues. Adverse reactions to this agent are far less frequent than those seen with iodinated compounds, with common reactions including nausea, vomiting, headache, paresthesias, or dizziness.

Hydrogen nuclei are favored for MR imaging. On placement of a patient in an MR scanner, the randomly oriented hydrogen nuclei align with the static magnetic field. In order to detect a signal, a perturbing rf pulse is transiently applied to the patient, resulting in a net change in alignment of these nuclei. When the rf pulse is turned off, the spins return to their equilibrium state by dissipating energy to the surrounding molecules. The rate of energy loss is mediated by the intrinsic relaxation properties of the tissue, designated as the longitudinal (T1) and transverse (T2) relaxation times. T1 represents the restoration of the longitudinal magnetization along the axis of the main magnetic field, whereas T2 represents the decay time of the magnetization in the transverse plane.

Technical advances in gradient hardware have resulted in faster and stronger gradients that permit subsecond image scan times. Newer pulse sequences have been developed that currently augment conventional MR pulse sequences (spin echo and gradient echo), increasing the sensitivity of clinical studies to disease detection. These rapid imaging techniques offer major advantages over conventional MR imaging, including decreased image acquisition times, minimized patient discomfort, and increased ability to image physiologic processes in the body. In addition, single-breath-hold scanning can be performed, reducing respiratory artifact.

Fast spin echo, fast gradient echo, diffusion imaging, perfusion imaging, and echo planar imaging (EPI) are examples of fast imaging techniques that can be performed on clinical scanners. Diffusion-weighted imaging is exquisitely sensitive to the microscopic molecular motion of water, demonstrating areas of limited (restricted) intracellular diffusion following an acute ischemic event. This sequence is utilized routinely in clinical neuroimaging protocols but is somewhat nonspecific for pathology, as diffusion changes that are characteristic of acute ischemia can be observed with infection and some tumors. Perfusion-weighted MRI, a less frequently used technique, provides information about the blood supply to a particular area of the brain following rapid bolus injection of gadolinium-based contrast agent. Echo planar imaging allows the collection of all data required for image reconstruction in a fraction of a second, after a single rf pulse. This technology has resulted in significant clinical and scientific advances, such as in stroke evaluation and functional brain imaging, respectively. Functional MRI studies of the human brain using EPI techniques have allowed physiological investigations of the functional organization of the brain.

MR angiography includes contrast-enhanced MR angiography and non-contrast-enhanced MR angiography. Three-dimensional contrast-enhanced magnetic resonance angiography (MRA) is used for noninvasive assessment of many vascular abnormalities, including aneurysms, dissection, vessel anomalies, and coarctation. It has evolved from the use of fast scanning techniques on high-gradient-strength units, in combination with contrast. Using this technique, volumetric acquisitions can be performed in a single breath hold. Improvements in contrast resolution are achieved, regardless of the plane of acquisition. This has allowed reductions in the number of image sections needed to display a large vascular territory, as well as overall imaging acquisition times. Multiphase dynamic imaging is usually performed after intravenous gadolinium administration, with the arteries best seen during the early phase and veins during the later phases. Noncontrast MRA methods, such as 3D time-of-flight (TOF) MR, is used to evaluate intracranial arterial (Figure 1-8) and carotid arteries. In addition, 2D TOF MR imaging is used to evaluate peripheral vascular diseases.

Clinical Applications

MRI has traditionally been used for neurologic indications, including brain tumors (Figure 1-9), acute ischemia, infection, and congenital abnormalities. MRI has been used for a number of nonneurologic indications, namely, spine, musculoskeletal (MSK), cardiac, hepatic, biliary, pancreatic, adrenal, renal, breast, and female pelvic imaging. Spine MR studies are useful for evaluating degenerative changes, disk herniation, infection, metastatic disease, and congenital abnormalities. Common MSK applications involve imaging of

▲ **Figure 1-8.** 3D reformatted image from noncontrast MR angiography shows absent signal in the right internal carotid artery (ICA), indicating complete occlusion of the right ICA or a high-grade stenosis with extremely slow blood flow. Flow in the right anterior and middle cerebral arteries (arrows) is supplied by a small anterior or posterior communicating artery. (Arrowhead: left internal carotid artery.)

▲ **Figure 1-9.** A midline sagittal T1-weighted contrast-enhanced MR image depicts a large tumor (T) in the region of the pineal gland.

large joints, such as knee, shoulder, and hip. The primary common indication for MRI of the knee is the assessment of menisci and ligaments following internal derangement. Rotator cuff tear is a typical shoulder indication. Cardiac studies are performed to identify complex malformations, cardiac function, myocardiac viability, valvular disease, myocardial perfusion, and congenital heart disease. In the abdomen, hepatic MRI studies are often used to diagnose atypical presentations of liver lesions, metastatic disease, and hepatocellular carcinoma. Adrenal studies are performed primarily to distinguish adrenal adenomas from metastatic disease. Atypical renal masses, found incidentally on US or CT, can often be better characterized on MRI. In addition, renal MRI is used to establish the presence and extent of tumor thrombus in cases of renal-cell carcinoma for tumor staging purposes. Breast MRI is utilized to stage cancer, to screen patients at high risk, to look for unknown primary cancer in patients with positive axillary nodes, for delineation of residual cancer after chemotherapy, and sometimes for patients with equivocal mammographic and/or US findings. Finally, oncologic applications in the female pelvis include the diagnosis and characterization of cervical and endometrial carcinomas, as well as adnexal lesions. MR enterography is used in the evaluation of small-bowel disease (Figure 1-10).

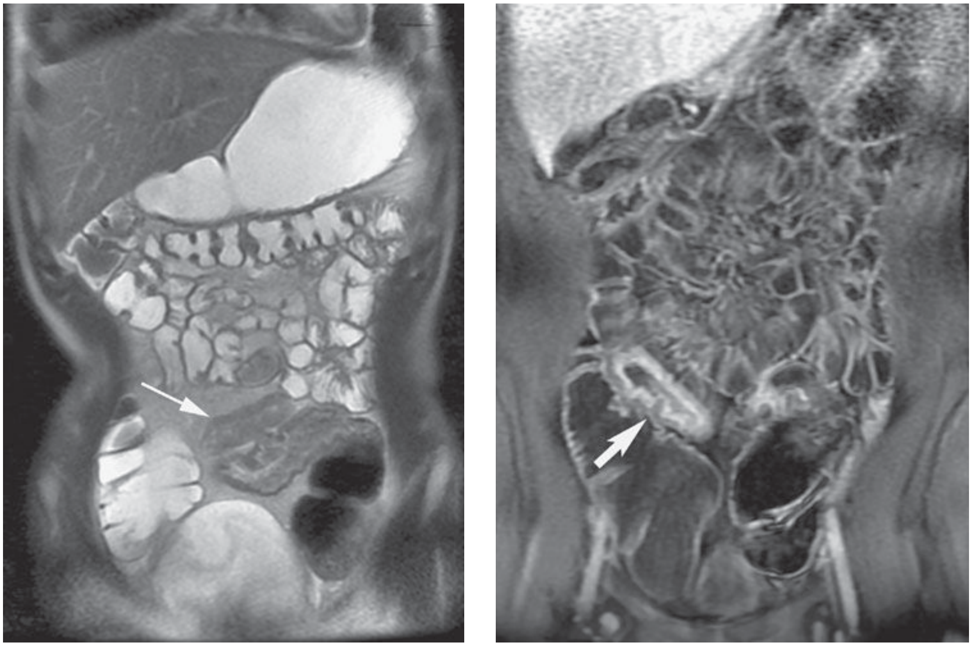

A B

▲ **Figure 1-10.** MR enterography on a patient with Crohn disease. **A.** Coronal T2-weighted image shows wall thickening and stenotic ileum (arrow). **B.** Coronal gadolinium-enhanced fat suppressed T1-weighted image shows increased contrast enhancement of one thickened segment of ileum (arrow).

▲ **Figure 1-11.** An unenhanced MRI of the upper abdomen consisting of MRCP sequences showing the dilated common bile duct (C). Within the common bile duct, there is an ovoid filling defect (arrow) measuring 3.8 × 1.7 cm in the coronal plane, indicating a biliary calculus. The intrahepatic and extrahepatic biliary ducts are markedly dilated.

Magnetic Resonance Cholangiopancreatography

Magnetic resonance cholangiopancreatography (MRCP) is used to evaluate choledocholithiasis, retained gallstones, pancreatobiliary neoplasms, strictures, primary sclerosing cholangitis, and chronic pancreatitis (Figure 1-11). This noncontrast technique relies on the relatively stationary nature of bile (compared with blood) to depict the predominantly fluid-filled pancreatic ducts and biliary tree. Rapid heavily T2-weighted breath-hold sequences are utilized, resulting in visualization of high signal-intensity ductal structures. In patients who have failed endoscopic retrograde cholangiopancreatography (ERCP), or who are unable to tolerate this procedure, MRCP has become a suitable alternative. MRCP is particularly useful in postoperative patients, patients with biliary system anomalies, and as a screening tool in patients with an otherwise low probability of a biliary abnormality. ERCP is generally reserved for therapeutic purposes, such as stent placement, stone extraction, or stricture dilatation.

Nephrogenic Systemic Fibrosis

Since 2006, it has been reported that the administration of gadolinium-based contrast agents for MR imaging is associated with the development of nephrogenic systemic fibrosis (NSF) in some patients with renal insufficiency. Although NSF was first reported in 1997, the exact cause of development of NSF remains unknown. The dissociation of gadolinium ion from the chelating ligand recently has been proposed as an etiologic factor in the development of NSF. The incident of NSF ranges from 0.003% to 0.039% depending on the report cited. The incidence of NSF may increase to 1% to 7% in patients with severe chronic kidney disease following exposure to gadolinium-based contrast media. All patients in published case reports developed NSF within 6 months following administration of gadolinium-based contrast agent. The majority of patients with renal insufficiency in these published reports, however, did not develop NSF following administration of gadolinium chelates. The development of NSF following the administration of a gadolinium chelate contrast has been reported to be particularly associated with patients who have acute or chronic renal disease with a glomerular filtration rate (GFR) lower than 30 mL/min/1.73 m^2, and in those with acute renal insufficiency. The estimated GFR was calculated by using the patient's age, weight, and race and serum creatinine level. Some risk factors, such as concurrent proinflammatory conditions, metabolic conditions including acidosis and high calcium-phosphate products, or concurrent tissue injury, surgery, and ischemia, are associated with the development of NSF in patients who underwent gadolinium-based contrast MR imaging.

In 2007, the US Food and Drug Administration (FDA) requested that a warning be added to all five FDA-approved gadolinium-based contrast agents regarding the potential risk of NSF in patients with renal failure. These five FDA-approved products include gadodiamide (Omniscan, GE Healthcare, Oslo, Norway), gadopentetate dimeglumine (Magnevist, Bayer Healthcare, Wayne, NJ), gadobenate dimeglumine (MultiHance, Bracco Diagnostics, Princeton, NJ), gadoteridol (ProHance, Bracco Diagnostics, Princeton, NJ), and gadoversetamide (OptiMARK, Tyco-Mallinckrodt, St Louis, MO). One recent recommendation aimed at decreasing the risk of NSF has been to use 0.1 mmol/kg of gadolinium contrast for patients with GFR lower than 30 mL/min. If a patient is in a dialysis program, some experts believe that it may be prudent to dialyze after administration of gadolinium-based contrast agent. Alternative imaging examinations, such as arterial spin-labeling perfusion MRI, may replace administration of gadolinium for some.

MR imaging is contraindicated for patients with metal implants or foreign bodies, such as intracranial aneurysm clips, intraorbital metallic foci, cardiac pacemakers, or specific types of cardiac valves. In these instances, these objects may be dislodged or damaged by the magnetic field. MR imaging may also be contraindicated for claustrophobic or uncooperative patients who may not respond to conscious sedation protocols.

NUCLEAR MEDICINE

Nuclear medicine studies, in general, are very sensitive, but relatively nonspecific in the detection of pathology. It is very important, therefore, to correlate nuclear medicine examinations with pertinent history, physical findings, laboratory data, and other diagnostic imaging studies in order to optimize the diagnostic utility of these studies. Nuclear medicine imaging examinations are performed by administering various radiopharmaceuticals to the patient and subsequently recording in vivo distribution. Radiopharmaceuticals consist of two main components: (1) the main component that is distributed to various organs via a number of different mechanisms, and (2) the radionuclide that is tagged to the main component, which emits gamma rays, permitting detection of the compound in the body.

Most nuclear medicine studies are performed with gamma cameras, which provide planar (2D) images. Single photon emission computed tomography (SPECT) is a special technique that creates tomographic images using a rotating gamma camera system. Positron emission tomography (PET) is another unique technique that creates tomographic images by detecting gamma rays produced when positrons interact with electrons.

Some common nuclear medicine procedures include (1) cardiac studies to evaluate myocardial perfusion and/or ventricular function; (2) skeletal studies to evaluate for early bony metastases (Figure 1-12), skeletal trauma, osteomyelitis, and primary bone neoplasms; (3) renograms and renal scans to evaluate kidney function and morphology; (4) ventilation-perfusion studies to evaluate for suspected pulmonary emboli; and (5) PET studies to diagnose or stage tumors (eg, lung, lymphoma, melanoma, colorectal, breast), evaluate dementia, monitor for brain tumor recurrence, track post-therapy changes, and evaluate myocardial viability.

Less common nuclear medicine studies include (l) thyroid evaluation of nodules and therapy for hyperthyroidism and thyroid cancer; (2) hepatobiliary studies to evaluate for acute cholecystitis and bile duct patency; (3) brain imaging to evaluate dementia and brain death; (4) white blood cell studies to detect infection and inflammation; (5) gastrointestinal bleeding studies to detect and localize small gastrointestinal bleeds; (6) lymphoscintigraphy to identify sentinel lymph nodes for surgery; and (7) parathyroid studies to identify adenomas and hyperplasia.

Positron Emission Tomography/CT (PET/CT)

Positron emission tomography (PET) with fluorine (^{18}F) fluorodeoxyglucose (FDG) is a functional imaging method that plays an important role in the diagnosis and staging of malignancy, as well as in treatment monitoring. CT is an anatomic imaging modality that provides excellent spatial localization of pathology. The first combined PET/CT scanner was in operation in 2001. Combined PET/CT scanners have separate individual imaging components that reside in the same unit. In general, a CT scan is performed first and the PET scan follows. Output from PET/CT imaging includes separate CT and PET images, as well as the coregistered fused images that overlay the anatomic CT and metabolic data. The combined anatomic and functional images can be acquired in a single examination. The use of CT images for attenuation correction of the PET emission data also significantly reduce PET scan time. The combined PET/CT is more sensitive and specific for detecting otherwise occult malignancy, tumor staging, and detecting disease recurrence and/or metastasis. PET/CT has also proven useful for following post-therapy changes, such as squamous-cell carcinoma of the head and neck. Fused PET/CT images consistently outperform separately collected CT and PET images for the detection of pathology, even when the separate nonfused imagines are viewed simultaneously.

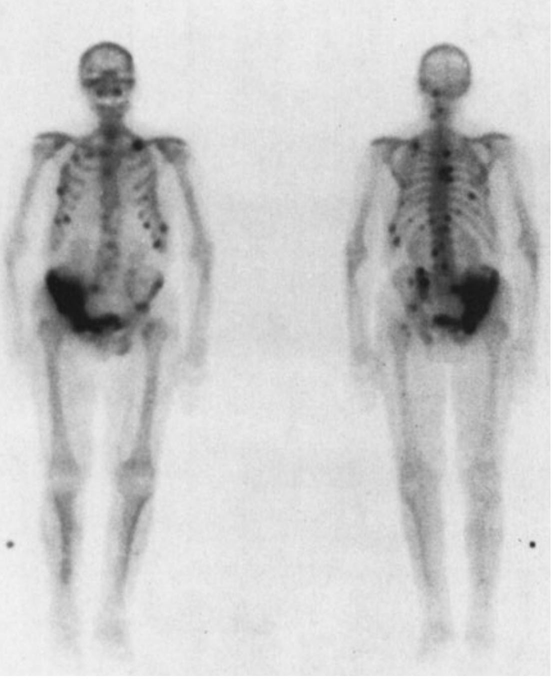

▲ **Figure 1-12.** A ^{99m}Tc-MDP bone scan in the anterior and posterior projections demonstrates multiple foci of increased radiopharmaceutical accumulation (spine, ribs, pelvis, and left clavicle) with the typical appearance of bone metastases.

Acknowledgments *Special thanks to my colleagues, Drs. John Leyendecker, MC, and Caroline Chiles, MD, for providing me with the CT and MR images used in this chapter.*

SUGGESTED READING

1. McAdams HP, Samei E, Dobbins J III, Tourassi GD, Ravin CE. Recent advances in chest radiography. *Radiology*. 2006;241:663-683.
2. Rubesin SE, Levine MS, Laufer I. Double-contrast upper gastrointestinal radiograph: a pattern approach for diseases of the stomach. *Radiology*. 2008;246:33-48.
3. Steenburg SD, Ravenel JG. Acute traumatic thoracic aortic injuries: experience with 64-MDCT. *AJR Am J Roentgenol*. 2008;191:1564-1569.
4. Nandalur KR, Hussain HK, Weadock WJ, et al. Possible biliary disease: diagnostic performance of high-spatial resolution isotropic 3D T2-weighted MRCP. *Radiology*. 2008;249:883-890.
5. Maccioni F, Bruni A, Viscido A, et al. MR imaging in patients with Crohn disease: value of T2- versus T1-weighted gadolinium-enhanced MR sequences with use of an oral superparamagnetic contrast agents. *Radiology*. 2006;238:517-530.
6. Prince MR, Zhang H, Morris M, et al. Incidence of nephrogenic systemic fibrosis at two large medical centers. *Radiology*. 2008;248:807-816.
7. von Schulthess GK, Steinert HC, Hany TF. Integrated PET/CT: current applications and future directions. *Radiology*. 2006;238:405-422.
8. Miyazaki M, Lee VS. Nonenhanced MR angiography. *Radiology*. 2008;248:20-43.
9. American College of Radiology. *Manual on Contrast Media*. 6th ed. Reston, Va: American College of Radiology; 2008:23-37.

The Physical Basis of Diagnostic Imaging

2

Robert L. Dixon, PhD
Christopher T. Whitlow, MD, PhD

IMAGING WITH X-RAYS

What Is an X-ray?

An x-ray is a discrete bundle of electromagnetic energy called a photon. In that regard, it is similar to other forms of electromagnetic energy such as light, infrared, ultraviolet, radio waves, or gamma rays. The associated electromagnetic energy can be thought of as oscillating electric and magnetic fields propagating through space at the speed of light. The various forms of electromagnetic energy differ only in frequency (or wavelength). However, because the energy carried by each photon is proportional to the frequency (the proportionality constant is called Planck's constant), the higher frequency x-ray or gamma ray photons are much more energetic than, for example, light photons and can readily ionize the atoms in materials on which they impinge. The energy of a light photon is of the order of one electron-volt (eV), whereas the average energy of an x-ray photon in a diagnostic x-ray beam is on the order of 30 kiloelectron volts (keV) and its wavelength is smaller than the diameter of an atom (10^{-8} cm).

In summary, an x-ray beam can be thought of as a swarm of photons traveling at the speed of light, each photon representing a bundle of electromagnetic energy.

Production of X-rays

Electromagnetic radiation may be produced in a variety of ways. One method is the acceleration or deceleration of electrons. For example, a radio transmitter is merely a source of high-frequency alternating current that causes electrons in an antenna wire to which it is connected to oscillate (accelerate and decelerate), thereby producing radio waves (photons) at the transmitter frequency. In an x-ray tube, electrons boiled off from a hot filament (Figure 2-1) are accelerated toward a tungsten anode by a high voltage on the order of 100 kilovolts (kV). Just before hitting the anode, the electrons will have a kinetic energy in kiloelectron volts equal in magnitude to the kilovoltage (eg, if the voltage across the x-ray tube is 100 kV, the electron energy is 100 keV). When the electrons smash into the tungsten anode, most of them hit other electrons, and their energy is dissipated in the form of heat. In fact, the anode may become white-hot during an x-ray exposure,

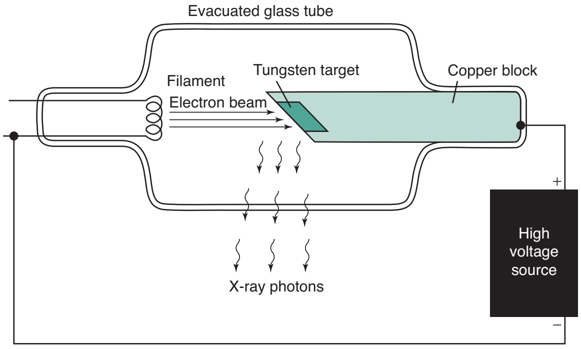

▲ **Figure 2-1.** Simple x-ray tube.

which is one reason for choosing an anode made of tungsten, with a very high melting point. The electrons penetrate the anode to a depth less than 0.1 mm.

A small fraction of the electrons, however, may have a close encounter with a tungsten nucleus, which, because of its large positive charge, exerts a large attractive force on the electron, giving the electron a hard jerk (acceleration) of sufficient magnitude to produce an x-ray photon. The energy of the x-ray photon, which is derived from the energy of the incident electron, depends on the magnitude of the acceleration imparted to the electron. The magnitude of the acceleration, in turn, depends on how closely the electron passes by the nucleus. If one imagines a target consisting of a series of concentric circles, such as a dart board, with the bull's-eye centered on the nucleus, more electrons clearly will impinge at larger distances than in the bull's-eye; hence, a variety of x-ray photon energies will be produced at a given tube voltage (kV) up to a maximum equal to the tube voltage (a hit in the bull's-eye), where the electron gives up all its energy to the x-ray photon. Increasing the voltage will shift the x-ray photon spectrum to higher energies, and higher-energy photons are more penetrating. The radiation produced in this manner is called Bremsstrahlung (braking radiation) and represents only about 1% of the electron energy dumped into the anode by the electron beam; the other 99% goes into heat.

The electron current from filament to anode in the x-ray tube is called the mA, because it is measured in milliamperes. The mA is simply a measure of the number of electrons per second making the trip across the x-ray tube from filament to anode. The rate of x-ray production (number of x-rays produced per second) is proportional to the product of milliamperage and kilovoltage squared. The quantity of x-rays produced in an exposure of duration s (in seconds) is proportional to the product of mA and time and is called the mAs. The quantity of x-rays at a given point is generally measured in terms of the amount of ionization per cubic centimeter of air produced at that point by the x-rays and is measured in roentgens (R) or in coulombs per kilogram of air. This quantity is called exposure, and 1 R of exposure results in 2×10^9 ionizations per cubic centimeter of air.

The electron beam is made to impinge on a small area on the anode of the order of 1 mm in diameter in order to approximate a point source of x-rays. Because a radiograph is a shadow picture, the smaller the focal spot, the sharper the image. By analogy, a shadow picture on the wall (such as a rabbit made with one's hand) will be much sharper if a point source of light such as a candle is used rather than an extended light source such as a fluorescent tube. The penumbra (or unsharpness) of the shadow will depend not only on the source size, but also on the magnification, as can be illustrated by making a shadow of one's hand on a piece of paper using a small light source such as a single light bulb. The closer you bring your hand to the paper (the smaller the magnification), the sharper the edges of the shadow. Similarly, magnification of the x-ray image produced by the point source is less, the closer the patient is to the film and the farther the source is from the film. The magnification factor (M) is defined as the ratio of image size to object size and is equal to the ratio of the focal-to-film distance divided by the focal-to-object distance ($M \geq 1$, and $M = 1$ means no magnification is produced; ie, either the object is right against the film, or the focal spot is infinitely far away). The penumbra, blurring, or unsharpness (Δx) produced on an otherwise perfectly sharp edge of an object and due to the finite focal spot size of dimension *a* is expressed by the equation

$$\Delta x = a(M - 1)$$

Unfortunately, the smaller the focal spot, the more likely it is that the anode will melt. The power (energy/per second) dumped into the anode is equal to the product of the kilovoltage and milliamperage; ie, at 100 kV and 500 mA, 50,000 watts of heat energy is deposited into an area on the order of a few square millimeters (imagine a 50,000-watt light bulb to get an idea of the heat generated).

Interaction of X-rays with Matter

X-rays primarily interact with matter through interaction of their oscillating electric field with the atomic electrons in the material. Having no electrical charge, the x-rays are more penetrating than other types of ionizing radiation (such as alpha or beta particles) and are therefore useful for imaging the human body. The x-rays may be absorbed or scattered by the atomic electrons. In the absorption process (photoelectric absorption), the x-ray is completely absorbed, giving all its energy to an inner shell atomic electron, which is then ejected from the atom and goes on to ionize other atoms in the immediate vicinity of the initial interaction. In the scattering process (Compton scattering), the x-ray ricochets off an atomic electron, losing some of its energy and changing its direction. The recoiling electron also goes on to ionize hundreds of atoms in the vicinity. Electrons from both processes go on to ionize many other atoms and are responsible for the biological damage produced by x-rays.

The attenuation of the x-ray intensity with thickness of material follows an exponential law due to the random hit-or-miss nature of the interaction. The process is similar to firing a volley of rifle bullets into a forest, where the bullets may either stick in a tree (be absorbed) or ricochet off a tree (scatter). The deeper you go into the forest, the fewer bullets there are; however, a bullet still has a chance of traveling through the forest without hitting a tree. Likewise, an x-ray can make it all the way through a patient's body without touching anything and remain unchanged, as if it had passed through a vacuum instead. These are called primary x-rays. Typically, only about 1% of the incident x-rays penetrate the patient, and only about a third of these are primary x-rays; the rest are scattered x-rays that do not contribute to the anatomic image. An x-ray image is a shadow or projection image which assumes that x-rays reaching the film have traveled in a straight line from the source, but this is true only for the primary x-rays. As Figure 2-2A shows, the film density (blackness) at point P on the film is related to the anatomy along line FP. The scattered photon reaches the film along the path FSP and is relaying information about the anatomy at the random point S to point P on the film. Scatter simply produces a uniform gray background; it does not contribute to the image. Because scatter reduces image contrast, it is desirable that the scatter be removed. This task is accomplished by use of an antiscatter grid (Figure 2-2B). This grid consists of a series of narrow lead strips with radiolucent (low-attenuation) interspace material to remove some of the scatter. With the grid, the scattered photon shown in the figure can no longer reach the film, but the primary x-rays can. More of the scatter than primary x-rays is eliminated by the grid; hence, image contrast increases, but at the cost of an increase of a factor of 2 to 3 in patient dose. This increase occurs because the scatter, which was previously blackening the film, has been reduced, and therefore, higher x-ray exposure to the front of the patient is necessary to get the requisite number of x-rays through the grid to blacken the film. The grid is usually made to move a few interspaces during the exposure by a motor drive, in order to wash out the grid lines.

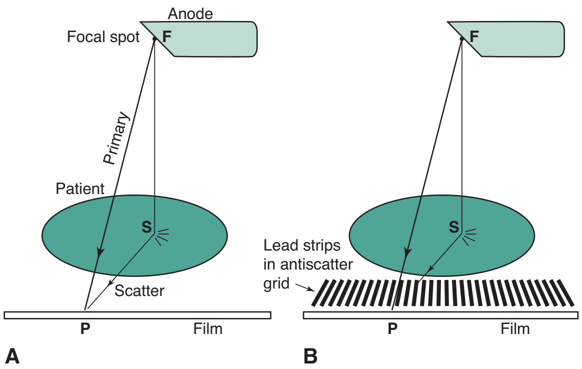

▲ **Figure 2-2.** (**A**) Scattered and primary x-ray photons reaching the same point P on film. (**B**) Scattered photon is removed by antiscatter grid, while primary photon gets through.

The absorption process is more prevalent at lower kilovoltages and in materials with higher atomic numbers. Bones appear white on an x-ray film because photoelectric absorption of x-rays is greater in bone than in soft tissue as a result of the higher atomic number of bone. Lead is a useful shielding material for x-rays because of its high atomic number. The probability of the absorption process decreases rapidly with photon energy (as $1/E^3$) and the scattering process decreases slowly (as $1/E$); hence, the x-ray beam becomes more penetrating as kilovoltage increases. The scattering process is roughly independent of the atomic number of the attenuating material (all electrons look alike to the photon for the scattering process), whereas the absorption process is more probable for tightly bound electrons such as the inner electrons in heavier elements.

Increasing the kilovoltage is therefore beneficial to the patient in that it reduces the radiation dose: that is, fewer x-rays must penetrate the front of the patient to get the requisite number out the back to blacken the film. However, an increase in kilovoltage will reduce image contrast because the absorption process, which is sensitive to atomic number, will decrease and the scattering process is independent of the atomic number of the materials. Even with materials of the same atomic number, contrast improves at lower kilovoltage settings because of higher attenuation, which results in greater differential attenuation between different thicknesses of the same material. Thus there is a tradeoff between image quality (contrast) and patient dose that must be weighed in the selection of kilovoltage.

The Radiographic Image

For production of radiographic images, the x-ray film is placed in a cassette and sandwiched between two fluorescent screens that glow under x-ray exposure, and it is primarily the light from these fluorescent screens that blackens the film. Although x-ray film, which is quite similar to ordinary photographic film, can be blackened by direct x-ray exposure, the film does not absorb the penetrating x-rays very efficiently, because the emulsion consists of silver halide crystals embedded in a low-atomic-number gelatin base. The fluorescent screens, called intensifying screens, are made of high-atomic-number materials, which therefore absorb x-rays very efficiently and also emit hundreds of light photons per x-ray absorbed. These light photons, in turn, are efficiently absorbed by the film. As a result, x-ray exposure to the patient is reduced by a factor on the order of 100 compared to direct x-ray exposure of the film. The screens do produce a loss of sharpness of the image due to the spreading out of the light from the point of x-ray absorption before the light reaches the film. This effect can be reduced by making the screen thinner; however, it then absorbs a smaller fraction of the incident x-rays and therefore results in a "slower" system (more patient exposure is required).

In recent years digital image receptors have come into use. One type called CR (computed radiography) utilizes a cassette with a photostimulable phosphor material that stores the x-ray image in the form of trapped electrons for later readout by a scanned laser beam, which releases the electrons from their traps. On release, these electrons cause the phosphor to emit light that has a shorter wavelength than that of the laser beam. This light signal is read out and digitized, thereby forming a digital image. Another type called DR (direct radiography) consists of a flat-panel digital detector plate that is built into the x-ray unit itself. In these, the x-ray image is converted to an electrical signal from a fine matrix of thin-film transistor elements, which creates a digital image having a pixel size of 0.2 mm or less. These digital images, which consist of an array of numbers in a matrix, can be processed to improve image quality; displayed and manipulated on a viewing monitor; and then printed onto film using a laser film printer. The advantage of these digital systems is that the image can be processed to improve contrast and provide edge enhancement, and the film can be printed to the appropriate darkness regardless of the x-ray exposure.

Recall that the quantity of x-rays produced during an exposure is proportional to

$$mAs \cdot kV^2$$

However, because the beam is more penetrating at high kilovoltage, the x-ray exposure that reaches the film through a patient is roughly proportional to

$$mAs \cdot kV^4$$

That is, it depends very strongly on kilovoltage. The exposure time required to blacken the film is thus proportional to

$$s \approx \frac{1}{mA \cdot kV^4}$$

The heat deposited in the anode is proportional to the product of kV and mAs.

Choice of an exposure technique is generally made by first selecting the kilovoltage. A lower kilovoltage gives greater image contrast but also higher patient exposure and requires a longer exposure time at a given milliampere setting, because the x-ray beam is less penetrating and x-ray production is lower at the lower kilovoltages. Thus, for thick body parts, care must be taken not to choose too low a kilovoltage.

Generally, x-ray tubes have two focal spot sizes produced by two different (selectable) filament sizes. That is, they have a large and a small focal spot (eg, 1.25 and 0.6 mm). With the small focal spot, however, the electron energy is deposited in a smaller area, thereby creating a higher anode temperature; hence, at a given kilovoltage, the maximum milliamperage that can be used without melting the anode is limited to a lower value, thereby resulting in a longer exposure time. The small focal spot will result in a sharper image, however, if the longer exposure time required by its selection does not "stop" patient motion; then motion of the patient during the exposure may blur out any sharpness gain realized by use of the small focal spot. In any case, the small focal spot is useful only for looking at fine detail, such as bony detail, and its use does not significantly improve, for instance, an abdominal radiograph in which soft-tissue contrast is the objective. The small focal spot might be used for radiographs of the skull or extremities. The exposure time selected should be short enough to stop the motion of the anatomic part being radiographed. A very short time would be required for the heart and somewhat longer times for the abdomen or chest. Exposure time is less critical for the head or extremities, which are not subject to motion in most cases.

Having selected the kilovoltage and exposure time, one must then select the milliamperage so that the milliampere-seconds (the product of milliamperage and time) is large enough to blacken the film suitably. If the milliamperage required is above 200 mA to 300 mA, a small focal spot generally cannot be used, because it will not allow this high a value of milliamperage without melting the anode.

On many x-ray units, a phototimer sensor (automatic exposure control) is used to automatically terminate the exposure when a given x-ray exposure has been accumulated at the cassette position. In this way, the film is blackened sufficiently regardless of patient thickness and kilovoltage selection. When using this feature, however, the operator loses control of the exposure time. Choosing the highest milliamperage allowable by the tube will ensure the minimum exposure time.

Fluoroscopy

If, instead of using the light from a fluorescent screen to blacken a film, one viewed the fluorescent screen directly with the naked eye, then one would be performing fluoroscopy as it was done in the early days of medical x-ray use. Unfortunately, the image made in this fashion was very dim, even at a high exposure rate to the patient, so modern fluoroscopy uses an image intensifier that amplifies the light from a fluorescent screen. A typical fluoroscopic imaging system is shown in Figure 2-3. The image intensifier tube is an evacuated glass or metal tube with a fluorescent screen (input phosphor) that glows with the image produced by the x-ray pattern that exits the patient. The light from the

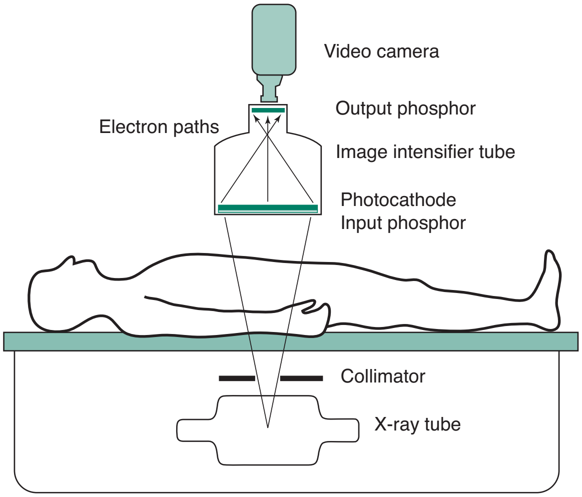

▲ **Figure 2-3.** Fluoroscopic imaging system.

input phosphor causes ejection of electrons from a photoelectric material adjacent to the input phosphor. These electrons are accelerated via a high voltage (30 kV), as well as being focused to preserve the image onto a small (1-inch diameter) screen (the output phosphor), which glows with the image because of the energy deposited by the impact of the accelerated electrons. The output phosphor glows much more brightly than the input phosphor (about 3000 times) because of the energy gain provided by the acceleration of the electrons and also because of minification of the image on the output phosphor. The image on the output phosphor can be viewed with the naked eye, usually with a series of lenses and mirrors, but the image is more commonly viewed by focusing a video camera onto the output phosphor and viewing the image on a TV monitor via a closed-circuit TV system. The fluoroscopic image generally has less contrast and less resolution of fine detail than a radiographic image; however, it is clearly convenient to view the image in real time—particularly when observing the flow of radiopaque contrast agents ingested or injected into the body. (These contrast materials, such as iodine or barium compounds, have a higher atomic number than soft tissue, hence, absorb more x-rays.) During fluoroscopic examinations, the x-ray tube is typically operated below 100 kV and below 3 mA tube current. Even so, entrance exposure rates (at the point where the x-ray beam enters the patient) are about 2 to 5 R/min, depending on patient thickness; hence, fluoroscopic examinations generally result in significantly higher patient exposures than do radiographic examinations.

Fluoroscopic systems generally have an automatic brightness control in which the brightness of the output phosphor is sensed by a light detector. The brightness signal from this detector is compared to a reference level, and the difference signal is used to instruct the x-ray generator to vary milliamperage or kilovoltage (or both) in order to maintain a constant brightness at the output phosphor. For example, after ingestion of barium in a barium-swallow examination, the barium absorbs significantly more x-rays, and the image would tend to go dark without such a system; however, as the brightness falls below the reference level, the automatic brightness control causes the x-ray generator to increase the milliamperage or kilovoltage to maintain a constant brightness on the monitor.

▶ Recording of Fluoroscopic Images

Fluoroscopic images can be recorded for later viewing by several methods. The TV image can be recorded using a videotape recorder or a videodisc recorder, the latter having the advantage of being able to view one frame at a time as well as providing random access rather than the sequential viewing required by videotape.

In addition, some systems have the capability of digitizing the electric signal from a TV frame and storing it in computer memory chips. These systems often have a "last image hold" capability that holds the last TV frame on the monitor. This method is also used in digital subtraction angiography (DSA); that is, the analog signal from the TV camera is digitized and stored frame by frame in a computer memory in a 512×512 or 1024×1024 image matrix. A short radiographic x-ray pulse is usually used for making the image. Images made just before and after injection of contrast material into the arteries can be subtracted digitally, so that only the vascular system appears in the subtracted image.

▶ Spot Film Devices

The aforementioned image recording methods merely store the image recorded by the TV camera, which is of lower quality than a radiographic image and has even poorer resolution than the image appearing on the output phosphor of the image-intensifier tube because of the limitations of the TV imaging process. In order to record higher quality images during a fluoroscopic examination, spot film devices are used. The most common device transports a conventional radiographic screen/film cassette to a position in front of the image intensifier at the push of a button on the fluoroscopic carriage. The x-ray tube is then switched into a radiographic mode (ie, the milliamperage is increased from low mA to 200 to 400 mA to shorten exposure time), and a conventional radiographic image is obtained on film. Digital spot films can be obtained by digitizing a TV frame from the image intensifier acquired with a short exposure burst at a higher exposure value than that of a single continuous fluoroscopic frame. These produce an image of higher quality (lower noise) than that obtained from the fluoroscopic image.

Computed Tomography

In radiography or fluoroscopy, one is creating a shadow picture or a projection of the attenuation properties of the human body onto a plane. Thus, each ray from the source to a given point on the film, such as ray FP in Figure 2-2, conveys information about the sum of the attenuation along a line in the body; that is, anatomic structures are piled on top of each other and flattened into the radiographic image. In an attempt to give a different perspective, one may obtain projections from two different directions (eg, a lateral and an anteroposterior radiograph), so that the structures that are piled on top of each other differ in each projection. In the late 1960s a British engineer, Geoffrey Hounsfield, concluded that if one obtained projection data from a sufficient number of different angles, one could reconstruct the attenuation properties of each volume element in the body and display these as a cross-sectional image. This required the computational power of a computer to accomplish, and the basic idea is illustrated in Figure 2-4. The x-rays from a source are detected by a series of individual detectors (rather than film) after penetrating the body, and each detector defines a ray from the source through the body, thereby creating a projection. The width of the x-ray beam in the dimension perpendicular to the page is only about 10 mm; hence, only one slice of the body in the longitudinal direction is imaged at a time.

The x-ray tube and the detector bank are rotated 360 degrees about the patient to obtain, for example, 720 projections at 0.5-degree intervals. The computer is then able to reconstruct a cross-sectional image of the slice of the body by dividing the slice into an imaginary matrix. In a matrix of 512×512 pixels in the transverse plane, each pixel represents an area of about 0.5×0.5 mm in a 25-cm diameter body. The computer assigns a numerical value to each pixel, which represents the amount of attenuation contributed by the volume element of the body represented by that pixel, and these numbers are converted into a gray-scale image for viewing. In an axial scan series, after one slice is completed, the patient is advanced via a motorized couch by 10 mm in order to image the adjacent slice, and up to 30 slices (images) may be done to reconstruct the anatomy over a 30-cm length of the patient. Newer scanners, called helical (or spiral) CT scanners, use a continuous advance of the patient through the scan beam rather than the stepping couch motion utilized in axial scans, and axial slices are reconstructed by interpolation of data into the slice from a complete rotation. Multislice helical scanners with subsecond rotation times have been developed that collect data for reconstruction of several slices in each rotation; thus, a 30-cm length of patient anatomy can be imaged in 15 seconds or less.

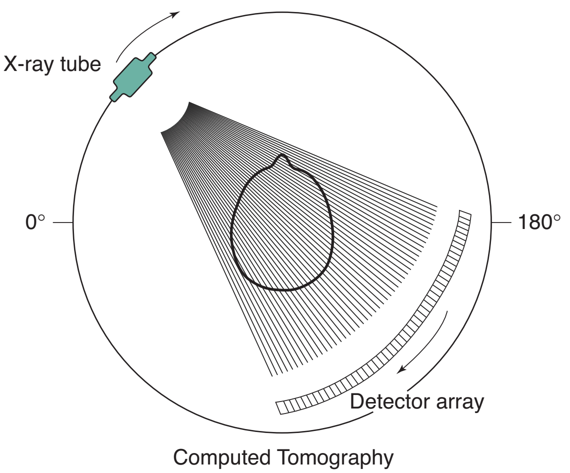

▲ **Figure 2-4.** Computed tomographic (CT) scanning geometry. A single projection of the head is illustrated.

MAGNETIC RESONANCE IMAGING

The technique called nuclear magnetic resonance, developed by physicists in the 1940s, was first utilized for imaging the human body in the late 1970s. The nuclei of some atoms (notably hydrogen nuclei in the body) have a fundamental angular momentum called spin, which causes them to behave like tiny spinning magnets. When placed in a uniform external magnetic field and excited by a radio pulse tuned to a resonant frequency that is proportional to the externally applied magnetic field strength (Larmor frequency), the axis of rotation of the nuclei will precess around the applied magnetic field direction in a similar fashion to the precession of a leaning gyroscope or top about the gravitational field direction (Figure 2-5). This precession can be detected, because the collection of processing magnets (protons in the body) induces an oscillatory voltage in a pickup or receiver coil. This oscillation at the Larmor frequency can be detected by connecting the pickup coil to a radio receiver, and one could therefore, in effect, hear the protons "singing" in unison into the coil at the Larmor frequency. This provides no imaging information; however, if the external magnetic field is made nonuniform in space in a known fashion (ie, a magnetic field gradient is utilized), then protons at different locations will precess at different frequencies, thereby creating a relationship between location in the body and precessional frequency. With application of such a gradient, the protons no longer sing in unison, but at different frequencies depending on their location, as in a chorus; that is, the sopranos would be located where the magnetic field was largest and the baritones where it was smallest. By listening to different frequencies, one could deduce from the signal strength at a given frequency how many protons were present at the location corresponding to that frequency. This method of imaging allows one to map the density of protons in the body in

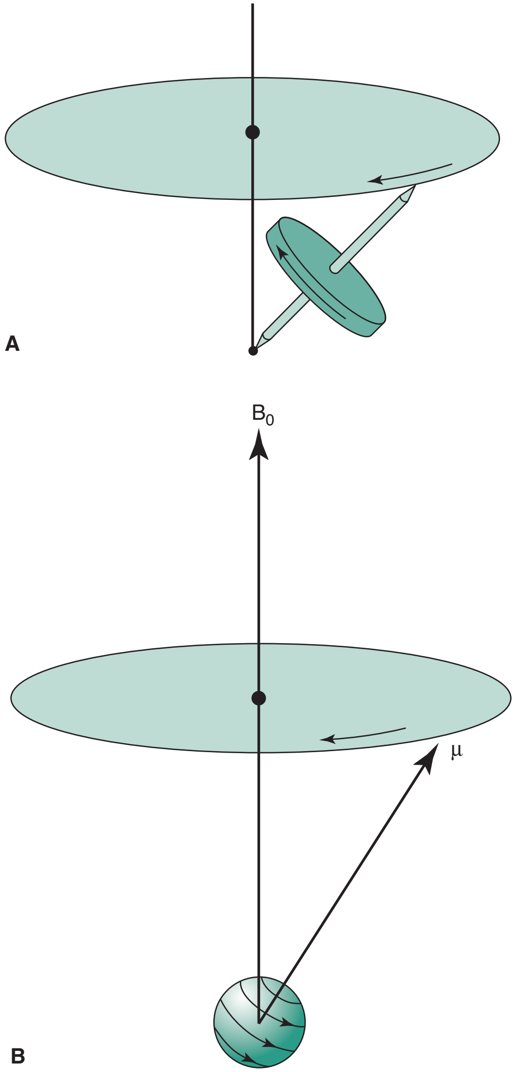

▲ **Figure 2-5.** (**A**) Precession of a gyroscope about the earth's gravitational field. (**B**) Precession of the spin axis of a proton of magnetic moment μ about an applied magnetic field B_0.

three dimensions; however, most images are obtained and displayed as planar cross-sectional images similar to those in CT scans and having a slice thickness of 10 mm and a matrix size that is typically 128 × 256. For greater contrast, the proton density images may also be weighted by the relaxation times (T1, T2), which are measures of the realignment times of protons with respect to the magnetic field direction. This weighting is typically accomplished by varying the radiofrequency pulse durations and spacings in a variety of pulse sequences, the spin-echo pulse sequence being the most commonly used.

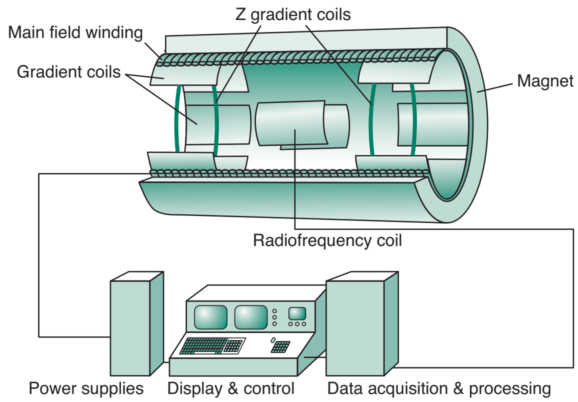

▲ **Figure 2-6.** Magnetic resonance imaging hardware.

The hardware of a (nuclear) magnetic resonance imaging machine (Figure 2-6) consists typically of a cylindrical superconducting coil surrounding the patient to generate a large, static magnetic field; auxiliary coils for generating the magnetic field gradients; radio transmitter/receiver coils in close proximity to the patient; electronics for radiofrequency transmitting and receiving; and a computer to orchestrate the events and to reconstruct the spatial image from the frequency spectra.

ULTRASOUND IMAGING

Sound (or pressure) waves in the 3 MHz to 10 MHz frequency range are used for imaging the body by detecting the intensity of the reflected waves from various organs and displaying this reflected intensity as a gray-scale (or color) image. The sound waves are generated by applying an electrical pulse to a piezoelectric crystal. This crystal also acts as a receiver of the reflected waves after the transmitter pulse is terminated. A typical ultrasound transducer contains a linear array of such crystals, which can be fired in sequence or operated as a phased array to cause the ultrasound beam to rapidly scan across an area 5 to 10 cm in width for real-time imaging. The useful imaging depth is determined by the frequency; the higher frequencies (shorter wavelengths) have less penetrability. For example, at 10 MHz the imaging depth is limited to a few centimeters. Unfortunately, the lower the frequency, the poorer the axial resolution, because objects that are closer together than a wavelength cannot be separated. Hence, there is a tradeoff between axial resolution and penetration depth. Because ultrasound radiation is nonionizing, no adverse biological effects have been observed at diagnostic power levels.

BIOLOGICAL EFFECTS OF X-RAYS

The biological effects of x-irradiation are due to the recoiling electrons produced by the absorption or scattering of the incident x-rays, these electrons having enough kinetic energy to ionize hundreds of atoms along their trajectory. These electrons may damage DNA molecules directly or produce free radicals that can cause chemical damage to genetic material; either effect may result in cell death or mutation. Magnetic resonance imaging and ultrasonic imaging do not utilize ionizing radiation, and there is no significant evidence that any biologic damage results from these imaging modalities.

Effect on the Patient

The primary risk to patients undergoing medical x-ray examinations is radiation-induced cancer, primarily leukemia, thyroid, breast, lung, and gastrointestinal cancer. These relative risks are considered to be related to radiation dose and effective dose, which is essentially the exposure to various critical organs multiplied by an organ-weighing factor (the units of radiation dose or exposure: a rem, a rad, and a roentgen are essentially equivalent for x- and γ-ray irradiation). Table 2-1 lists representative diagnostic procedures and associated typical effective dose in millirem, with the dose translated into relative increase in cancer risk per million persons, as well as the time required to receive the equivalent effective dose from natural background radiation. For example, if 1 million persons received lumbar spine examinations, there would be 51 additional (randomly occurring) cases of cancer above that occurring naturally in this population over their lifetime. In addition, it would take 155 days to receive a dose of radiation from natural background radiation equivalent to one lumbar spine radiograph.

According to a recent report by the National Council on Radiation Protection and Measurements (NCRP), Americans were exposed to greater than seven times the ionizing radiation in 2006, as compared to the early 1980s. This increase was primarily due to the increased utilization of computed tomography, which, when combined with nuclear medicine imaging, constituted 36% of total radiation exposure and 75% of medical-associated radiation exposure received by the US population. Indeed, the NCRP estimated that 67 million CT scans were performed in the United States in 2006. Such markedly increased utilization and associated increase in radiation exposure raise concern about subsequent long-term risk of malignancy. Future research evaluating the diagnostic benefit of imaging compared to the exposure risk to the population will undoubtedly shape the environment and context of medical imaging over the next decade.

The Pregnant Patient

The fetus consists of rapidly dividing cells; hence, it is more sensitive to radiation, particularly in the first trimester. The principal risks to the fetus from in utero irradiation are cancer induction, malformation (eg, small head size), and mental retardation.

Every fertile female patient should be asked if she might be pregnant; if so, the relative risks of the diagnostic x-ray procedure versus the expected benefit should be weighed before the procedure is performed, or alternate imaging procedures such as MR imaging or ultrasound should be considered. It should be noted, however, that the added risk from diagnostic x-ray procedures is generally negligible compared to the normal risks of pregnancy, because fetal doses are typically below 5 rad in these procedures.

Table 2-1. Typical Effective Doses and Resulting Increased Risk of Fatal Cancer for Various X-ray Examinations

X-ray examination	Typical effective dose, mrem (1 mrem = 0.01 mSv)	Lifetime risk of fatal cancer per million persons	Time period for equivalent effective dose from natural background radiation
Chest (PA and lateral)	8	3	10 d
Lumbar spine	127	51	155 d
Upper gastrointestinal tract	244	98	297 d
Barium enema	870	348	2.9 y
Abdomen (KUB)	56	22	68 d
Pelvis	44	18	54 d
Head CT	180	72	219 d
Abdominal CT	760	304	2.53 y

The National Council on Radiation Protection (NCRP) in its report NCRP No. 54 states:

> The risk (to the fetus) is considered to be negligible at 5 rad or less when compared to the other risks of pregnancy, and the risk of malformations is significantly increased above control levels only at doses above 15 rad. Therefore, exposure of the fetus to radiation arising from diagnostic procedures would rarely be cause, by itself, for terminating a pregnancy.

If the x-ray examination involves the abdomen in such a way that the fetus is in the direct x-ray beam, then fetal doses are typically in the 1 to 4 rad (1 rad = 1 cGy) range depending on the number of films and fluoroscopic time (if any). If the examination does not involve the abdomen, and the fetus receives only scatter radiation, the fetal dose is generally small (typically, well below 1 rad).

SUGGESTED READING

1. National Council on Radiation Protection and Measurements. Ionizing radiation exposure of the population of the United States (2009). NCRP Report No. 160. Bethesda, Md: National Council on Radiation Protection and Measurements; 2009.
2. Mettler FA Jr, Huda W, Yoshizumi TT, Mahesh M. Effective doses in radiology and diagnostic nuclear medicine: a catalog. *Radiology.* 2008;248:254-263.

Imaging of the Heart and Great Vessels

3

James G. Ravenel, MD

The heart is often the "forgotten" structure in thoracic imaging studies. Yet a tremendous amount of information regarding cardiac structure and function can be gleaned from careful analysis of studies, regardless of whether they are dedicated to cardiac imaging. This chapter describes the normal radiographic appearance of the heart, pericardium, and great vessels (aorta and pulmonary vessels) and briefly outlines some of the more common pathologic entities in this organ system. Critical evaluation of the findings on the imaging examinations of this region is not possible without paying attention to the lungs, as these two organ systems mirror changes in each other. The most common abnormalities encountered in the cardiovascular system are hypertension, pulmonary arterial hypertension (usually secondary to chronic pulmonary disease), congestive heart failure, atherosclerotic disease, and valvular disease. Less common cardiac and great vessel diseases such as congenital heart disease, neoplasms, and diseases of the pericardium are described in less detail. The last topic, monitoring devices and postoperative changes, is one with which students should be familiar.

It is assumed that the student understands the basic normal anatomy of the cardiovascular system from the basic science and clinical years. At the completion of this chapter, the student should have an understanding of the wide range of imaging modalities used, an appreciation for the potential yield from these examinations, a basic knowledge of the normal imaging anatomy on the conventional radiograph, a familiarity with more common postoperative alterations, and the various monitoring devices that may be present in the intensive care unit (ICU).

TECHNIQUES AND NORMAL ANATOMY

A variety of techniques have been developed to evaluate the heart and great vessels (Table 3-1). In this section, we briefly describe the major tests used in imaging this system.

Conventional Radiographs

The most common imaging test for evaluating the heart and great vessels is the chest radiograph, which consists of an upright posterior-to-anterior (PA) and left lateral (LAT) projections. The terms *PA* and *left lateral* refer to the direction the x-ray beam takes through the body before it reaches the

Table 3-1. Imaging Tests for Heart, Great Vessels, and Pericardium

Conventional radiographs Posteroanterior (PA) and lateral Oblique Portable anteroposterior (AP)
Computed tomography (CT)
Echocardiography Transthoracic Transesophageal
Magnetic resonance (MR) imaging
Angiography Coronary arteriography Aortography Pulmonary arteriography
Radionuclide imaging
Positron emission tomography

radiographic cassette. Chest radiographs are usually obtained with high kilovoltage and milliamperage to minimize exposure time and cardiac motion. When possible, the distance between the x-ray tube source and the film is at least 6 feet to minimize magnification and distortion.

The examination is ideally performed with the patient at maximal inspiration. A good rule of thumb for estimating adequate inspiration is to be able to count 9 to 10 posterior ribs or 5 to 6 anterior ribs from the lung apices to the hemidiaphragms through the aerated lungs (Figure 3-1). When a chest radiograph is taken in the expiratory phase of respiration, the patient may appear to have cardiomegaly, vascular congestion, and even pulmonary edema. This appearance, however, is merely artifactual and caused by the lack of inspiration (Figure 3-2).

Severely ill, debilitated patients or patients who cannot be transported to the radiology department can have their chest radiographs obtained with a portable x-ray machine. Patients in the ICU who have intravascular catheters or who are undergoing mechanical ventilation frequently have chest radiographs performed as a survey for complications that may not be revealed by physical examination or laboratory data. These examinations are done with the cassette placed behind the patient in bed and are therefore anterior-to-posterior (AP) projections. The technical factors, which are controlled by the technologist at the time of the examination, vary with the size of the patient and the distance of the radiographic plate from the x-ray source (or machine). An attempt is still made to obtain the examination during maximum inspiration, but this objective may be difficult to achieve in some patients, especially those who have dyspnea.

With the patient in the supine position, there is normally a redistribution of blood flow to the upper lobe pulmonary veins (cephalization), and the heart may appear enlarged relative to its appearance on the upright PA radiograph, because of magnification (Figure 3-3). Some patients are able to sit for their examinations, whereas others are radiographed in a semiupright position. Ideally, the technologist should mark the exact position of the patient when the radiograph is obtained, and the date and time of the examination should be recorded in all cases. Changes in patient positioning and ventilator settings can have substantial effects on the radiographic appearance and must be taken into account when evaluating any change in the radiograph from a previous study.

The chest radiograph, whether it is obtained in the upright, semiupright, sitting, or supine position, should almost always be the initial screening examination in the evaluation of the cardiovascular system. Because it is essentially a screening study, the chest x-ray must be correlated with the clinical symptoms and physical examination to determine the overall significance of the radiographic findings. This information is also used to decide if other imaging tests are appropriate and which ones will potentially result in the highest diagnostic yield. Decisions regarding further imaging also depend on the impact on the clinical management of the patient, the potential for treatment of any abnormality that may be discovered, the cost and availability of the technique, and the expertise of the interpreting radiologist.

The conventional radiograph is an excellent screening test for the patient suspected of having disease involving the heart and great vessels, because the overall anatomy of these areas is demonstrated well. Whenever possible, all radiographs should be reviewed with all prior relevant imaging studies. Even when a prior chest radiograph is not available, additional information may be ascertained by reviewing other prior images such as thoracic spine or rib-detail image when available. Advanced imaging studies such as computed tomography (CT) and magnetic resonance (MR) imaging can also be used to help clarify complex findings on chest radiographs.

The normal cardiac silhouette size may be determined by the cardiothoracic ratio, a measurement obtained from the PA view. This ratio is calculated by dividing the transverse cardiac diameter (measured from each side) by the widest diameter of the chest (measured from the inner aspect of the right and left lungs near the diaphragm). The average normal value for this ratio in adults is 0.50, although up to 60% may be normal (Figure 3-4). A measurement over 50% is generally considered abnormal in an upright inspiratory-phase PA film, although this may not always be clinically significant. The cardiothoracic ratio cannot be reliably used for the AP projection of the chest, because the heart is magnified (see Figure 3-3). The size of the patient and the degree of lung expansion also should be considered. For instance, in a small person with a petite frame and a small thoracic cage, the heart size may be normal, but the cardiothoracic ratio may

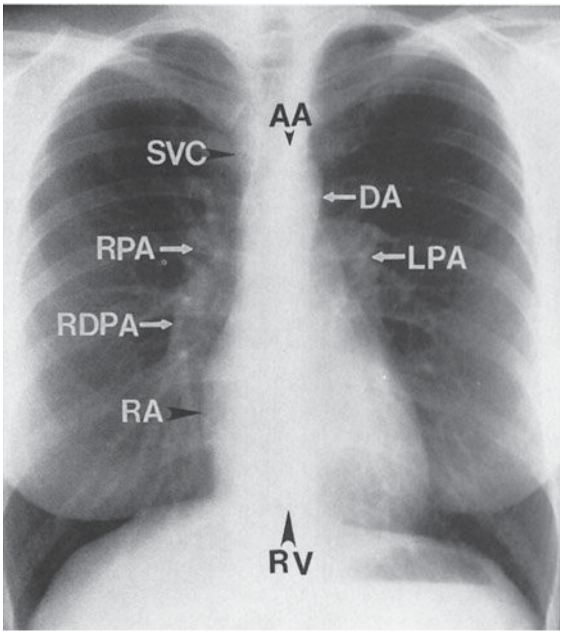

A

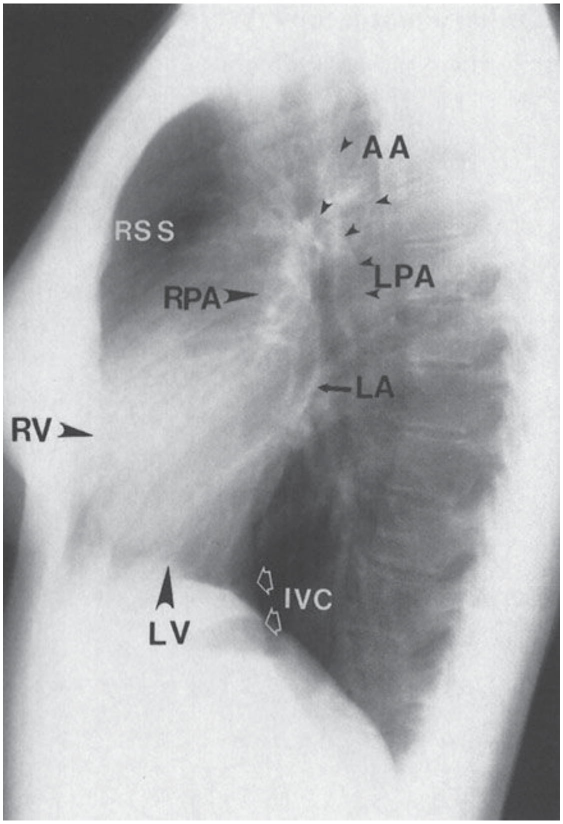

B

▲ **Figure 3-1.** Normal PA and lateral radiographs. (**A**) PA view of normal chest. RA, right atrium; RDPA, right descending pulmonary artery; RPA, right main pulmonary artery; SVC, superior vena cava; AA, aortic arch; DA, proximal descending thoracic aorta; LPA, left pulmonary artery; RV, right ventricle. (**B**) Lateral view of normal chest. RV, right ventricle; RSS, retrosternal clear space; AA, ascending aorta; LPA, left pulmonary artery; RPA, right pulmonary artery en face; IVC, inferior vena cava; LA, left atrium; LV, left ventricle.

measure over 50%. Similarly, if the patient has pulmonary disease such as emphysema, the heart may be enlarged, but because of the overinflation of the lungs, the cardiothoracic ratio may still be normal. In clinical practice, most radiologists do not perform this measurement and rely on experience and "gestalt" to evaluate heart size.

The contours of the heart, mediastinum, and great vessels on the PA view should be evaluated on each chest film (see Figure 3-1A). A reasonable approach is to begin in the upper right side of the mediastinum just lateral to the spine and below the right clavicle. The curved soft-tissue shadow represents the right border of the superior vena cava (SVC). The border of the SVC forms an interface with the lung and should not be confused with the right paratracheal stripe. Below the SVC is the right cardiac border formed by the right atrium. The inferior heart border, or base of the heart, is the area just above the diaphragm and is composed primarily of the right ventricle, although there is some contribution from the left ventricular shadow. The left ventricle makes up the majority of the apex of the heart, which points to the left of the spine. The origins of the right and left pulmonary arteries are generally well demarcated on the normal PA film as they emerge from the mediastinum. The most prominent and recognizable component of the right pulmonary artery, the right descending pulmonary artery (RDPA), is seen just to the right of the superior cardiac border and descends inferiorly. It can usually be easily followed until it branches. The left main pulmonary artery is less well defined, but its origin can usually be seen above and lateral to the left atrial appendage just before it branches. When enlarged, the main pulmonary artery may be seen superimposed over the left pulmonary artery and filling in the normal space

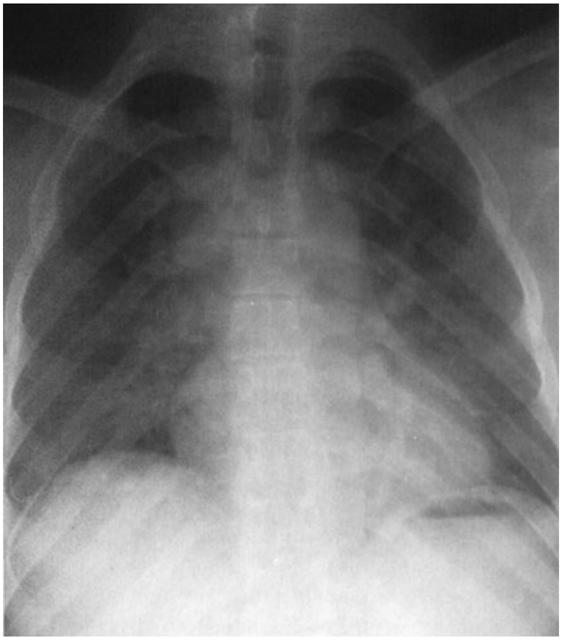

▲ **Figure 3-2.** Expiratory phase on a PA radiograph. Note the low lung volumes, apparent enlargement of the cardiac silhouette, and crowding of bronchovascular structures at the bases. Findings may be misinterpreted as heart failure if analysis of depth of inspiration is not performed.

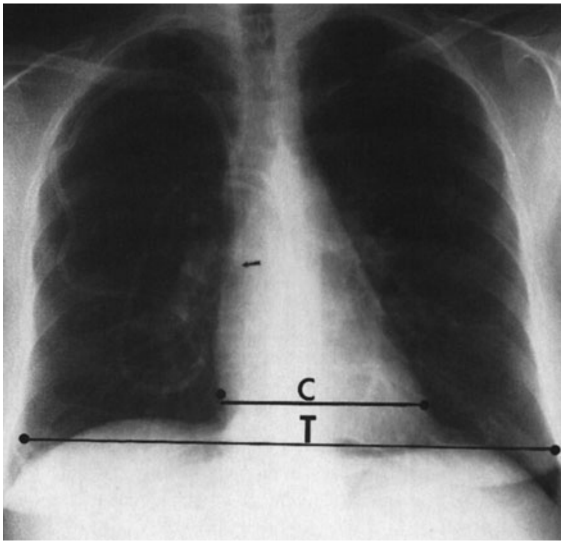

▲ **Figure 3-4.** Upright PA chest radiograph in a patient with leukemia shows normal cardiothoracic (C/T) ratio and how it is measured. Incidentally noted is the tip of an internal jugular triple-lumen catheter in the superior vena cava (arrow).

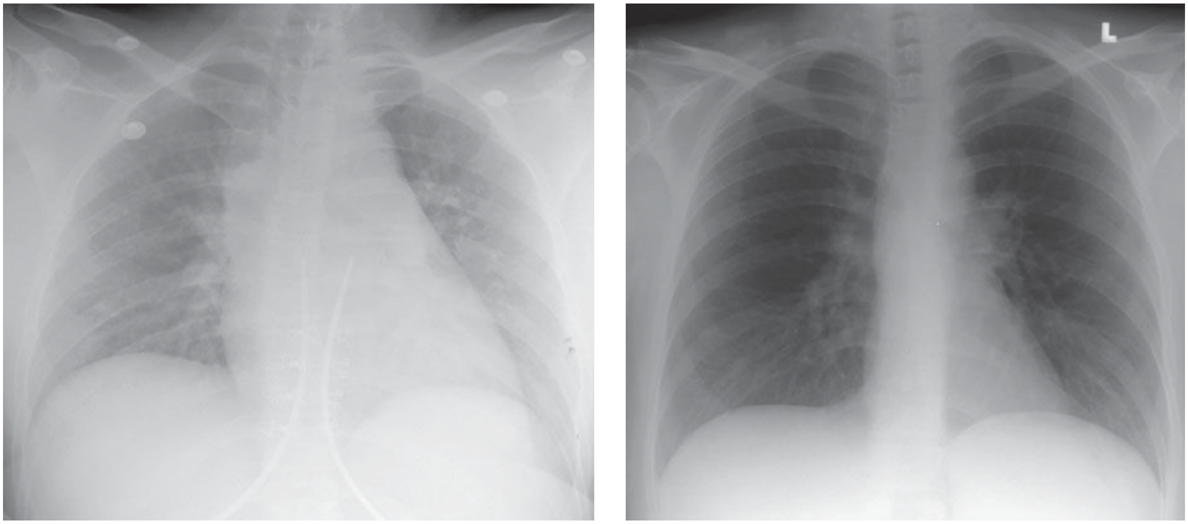

A B

▲ **Figure 3-3.** AP (**A**) and PA (**B**) radiographs of the chest in same patient on same day. Note that the cardiac silhouette appears larger on the AP radiograph and may be mistaken for disease if patient position is not considered in the interpretation.

between the left pulmonary artery and transverse aortic arch (the AP window). The aorta originates posterior and to the right of the main pulmonary artery, and the border of the ascending portion of the aorta can usually be seen superimposed on the inferior portion of the SVC. The majority of the transverse arch is not outlined by air and therefore cannot be seen as it crosses the mediastinum. However, the distal transverse and descending aorta can be seen to the left of the mediastinum as it turns inferiorly. The left border of the descending thoracic aorta should be followed down to the aortic hiatus. Any loss of this contour or any contour abnormality may indicate pathology and should be investigated. Dilation or ectasia, localized bulges, and calcification may occur within the aorta as a normal part of the aging process, but should be viewed as abnormal in younger individuals. Of course, the spine, ribs, adjacent soft tissues, and upper abdominal contents should all be scrutinized. The left atrium lies just inferior to the tracheal carina, but it is usually not visualized as a discrete structure on the normal PA view.

The lateral view of the chest also reveals important information regarding the cardiac contour (see Figure 3-1B). Just behind the sternum there is normally a radiolucent area called the retrosternal clear space (RSS). This region represents lung interposed between the chest wall and the anterior margin of the ascending aorta. Any density present within the RSS may be due to an anterior mediastinal mass or post-surgical changes. The anterior border of the cardiac shadow is composed primarily of the anterior wall of the right ventricle. Right ventricular enlargement may also encroach into the retrosternal clear space. The posterior margin of the cardiac silhouette is formed by the left atrium and left ventricle. Just posterior and inferior to the left ventricle is a linear soft-tissue shadow leading into the heart formed by the inferior vena cava (IVC). The left ventricular shadow should not project more than 2 cm posterior to the posterior border of the IVC. The transverse aortic arch can usually be discerned on the normal lateral chest film as a smooth curving shadow originating anteriorly, crossing the mediastinum in a semilunar fashion, and then descending posteriorly as a linear shadow superimposed over the vertebral bodies. The left pulmonary artery (LPA) produces a similar curvilinear shadow just below the aortic arch before it branches. Just below the LPA, the left main/left upper lobe bronchus can be seen (projected end-on) as a round lucency. The right pulmonary artery (RPA) is seen en face down its lumen as an oval soft-tissue structure anterior to the bronchus intermedius and below and anterior to the left pulmonary artery.

Echocardiography

Echocardiography uses high-frequency ultrasound to evaluate the heart and great vessels. The major indications for the technique are listed in Table 3-2. The examination provides a dynamic rendition of cardiac great vessel anatomy and, when combined with the Doppler technique, yields information regarding cardiac and great vessel blood flow (hemodynamics) as well. Because of the high frame rates inherent in ultrasonography, echocardiography can image the heart in a dynamic real-time fashion, so that the motion of cardiac structures can be reliably evaluated. Echocardiography is useful in assessing ventricular function, valvular heart disease, myocardial disease, pericardial disease, intracardiac masses, and aortic abnormalities (Figures 3-5 and 3-6). With Doppler technology, cardiac chamber function, valvular function, and intracardiac shunts frequently seen in congenital heart disease can be assessed. Combined Doppler echocardiography is a commonly performed procedure because it is relatively inexpensive and widely available, provides a wealth of information, is noninvasive, has no risk of ionizing radiation, and can also be performed at the bedside in critically ill patients. Furthermore, the results are immediately available because no special postexamination image processing is required. However, this technique is technically challenging and requires a great deal of operator expertise. Also, a small percentage of patients have poor acoustic windows that can severely degrade image quality. This disadvantage can be obviated by placing the sonographic probe in the esophagus, a procedure called transesophageal echocardiography (TEE). Transesophageal echocardiography yields consistently excellent images of the heart and great vessels, but involves a small amount of discomfort and risk to the patient. More recently, echocardiography has been combined with stress-testing modalities to assess inducible myocardial ischemia using wall motion analysis of left ventricular function.

Table 3-2. Indications for Echocardiography

Ventricular function
Congenital heart disease
Valvular heart disease
Cardiomyopathy
Pericardial effusion
Suspected cardiac masses
Aortic disease (proximally)

Radionuclide Imaging (Nuclear Medicine)

Cardiac radionuclide imaging, primarily used for the patient with suspected myocardial ischemia or infarction, requires an intravenous injection of radioactively labeled compounds that have an affinity for the myocardium. These compounds localize within the myocardium in diseased or damaged areas, and a radioactivity detector such as a gamma camera can image their distribution. These tests are most commonly

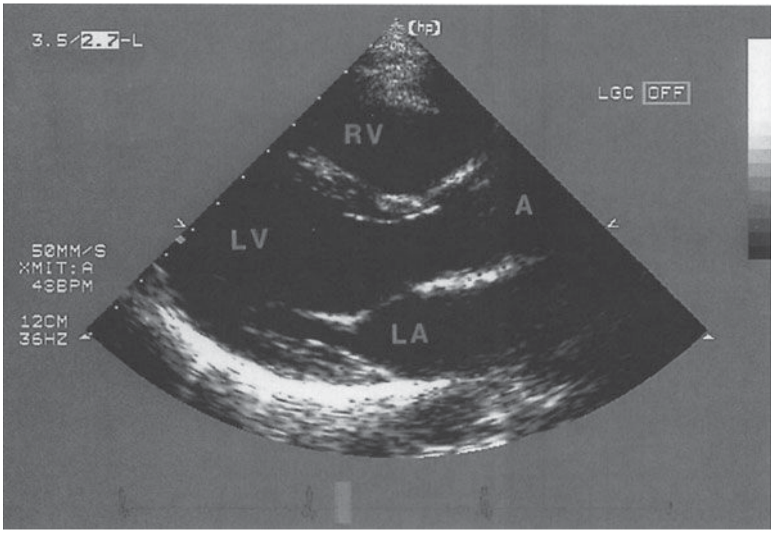

A

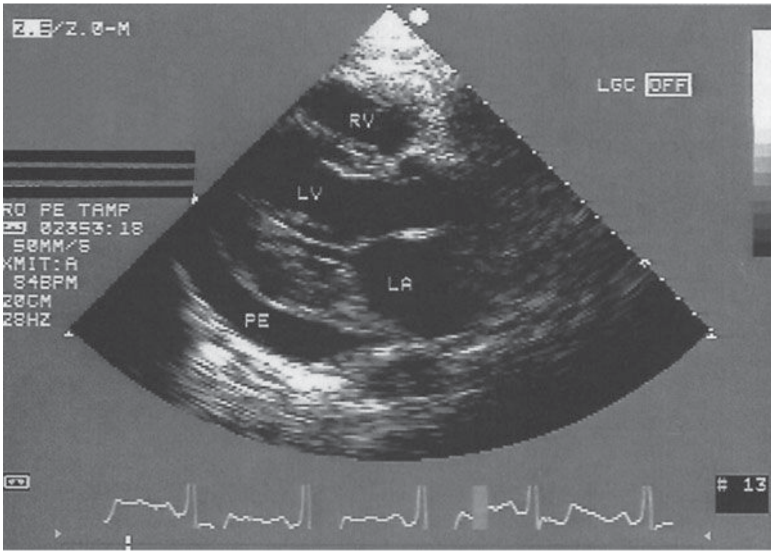

B

▲ **Figure 3-5.** (**A**) Normal transthoracic echocardiogram from a healthy subject. Views are taken from the left midparasternal region through an intercostal space. The structure closest to the apex of the screen is the chest wall. The mitral valve, separating the left atrium and left ventricle, is partially open in this image from early systole. A, aorta; LA, left atrium; LV, left ventricle; RV, right ventricle. (**B**) Transthoracic echocardiogram, left parasternal view, from a patient with a moderate-sized posterior pericardial effusion (PE), visualized as a sonolucent space between the epicardium and pericardium. RV, right ventricle; LV, left ventricle; LA, left atrium.

used in the evaluation of patients with angina and atypical chest pain (Figure 3-7). Gallium scans are occasionally used to assess for intrinsic myocardial disease such as myocardial sarcoidosis. Positron emission tomography (PET) with ^{18}F-FDG (^{18}F-fluorodeoxyglucose) is a problem-solving tool that has shown promise in assessing myocardial viability in patients with known coronary artery disease and to assess for metabolically active infiltrative disease (Figure 3-8). In addition, rubidium-82 and nitrogen-13 ammonia have been used as PET agents to evaluate myocardial perfusion.

Computed Tomography

Cardiac computed tomographic angiography has undergone a revolution over the past decade. Owing to improved detectors, increased detector rows, and decreased scan times, breath-hold imaging of the heart can now be performed in many cases without pharmaceutical intervention (Figure 3-9). The major indications for cardiac CT are to evaluate the coronary arteries in subjects with indeterminate nuclear stress tests, to characterize or confirm coronary or cardiac

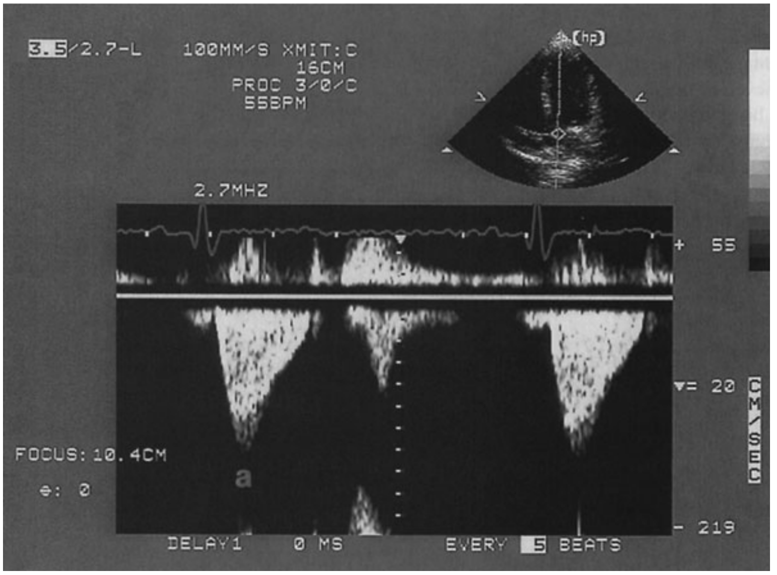

▲ Figure 3-6. Transthoracic spectral Doppler tracing taken from an intercostal space over the cardiac apex. The Doppler sample is placed in line with the left ventricular outflow and aorta (shown in miniature echocardiogram image at top right). Velocity of flow is denoted along left edge of tracing in cm/s. The Doppler tracing shows that aortic peak velocity (a) is normal (140 cm/s). This technique can reliably assess the presence of and quantitate the severity of aortic stenosis.

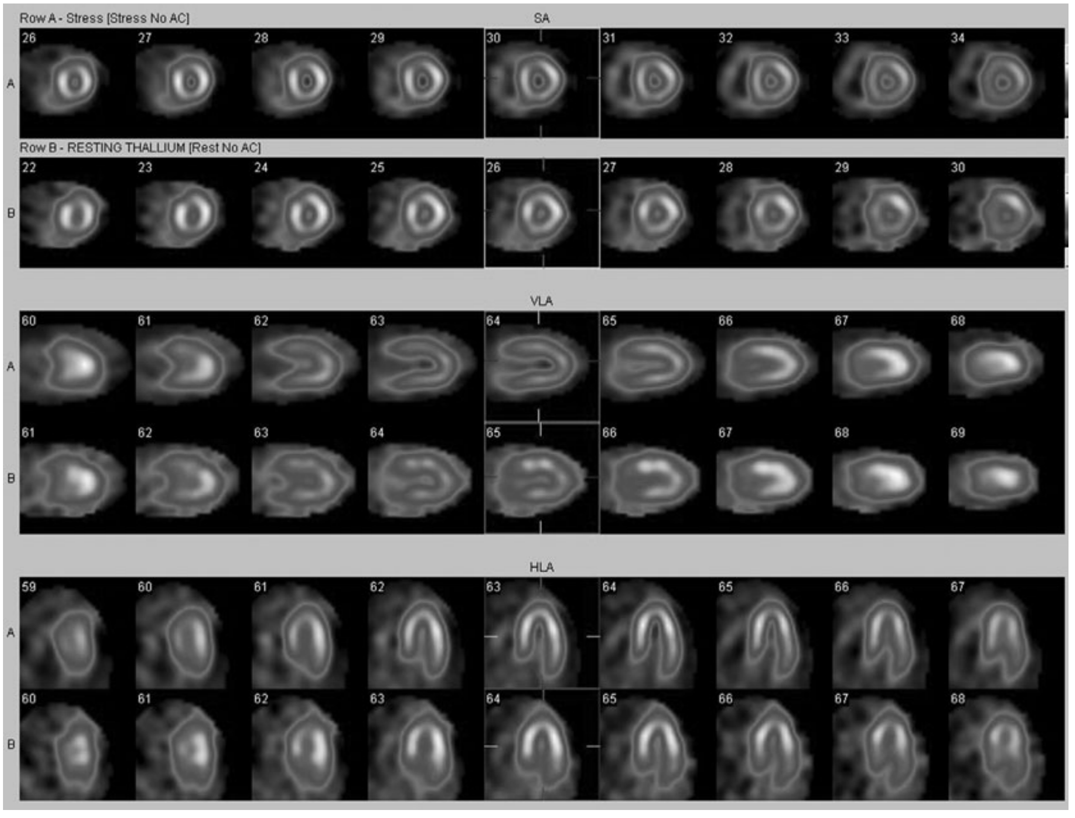

▲ Figure 3-7. Normal myocardial stress/rest study. Stress imaging performed with technetium-99m tetrofosmin following treadmill exercise achieving target heart rate. Resting images performed using thallium-201. Homogeneous perfusion of the left ventricular cavity is seen with both stress images (top of image pairs) and rest images.

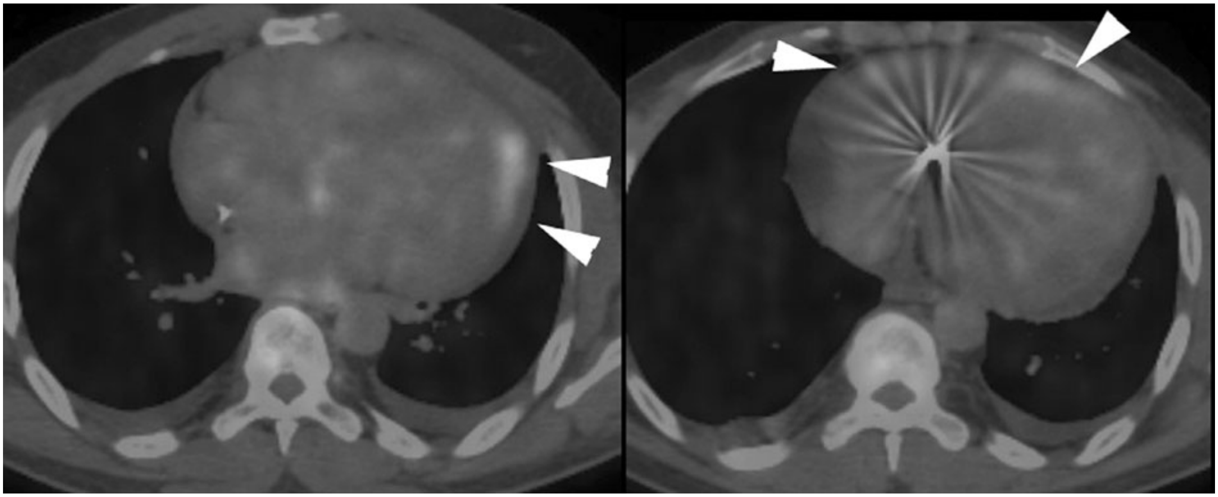

▲ **Figure 3-8.** ^{18}F-FDG-PET cardiac study performed after 24-hour fast shows patchy myocardial activity due to cardiac sarcoidosis (arrowheads). Normal myocardium is suppressed because of glucose deprivation and change in metabolism to free fatty acids.

anomalies, to assess location and patency of bypass grafts, and, in some cases, to assess for the presence of atherosclerotic disease in subjects presenting to the emergency department with atypical chest pain. The last is often performed with an extended coverage of the chest to concomitantly evaluate for pulmonary embolism and aortic dissection (triple rule-out). At the present time, some physicians also use the measurement of calcium in the coronary arteries detected at unenhanced ECG-gated CT to stratify the risk of future cardiovascular events (Figure 3-10). Contrast administration is mandatory when there are questions related to intrinsic cardiac anatomy or abnormalities of the thoracic aorta such as dissection or for evaluation of the pulmonary arteries for pulmonary embolism. For many of these applications, rapid administration of contrast is necessary (up to 4–5 mL per second), and a well-functioning large-bore (at least 18- to 20-gauge) IV catheter must be present to ensure a high-quality study.

The major drawback to CT for cardiac imaging at present is the use of ionizing radiation, which without careful management can be 4 to 5 times higher than for a standard chest CT. Fortunately, many techniques have been developed that lower radiation exposure. These include, but are not limited to, limiting scan distance, pulsing the x-rays to limit exposure during systole, prospectively gating rather than retrospectively reconstructing oversampled data, and modulating the x-ray beam based on patient size.

Magnetic Resonance Imaging

MR imaging has also gained rapid acceptance for cardiac evaluation, as it does not use ionizing radiation, can provide morphologic and physiologic data, and can be performed to give cine-loop images. MR cardiac imaging remains a challenge because of the inherent difficulty of simultaneously dealing with respiratory and cardiac motion, the competing needs for spatial and temporal data, and the hands-on approach to tailor the examination to the specific clinical question. Thus, MR imaging is largely a problem-solving tool, rather than a screening study. The major indications for MR imaging are congenital heart disease and suspected intracardiac masses, valvular dysfunction, pericardial disease, and aortic abnormality. From a functional standpoint, MR has the ability to asses cardiac function and motion, distinguish infarct from ischemia and help determine the advisability of revascularization (Figure 3-11), and measure flow across valves or coarctations. On the research side, MR imaging has also shown some promise in measuring the degree of damage from coronary artery atherosclerosis and evaluating the composition of atherosclerotic plaque.

Angiography

Conventional angiography is one of the most commonly performed imaging tests for evaluating the heart and great vessels. After the introduction of a catheter into a peripheral vessel (usually, the femoral or axillary vein or artery), the angiographer, under fluoroscopic visualization, positions the catheter in the region of interest, injects contrast material to confirm the location of the catheter, and then injects larger amounts of contrast material for diagnostic purposes. This injection of contrast material can be videotaped, recorded as standard or digital radiographs, or digitally stored for later review. There are four major types of angiography:

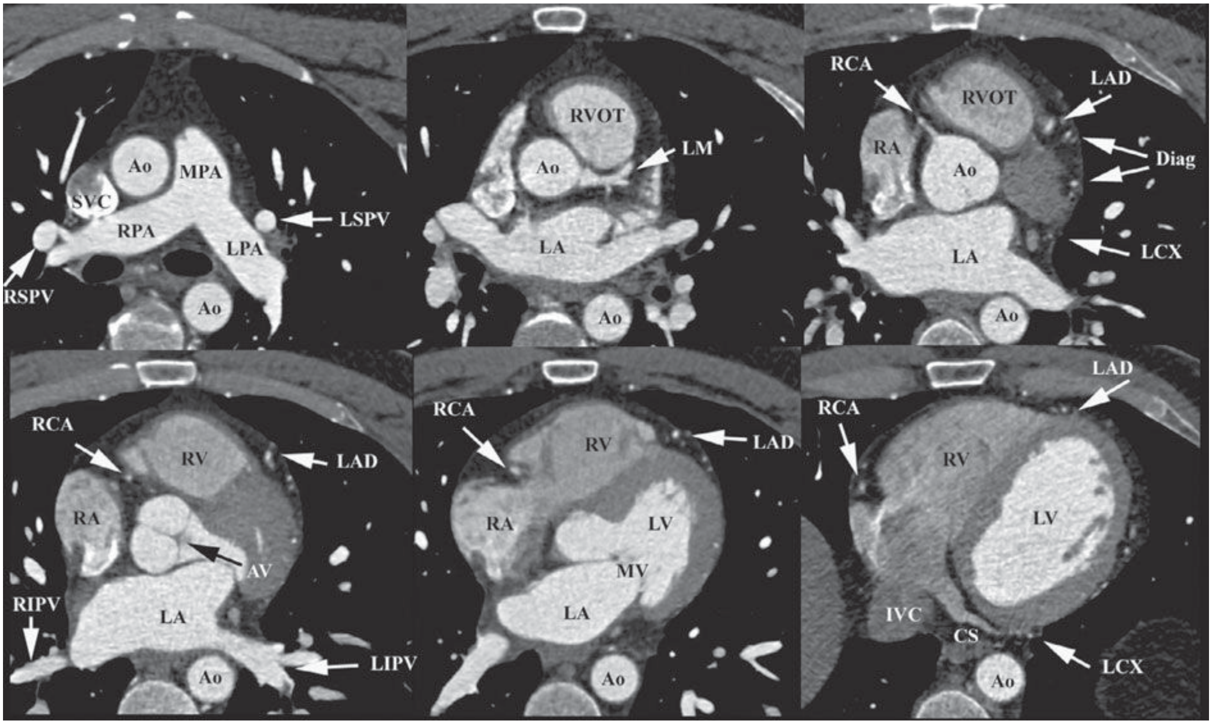

A

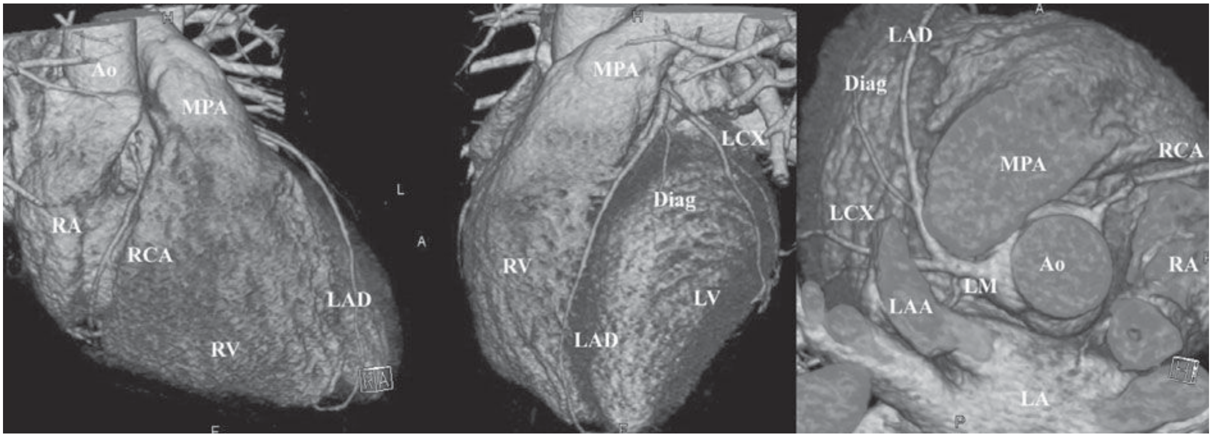

B

▲ **Figure 3-9.** Normal anatomy at cardiac CT angiography. (**A**) Axial composite image and (**B**) 3D volume rendered images in right anterior oblique, left anterior oblique, and cephalad projections (from left to right). Ao, aorta; AV, aortic valve; CS, coronary sinus; Diag, diagonal branch; IVC, inferior vena cava; LA, left atrium; LAA, left atrial appendage; LAD, left anterior descending artery; LCX, left circumflex artery; LM, left main coronary artery; LIPV, left inferior pulmonary vein; LPA, left pulmonary artery; LSPV, left superior pulmonary vein; LV, left ventricle; MV, mitral valve; MPA, main pulmonary artery; RA, right atrium; RCA, right coronary artery; RIPV, right inferior pulmonary vein; RPA, right pulmonary artery; RSPV, right superior pulmonary vein; RV, right ventricle; RVOT, right ventricular outflow tract; SVC, superior vena cava.

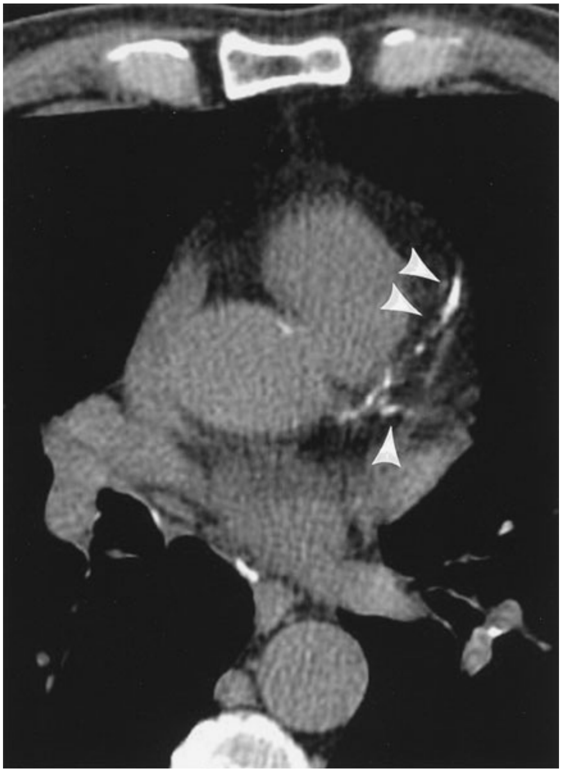

▲ **Figure 3-10.** Axial CT image shows atherosclerotic disease in the left anterior descending and left circumflex arteries (arrowheads) as evidenced by the presence of calcium.

angiocardiography (heart), coronary arteriography (coronary arteries) (Figure 3-12), aortography (aorta) (Figure 3-13), and pulmonary angiography (pulmonary arteries and lungs). Techniques developed by radiologists, angiocardiography and coronary arteriography, are now almost exclusively performed by cardiologists.

TECHNIQUE SELECTION

There is a wide array of imaging tests that can be used to evaluate the cardiovascular system (see Table 3-1). After a thorough history and physical examination, the initial screening study should always be a chest radiograph. Ideally, the PA and lateral views should be obtained with maximum inspiration. This study gives important information about the cardiac contour and the status of the lungs, and it is a good examination for excluding disorders that would require immediate treatment, such as pneumothorax. Furthermore, evaluation of the chest radiograph can often lead to a specific diagnosis and treatment, such as in congestive heart failure, or can help determine the need for another imaging study.

Depending on the history and physical examination findings, echocardiography, nuclear cardiac imaging, CT, MR, or conventional coronary angiography may follow. Echocardiography is a good screening test to assess cardiac and great-vessel valvular motion and structural abnormalities, cardiac chamber morphology, and flow. Angiography delineates the structural status of the coronary arteries and can give information on blood flow through the cardiac chambers, valves, and proximal great vessels, mainly in patients with suspected atherosclerosis. It is also used to guide interventions such as stent placement in the coronary arteries. Because of its inherent risks, coronary arteriography is usually reserved for patients with signs and symptoms of myocardial ischemia or infarction on the basis either of history or of results of electrocardiography, echocardiography, or radionuclide myocardial imaging.

In patients with suspected pulmonary emboli, helical CT is the most appropriate test in the setting of an abnormal chest x-ray (Figure 3-14). The ventilation-perfusion (V/Q) scan can be performed if the chest radiograph is normal and is also the preferred examination in young females because of the radiation dose to the breast by CT. Both of these tests can confirm the clinically suspected diagnosis of pulmonary embolic disease and often provide a useful "map" of the most suspicious regions of the lung for the angiographer if an angiogram is required for the definitive diagnosis of pulmonary embolism. CT can also detect important alternative diagnoses not detected by either V/Q scan or pulmonary angiography. More frequently, patients with atypical chest pain are being referred for the triple rule-out examination. This test is not appropriate for patients with clear signs or symptoms of myocardial ischemia and should be reserved for intermediate- to low-risk patients with a nondiagnostic ECG and negative first set of troponins.

Echocardiography, MR imaging, or CT or cardiac angiography may be selected for patients with suspected congenital heart disease. The advantages of MR imaging in this setting is that it is noninvasive, generally needs no contrast material administration, and uses no ionizing radiation, an important consideration in the pediatric patient. For these reasons, MR imaging has become the preferred imaging test in the pediatric population. As dose reduction techniques have improved, the use of CT for congenital heart disease has also increased.

Suspected aortic dissection (either atherosclerotic or traumatic in origin) can be evaluated by helical CT, TEE, aortography, or MR imaging. Helical CT is the imaging modality of choice for acute dissection because of its accuracy and availability (Figure 3-15). With multislice technology, CT angiography can provide images in multiple planes to show the relation of the dissection to key branch vessels. TEE has the advantages of being quick and noninvasive, and the examination can be performed expediently at the bedside. MR imaging is noninvasive, uses no ionizing radiation, is less operator-dependent, and can be performed in multiple planes. It is limited by availability and imaging time and because it cannot be used in patients with certain implanted

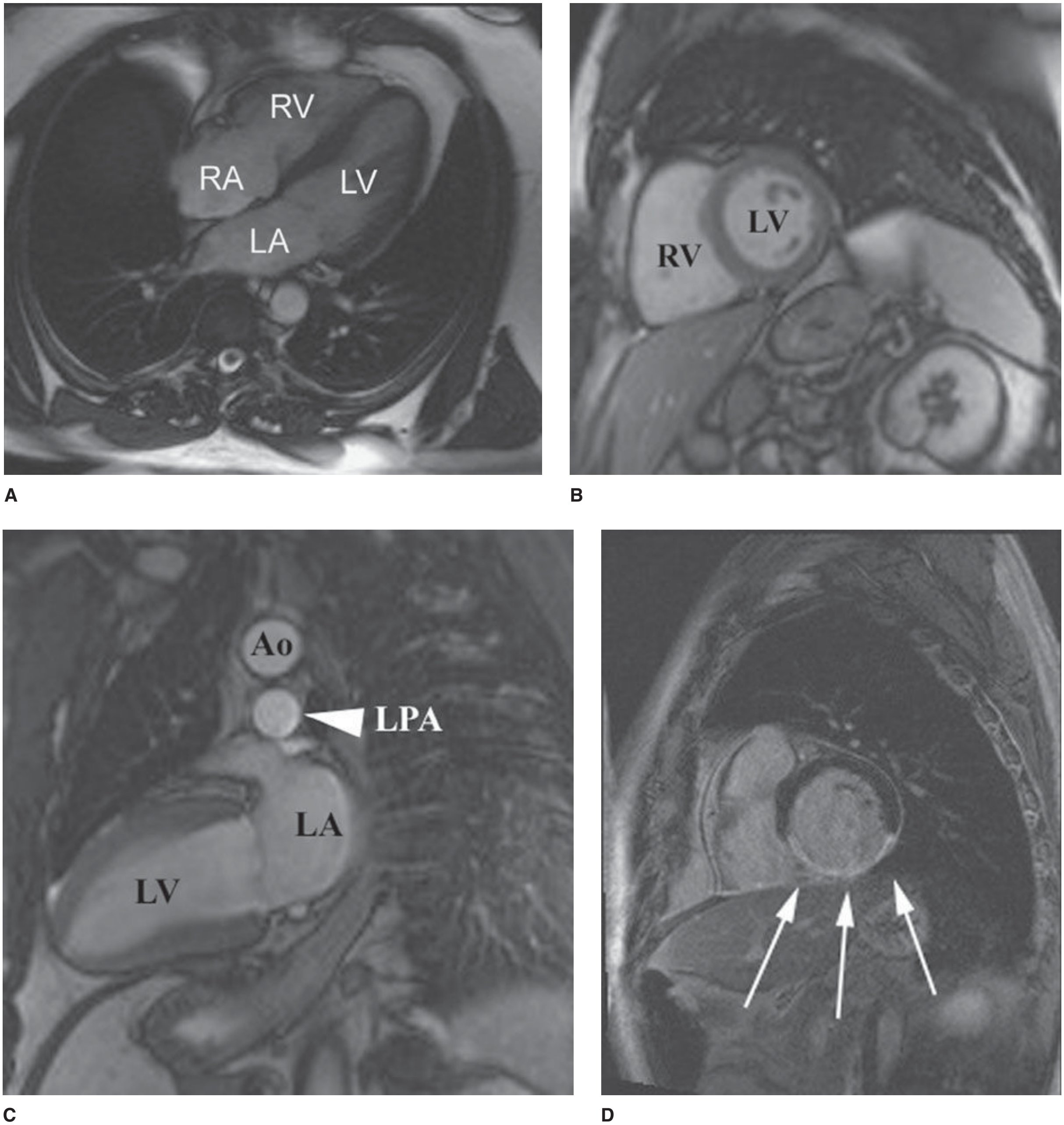

▲ **Figure 3-11.** Axial (**A**), short-axis (**B**), and long-axis (**C**) gradient echo "white blood" MR images with normal anatomy. (**D**) Delayed gadolinium enhancement study in a different case reveals extensive delayed enhancement of inferior wall (arrows) indicating infarct that is not amenable to revascularization. Ao, aorta; LA, left atrium; LPA, left pulmonary artery; LV, left ventricle; RA, right atrium; RV, right ventricle.

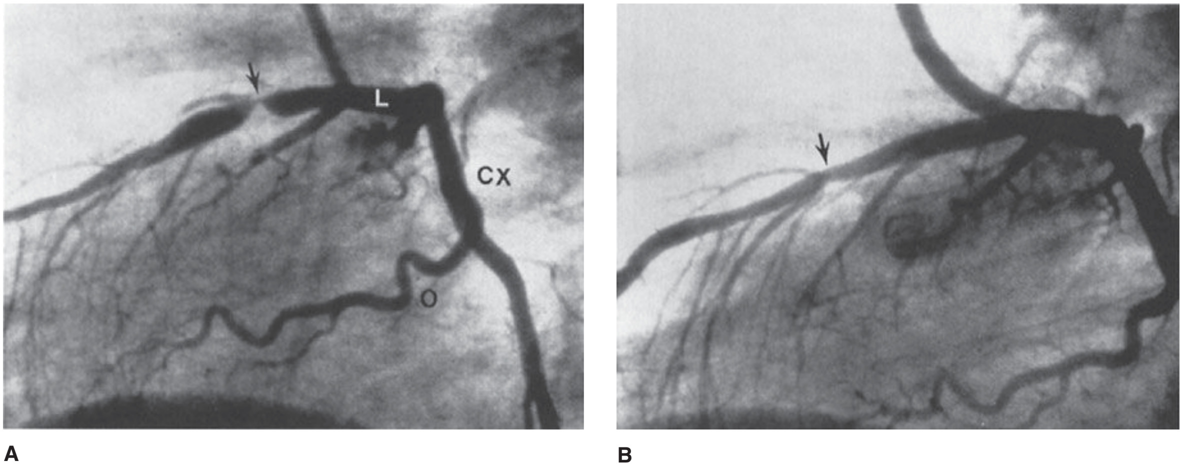

▲ **Figure 3-12.** (**A**) Coronary arteriogram. Images were obtained from the left lateral projection with contrast injection into the left main coronary artery. The left anterior descending (L), left circumflex (CX), and first obtuse marginal (O) branches are visualized. Severe stenosis is seen in the midportion of the left anterior descending artery (arrow) in this patient, who had unstable angina pectoris. (**B**) Coronary arteriogram, same projection and patient as in (A), obtained 1 day later. The stenosis in the left anterior descending coronary artery (arrow) has been reduced after percutaneous balloon angioplasty.

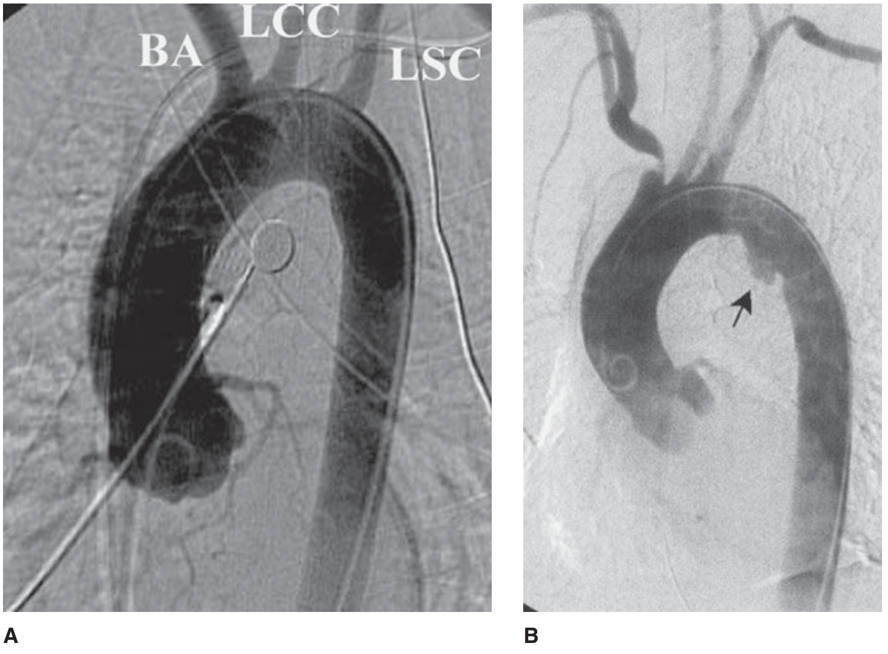

▲ **Figure 3-13.** (**A**) Normal aortogram of transverse arch in patient suspected of having traumatic aortic injury. Note the normal origins of the brachiocephalic artery (BA), left common carotid artery (LCC), and left subclavian artery (LSC) from the arch of the aorta. (**B**) Aortogram in a patient with acute traumatic aortic injury. The site of injury is the focal outpouching at the insertion of ductus arteriosus (arrow).

▲ **Figure 3-14.** Axial CT image shows filling defect (arrowheads) in right lower lobe artery and absence of flow in left lower lobe arteries (arrow) from pulmonary embolism.

devices, particularly pacemakers. Angiography has mostly been relegated to minimally invasive treatments such as stent-graft placement. Because survival rates often depend on early surgical intervention, availability and timeliness of the examinations is important.

In patients whose chest radiographs suggest intrinsic pulmonary or mediastinal processes, a standard chest CT is currently the preferred modality. The use of contrast depends on the indication, the preference of the radiologist, and any possible contraindications to administration of intravenous contrast for individual patients.

Finally, regardless of the situation, it is reasonable for the clinician and radiologist to decide together which imaging tests are most appropriate. In many instances, the choice of the next most efficacious and least costly imaging examination is not always clear-cut. In fact, in some circumstances, it is not necessary to perform another test because of the limited potential yield from the examination or because there is no adequate therapy for the suspected abnormality. It is hoped that future recommendations for test selection will be determined by well-designed prospective unbiased outcome studies comparing all of these modalities in various clinical scenarios. In the meantime, a commonsense approach, taking into consideration the history and physical examination findings, the information gleaned from the conventional radiograph, and the potential yield from the array of other available imaging tests, is the most appropriate. In all instances, communication between the clinician and radiologist is critical for the best patient care.

▶ Monitoring Devices

In clinical hospital practice, particularly in the ICU setting, a variety of catheters and tubes are used to monitor various

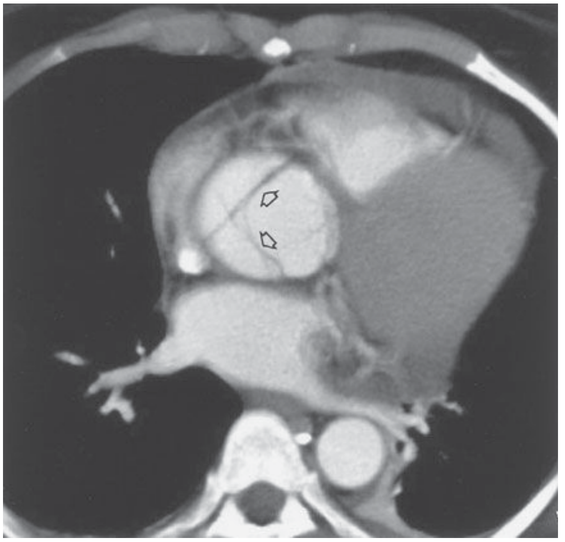

A

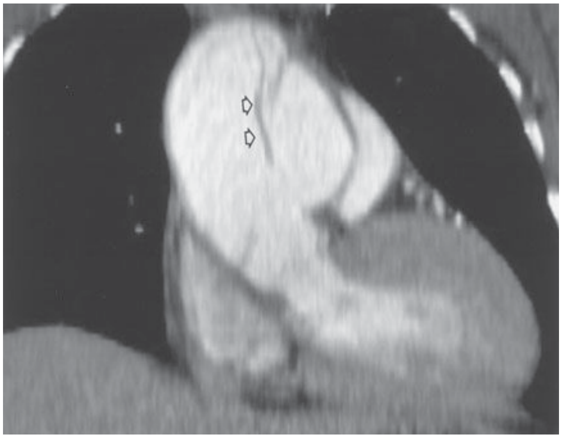

B

▲ **Figure 3-15.** Axial (**A**) and coronal (**B**) CT images show intimal flap of type A dissection (arrows).

parameters in patients (Figure 3-16). The student should be familiar with the normal routes and positions of these devices, as well as inappropriate positions and complications. Table 3-3 lists the most common monitoring devices.

Table 3-3. Common Monitoring Devices

Central venous catheters
Flow-directed pulmonary arterial catheters (Swan-Ganz catheters)
Intraaortic counterpulsation balloon
Cardiac pacemakers

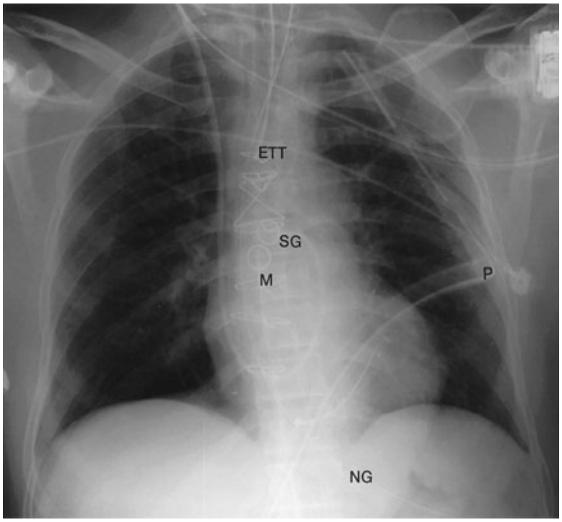

▲ **Figure 3-16.** Frontal radiograph immediately after coronary artery bypass surgery shows typical lines and tubes encountered in the ICU. Endotracheal tube (ETT), nasogastric tube (NG), Swan-Ganz catheter (SG), mediastinal drain (M), and left pleural drain (P) are present.

The basic venous anatomy of the upper mediastinum should be reviewed and kept in mind when evaluating catheter placement. The most common routes of catheter insertion in the chest include the internal jugular and subclavian veins. Radiographs obtained after insertion show the catheter following the course of either the internal jugular or subclavian vein and passing through the brachiocephalic vein. It then curves gently downward to terminate in the superior vena cava proximal to the right atrium (Figure 3-17). One normal variation of venous anatomy is the persistent left superior vena cava. In this situation the catheter descends down the left mediastinum terminating in the left SVC. The left SVC ultimately drains into the coronary sinus, which then enters the right atrium.

Intrathoracic central venous catheters are used mainly for monitoring central venous pressure (CVP), maintaining proper nutrition, delivering medication, and hemodialysis. It is standard practice to request a chest radiograph after catheter placement to verify its location (Figure 3-18) and to check for potential complications, such as pneumothorax (Figure 3-19) or hemothorax. Measurement of CVP is optimally obtained when the tip of the catheter is proximal to the right atrium and distal to the most proximal valves of the large veins. A catheter tip proximal to the veins gives an inaccurate

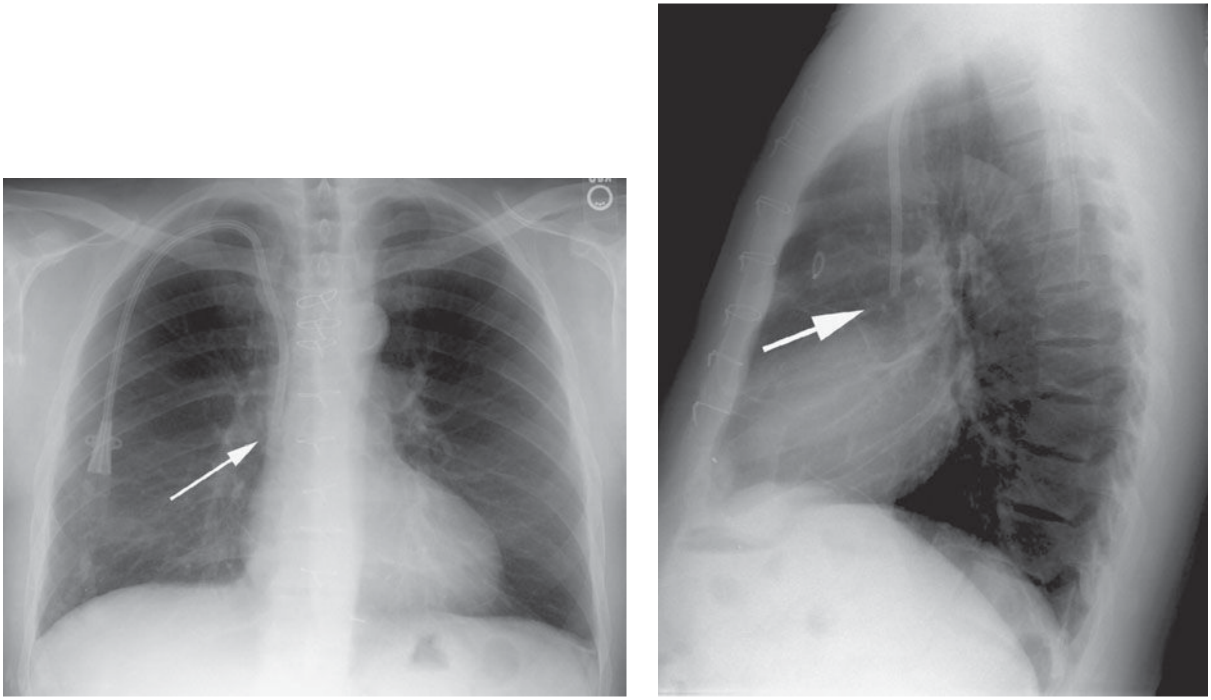

A

B

▲ **Figure 3-17.** PA (**A**) and lateral (**B**) view of a patient whose tunneled central venous catheter placement is normal with its tip in the superior vena cava above the right atrium (arrows).

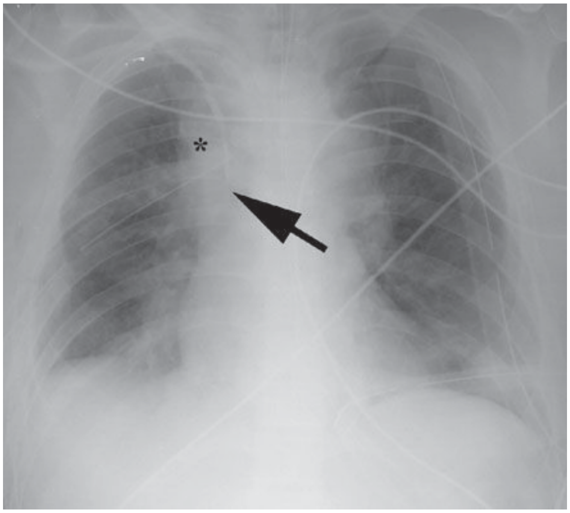

A

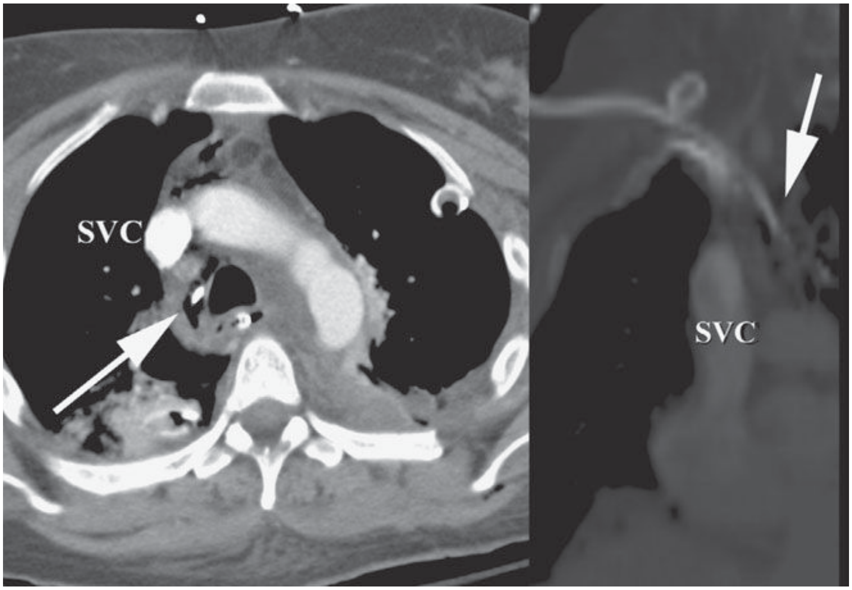

B

▲ **Figure 3-18.** Malposition of central venous catheter. (**A**) Portable frontal radiograph reveals central venous catheter overlying the expected region of superior vena cava (arrow). Because of lack of blood return, CT with contrast was obtained. Note also the widening of the right paratracheal stripe (*). (**B**) Axial and curved planar reformation reveal catheter has perforated the posterior wall of the superior vena cava with the tip residing in the mediastinum (arrows). SVC, superior vena cava.

reading of CVP, and a tip too close to the right atrium may cause arrhythmias from irritation of the right atrial myocardium. The reason for catheter insertion is critical for identifying its appropriate position. If it has been placed just for fluids and/or medications, a termination in the brachiocephalic vein is satisfactory. Conversely, a plasmapheresis catheter should never be located in the right atrium because of the risk of complications. More frequently, central venous catheters are being placed centrally via a peripheral vein. These catheters have minimal risk, can remain in place for longer periods of time without being exchanged, and are primarily used for the delivery of fluids and long-term antibiotics.

The major potential complications from catheter placement are outlined in Table 3-4. A malpositioned central venous catheter may result in inaccurate CVP measurement, thrombosis, catheter knotting, and infusion of substances into the mediastinum or pleura. Catheter tips against the wall of the SVC may erode into the mediastinum or may extend

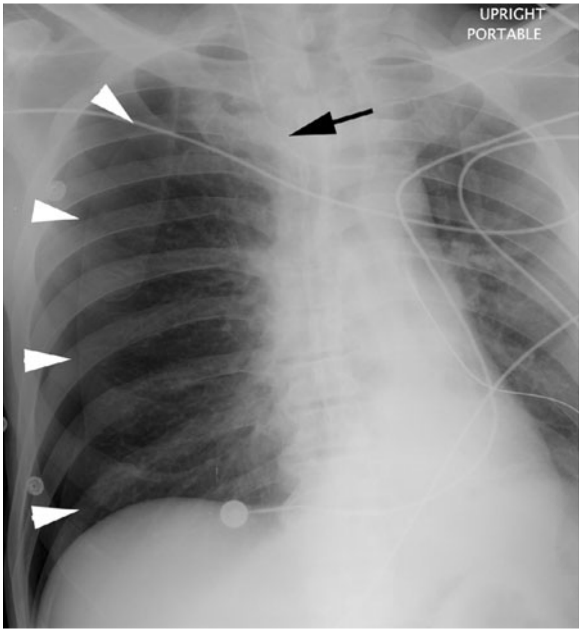

▲ **Figure 3-19.** Upright AP chest radiograph obtained after placement of right internal jugular (arrow) catheter shows a large right pneumothorax (arrowheads).

retrograde into tributary veins, particularly the azygous vein (Figure 3-20).

Flow-directed arterial catheters are also regularly used in cardiac and ICU patients to monitor cardiac output. The most common flow-directed catheter is the Swan-Ganz (SG) catheter (see Figure 3-16). It is usually inserted percutaneously

Table 3-4. Potential Complications of Intrathoracic Catheters

Malposition
Catheter knotting/fragmentation
Pneumothorax
Vascular injury
Thrombosis (venous)
Infarction (pulmonary arterial)
Infection/septic emboli/endocarditis
Air embolism
Cardiac arrhythmias
Fistulas Arteriovenous Venobronchial Arteriobronchial

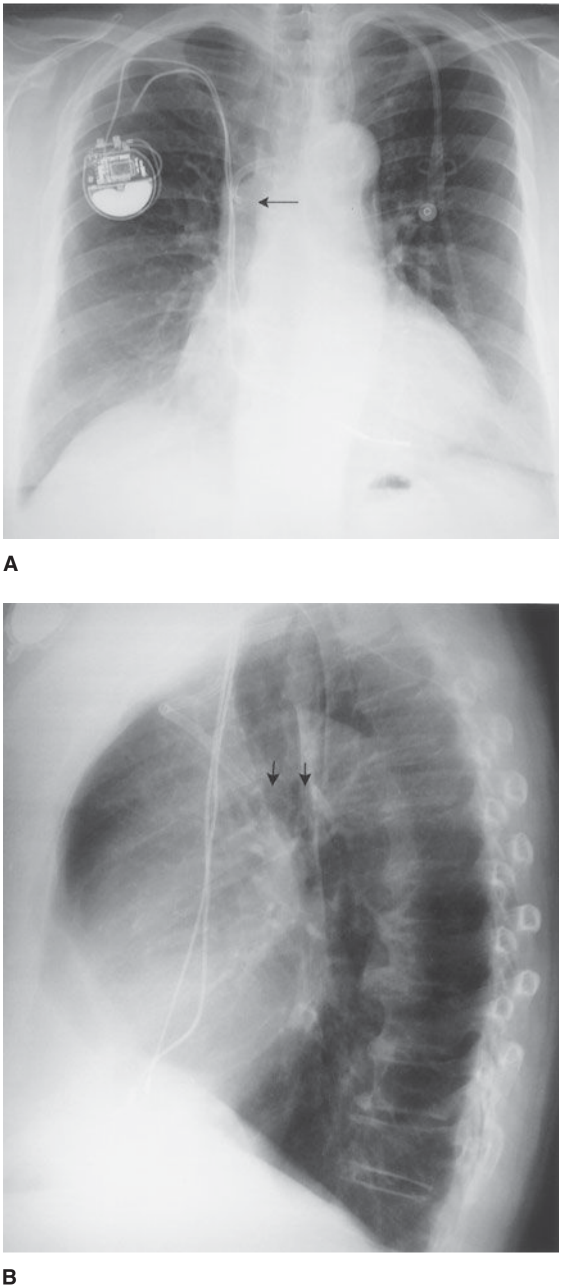

▲ **Figure 3-20.** PA (**A**) and lateral (**B**) views show central venous catheter with tip in azygous vein (arrows).

into the left or right subclavian vein and threaded through the brachiocephalic vein, superior vena cava, right atrium, tricuspid valve, right ventricle, pulmonic valve, and directed out into the main pulmonary artery. Usually terminating in the right or left pulmonary arteries, the SG tip should be distal to the pulmonary valve and proximal to the smaller pulmonary arterial vessels so it will not cause occlusion and, potentially, thrombosis. A simple rule of thumb is that the catheter should not extend past the mediastinal borders. It may then be intermittently "wedged" into a distal pulmonary artery branch to obtain a pulmonary capillary wedge pressure.

Complications of SG catheter placement are similar to those with other central venous catheters. The tip may be positioned in a number of inappropriate vessels or locations, and a chest radiograph should be obtained after catheter insertion to confirm its position (Figure 3-21). Introduction of any catheter into the subclavian vein, because of its close proximity to the lung apex, can cause pneumothorax (see Figure 3-19). A catheter tip position in the right ventricle can lead to ventricular arrhythmias, and leaving the catheter tip too distal may result in a pulmonary artery pseudoaneurysm or pulmonary infarct.

An intraaortic counterpulsation balloon pump (IABP) is occasionally used in patients with cardiogenic shock. This catheter measures approximately 26 cm in length and is surrounded by a balloon, which inflates with helium or carbon dioxide gas during diastole and deflates during systole. Deflation during systole decreases afterload and results in diminished left ventricular work and oxygen requirements, while the inflation of the balloon during diastole increases cardiac pressure to help ensure adequate perfusion of the coronary arteries. The catheter, introduced percutaneously into the thoracic aorta via the common femoral artery or placed into the ascending aorta at the time of surgery, should be positioned so that its tip is just distal to the origin of the left subclavian artery. The tip of the catheter has a small radiopaque marker so that this position can be ascertained on the chest radiograph (Figure 3-22). The major complications of the IAPB result from positioning of its tip proximal to the left subclavian artery, which may cause occlusion of the left subclavian vessel orifice, cerebral artery embolization, or aortic tear. If positioned too low, the balloon may occlude the celiac, superior mesenteric, and renal arteries.

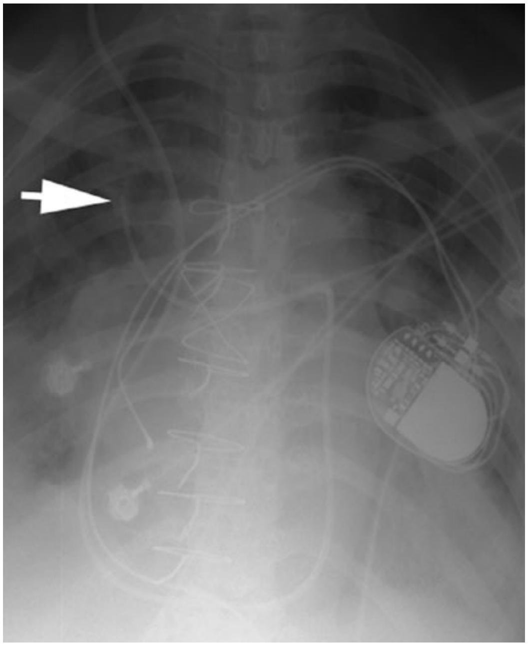

▲ **Figure 3-21.** Supine AP chest radiograph of a patient in the ICU in congestive failure shows a Swan-Ganz catheter tip positioned too far distally within the right upper lobe pulmonary artery (arrow).

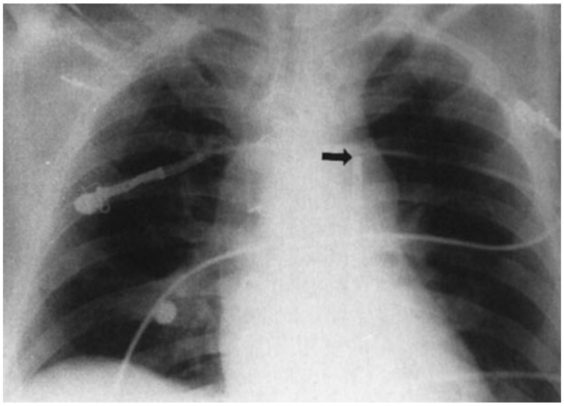

▲ **Figure 3-22.** Supine AP radiograph of patient 6 hours following coronary artery bypass surgery shows an IABP in normal position distal to the origin of the left subclavian artery (arrow).

Unipolar or bipolar pacemakers are most common and are usually implanted in the chest wall with leads inserted into the subclavian vein. The unipolar pacemaker tip is normally situated at the apex of the right ventricle. The bipolar pacemaker has a proximal lead that terminates in the right atrium and a distal lead that terminates within the right ventricle (similar to the unipolar pacemaker position). Biventricular pacemakers have a third lead present in the coronary sinus, appearing superior to the right ventricular lead (Figure 3-23). Its posterior position can be confirmed on the lateral view. Pacemakers that also have the ability to act as defibrillators have larger leads with a coil spring appearance. Leads are usually placed from a transvenous approach, although in certain circumstances they can be placed directly on the epicardium through the chest wall. The purpose of the chest radiograph after the pacemaker insertion is to document the appropriate placement of these leads, to check for complications from placement,

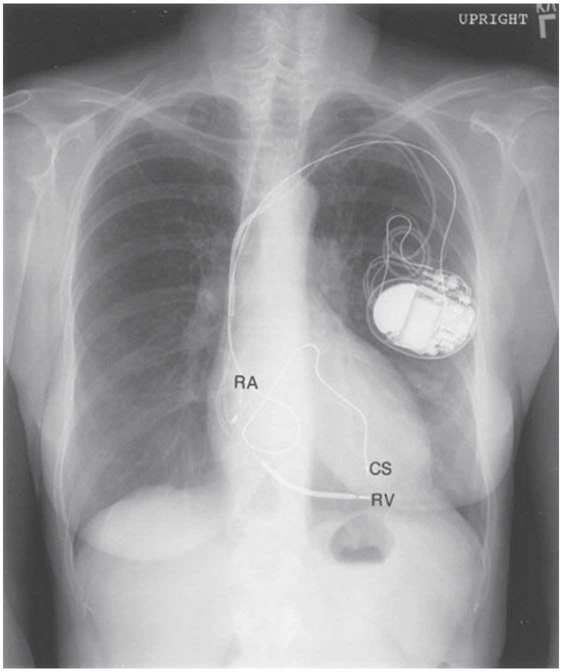

A

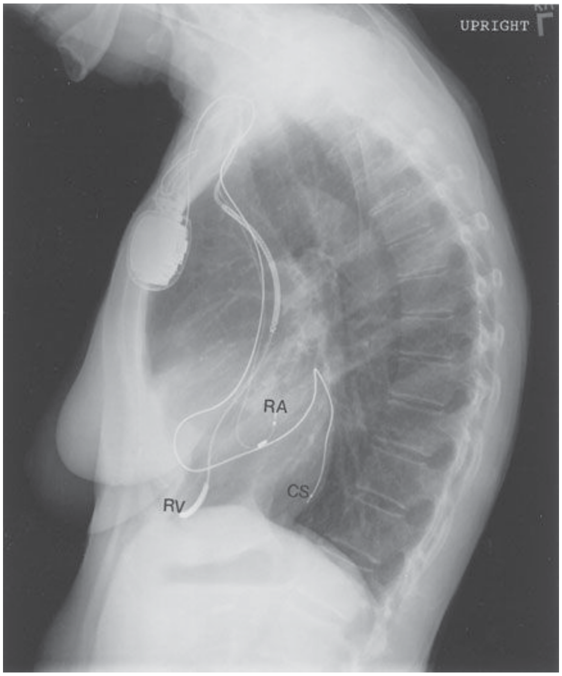

B

▲ **Figure 3-23.** PA (**A**) and lateral (**B**) views show the most common locations of pacing leads: RA, right atrium; RV, right ventricle; and CS, coronary sinus.

and to establish a baseline examination to compare with future chest radiographs.

EXERCISE 3-1. INCREASED HEART SIZE

3-1. The most likely diagnosis in Case 3-1 (Figure 3-24) is
A. congestive heart failure.
B. pericardial effusion.
C. intracardiac shunt.
D. expiratory phase of respiration.
E. pulmonic stenosis.

3-2. The most likely diagnoses in Case 3-2 (Figure 3-25) is
A. mediastinal mass.
B. intracardiac shunts (atrial septal defect [ASD] and ventricular septal defect [VSD]).
C. pericardial effusion or cardiomyopathy.
D. combined aortic and pulmonary arterial disease.
E. technical aberrations.

3-3. The most likely diagnosis in Case 3-3 (Figure 3-26) is
A. mediastinal mass.
B. intracardiac shunts (ASD and VSD)
C. pericardial effusion or cardiomyopathy
D. combined aortic and pulmonary arterial disease.
E. technical aberrations.

3-4. The most likely diagnosis in Case 3-4 (Figure 3-27) is
A. Ebstein's anomaly.
B. mediastinal mass.
C. intracardiac shunt.
D. pericardial effusion.
E. mitral and aortic stenosis.

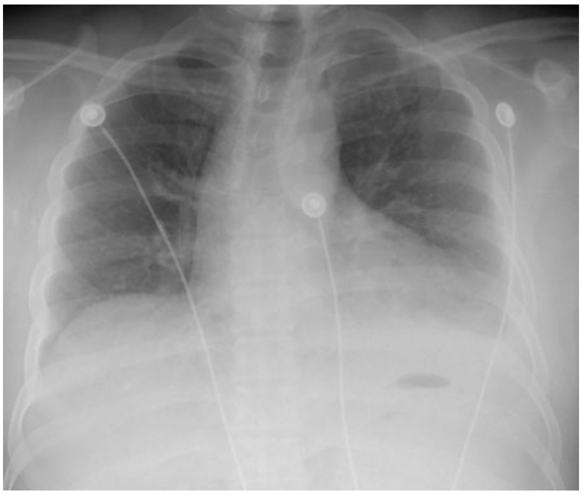

▲ **Figure 3-24.** Case 3-1: 20-year-old uncooperative man with minimal chest pain.

A

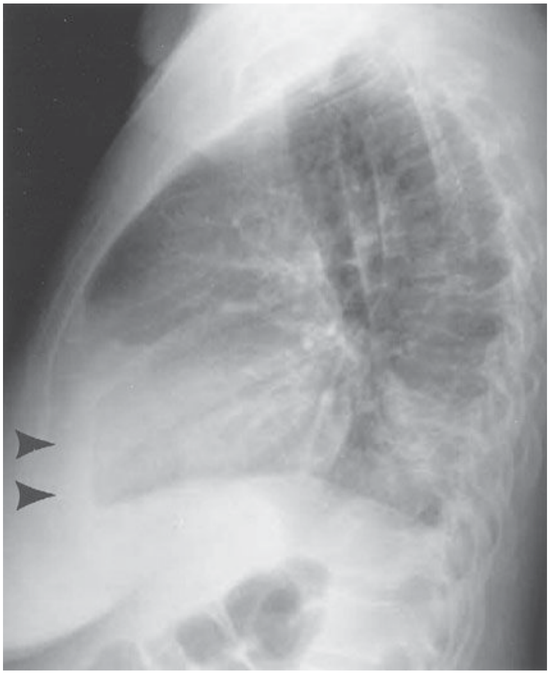

B

▲ **Figure 3-25.** (**A,B**) Case 3-2: 70-year-old man with uremia.

3-5. The most likely diagnosis in Case 3-5 (Figure 3-28) is
- **A.** congenital heart disease.
- **B.** congestive heart failure.
- **C.** pericardial effusion.
- **D.** acute pneumonia.
- **E.** aortic dissection.

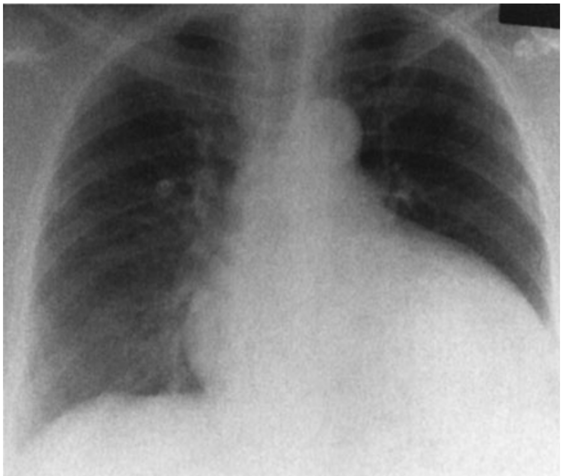

▲ **Figure 3-26.** Case 3-3: 60-year-old alcoholic man with shortness of breath.

Radiologic Findings

3-1. This case (Figure 3-24) represents an apparent "enlarged heart" due to an expiratory phase of respiration in an uncooperative patient (D is the correct answer to Question 3-1). Note the decreased lung volumes and the elevation of the hemidiaphragms. The resultant crowding of vessels obscures much of the cardiac border. The technique of inspiratory PA radiograph is preferred to avoid "diagnosing" diseases that a patient does not have.

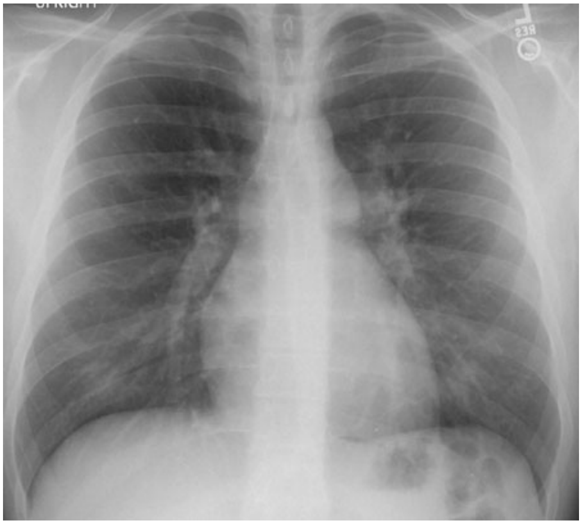

▲ **Figure 3-27.** Case 3-4: 28-year-old woman with a loud systolic murmur and without cyanosis.

A

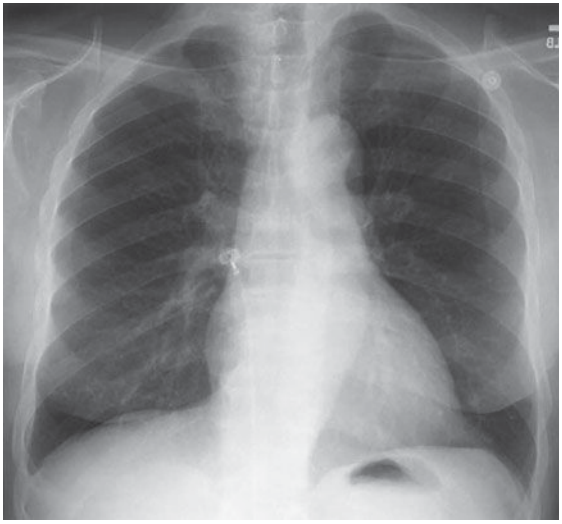

B

▲ **Figure 3-28.** (**A,B**) Case 3-5: (**A**) 55-year-old woman with an acute shortness of breath. (**B**) Chest radiograph of the same patient obtained 1 month earlier.

3-2. This case (Figure 3-25) is an example of pericardial effusion (arrowheads) (C is the correct answer to Question 3-2). The conventional radiograph findings on the frontal view are the so-called globular or water-bottle configuration of the heart.

3-3. This case (Figure 3-26) shows similar radiographic findings as in Case 3-2. This is the case of cardiomyopathy (C is the correct answer to Question 3-3).

3-4. This patient (Figure 3-27) has cardiomegaly, increased pulmonary vascularity, and prominent pulmonary arteries, findings suggestive of an intracardiac shunt, which in this case was an atrial septal defect (ASD) (C is the correct answer to Question 3-4). The lateral radiograph (Figure 3-29) shows the enlarged central pulmonary arteries and right ventricular prominence due to increased flow.

3-5. This case (Figure 3-28A) illustrates cardiomegaly, increased pulmonary vascularity, redistribution of blood flow to the upper lobes, and Kerley's B-lines typical of pulmonary edema (B is the correct answer to Question 3-5). Note the normal radiograph 1 month prior (Figure 3-28B).

Discussion

Pericardial effusion and cardiomyopathy have similar appearances on PA chest radiographs (Cases 3-2 and 3-3). This appearance is often referred to as a globular shape or a water-bottle heart. When this appearance is observed, an echocardiogram is the next best imaging test to differentiate between these two entities. However, this diagnosis may be suggested on the lateral radiograph by a separation of the pericardial and epicardial fat by pericardial fluid, as exhibited in Figure 3-25B (arrowheads). Additionally, the presence or absence of pulmonary edema may sometimes assist in the diagnosis. As a rule of thumb, pericardial effusions do not result in pulmonary edema, and therefore the

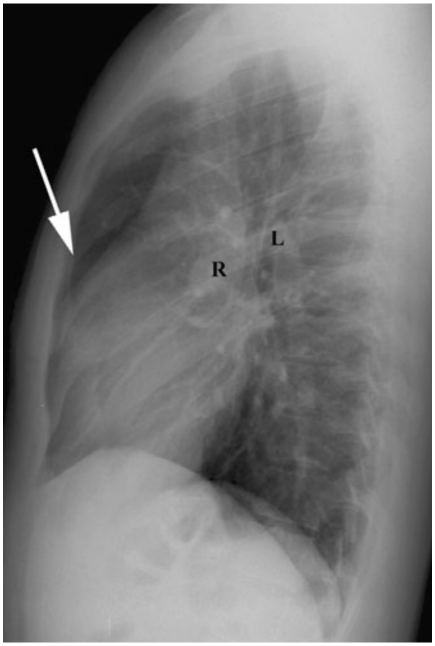

▲ **Figure 3-29.** Lateral view of patient in Case 3-4 shows filling in of the retrosternal space by the enlarged right ventricle (arrow) and large right (R) and left pulmonary arteries (L) from the pulmonary arterial hypertension.

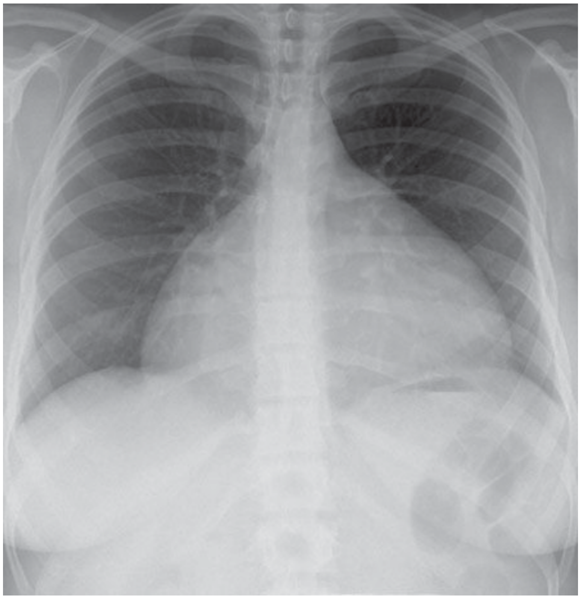

A

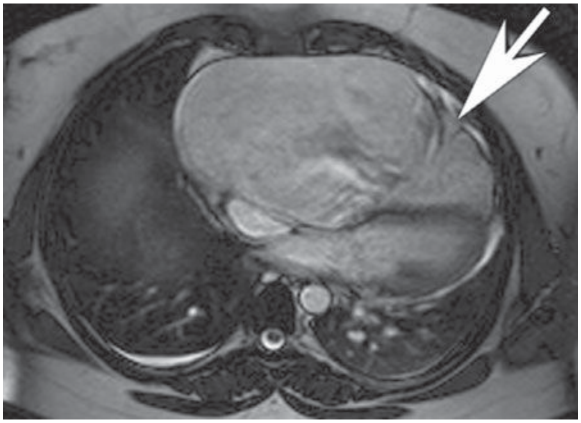

B

▲ **Figure 3-30.** (**A**) Upright PA view of chest in patient with Ebstein's anomaly reveals the globular-shaped heart characteristic of this disorder. (**B**) Axial gradient echo MR image reveals markedly enlarged right atrium with low-lying tricuspid valve (arrow) and small right ventricular chamber.

presence of edema should lead one to favor dilated cardiomyopathy. Mediastinal masses may occur in a location or a distribution that makes the heart appear enlarged on the chest radiograph. CT is the next best test to confirm a clinical suspicion of a mass and to evaluate mediastinal adenopathy.

Ebstein's anomaly, mentioned in Question 3-4, is an uncommon type of congenital heart disease that may also result in a globular appearance of the heart on the chest radiograph (Figure 3-30A). In these patients, the tricuspid valve is displaced downward, resulting in tricuspid regurgitation (Figure 3-30B). There is usually an associated ASD. The tricuspid insufficiency results in a massively enlarged right atrium, and the pulmonary vascularity is usually diminished due to decreased flow through the pulmonary arteries. These patients often present with congestive failure early in life, and echocardiography, MR imaging or cardiac angiography is necessary to make this diagnosis.

Increased heart size is a common clinical problem that may be caused by a variety of abnormalities. Cardiac enlargement may be diagnosed if the cardiothoracic ratio is greater than 60%. Often the lateral view is helpful for confirming left atrial and left ventricular enlargement. The most common cause of enlargement is atherosclerotic disease, although a number of other entities may cause an increased cardiac silhouette. In congestive heart failure (CHF), hydrostatic forces result in fluid collection in the interlobular septa, those connective tissue sheaths, veins, and lymphatics surrounding the secondary pulmonary lobule (Figure 3-31, arrows). As

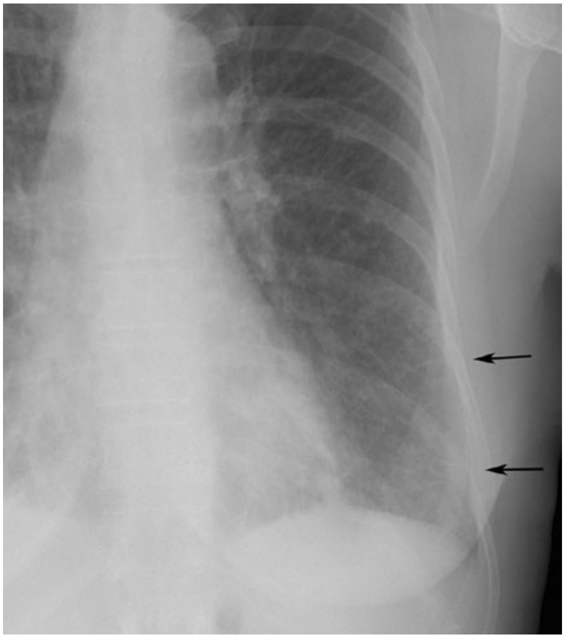

▲ **Figure 3-31.** Coned down frontal image of left hemithorax reveals fine reticular opacities extending to the pleural surface. These are Kerley B-lines (thickened interlobular septae) (arrows).

hydrostatic pressures increase, fluid may then accumulate in the alveoli giving an air-space pattern of disease. Intracardiac shunts, especially ventricular septal defect (VSD), can also cause cardiac enlargement because of the increased flow from the internal shunting. VSD is the most common congenital cardiac anomaly, and the intracardiac shunt must be at least 2 to 1 for the radiograph to show recognizable changes.

EXERCISE 3-2. ALTERATIONS IN CARDIAC CONTOUR

3-6. In Case 3-6 (Figure 3-32), the most likely cause of the radiographic abnormality is
A. syphilis.
B. cystic medial necrosis.
C. aortic stenosis.
D. congenital heart disease.
E. drug abuse.

3-7. In Case 3-7 (Figure 3-33), the abnormality is due to
A. mitral valve disease.
B. left ventricular hypertrophy.
C. pulmonic stenosis.
D. right atrial enlargement.
E. mediastinal mass.

3-8. In Case 3-8 (Figure 3-34), what is the cardiac contour abnormality?
A. Left atrial enlargement
B. Left ventricular enlargement
C. Right atrial enlargement
D. Left ventricular aneurysm
E. Right ventricular aneurysm

3-9. The diagnosis in Case 3-9 (Figure 3-35) is
A. situs inversus.
B. dextrocardia.
C. technical aberration.
D. tetralogy of Fallot.
E. pulmonary atresia.

3-10. The configuration of the heart in Case 3-10 (Figure 3-36) has been called the
A. boot-shaped heart.
B. third mogul of the heart.
C. snowman appearance.
D. double contour sign.
E. water-bottle heart.

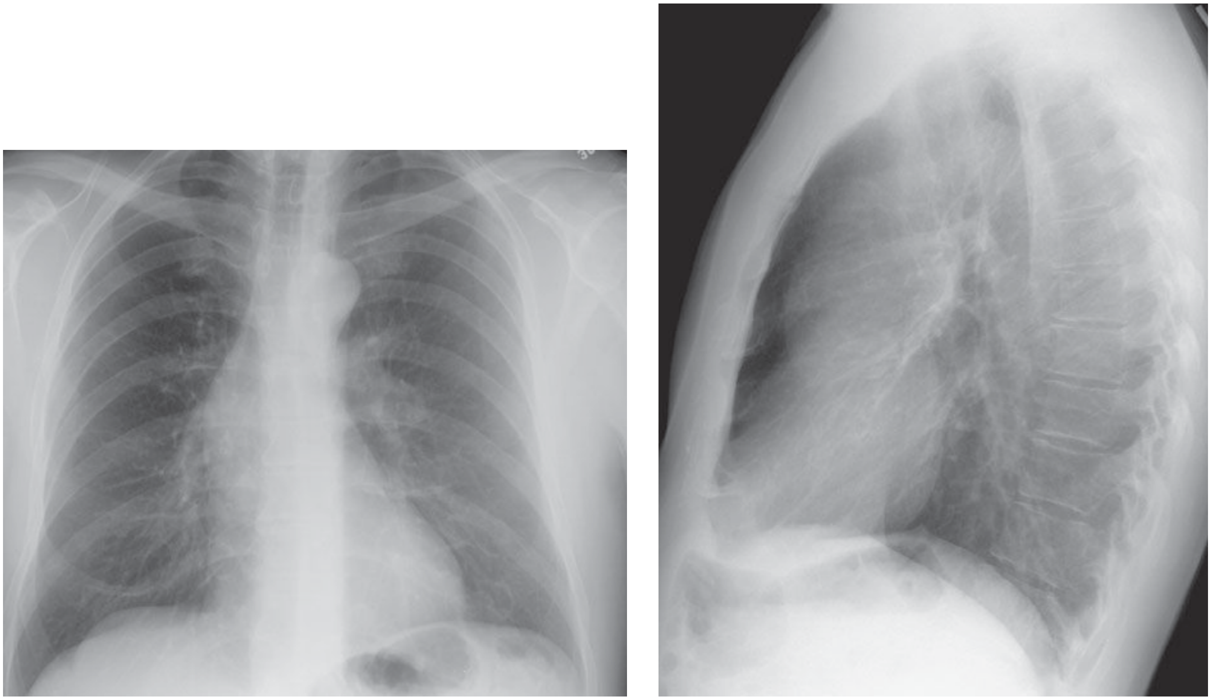

A B

▲ **Figure 3-32.** Case 3-6: 68-year-old man with a long history of elevated blood pressure and systolic murmur.

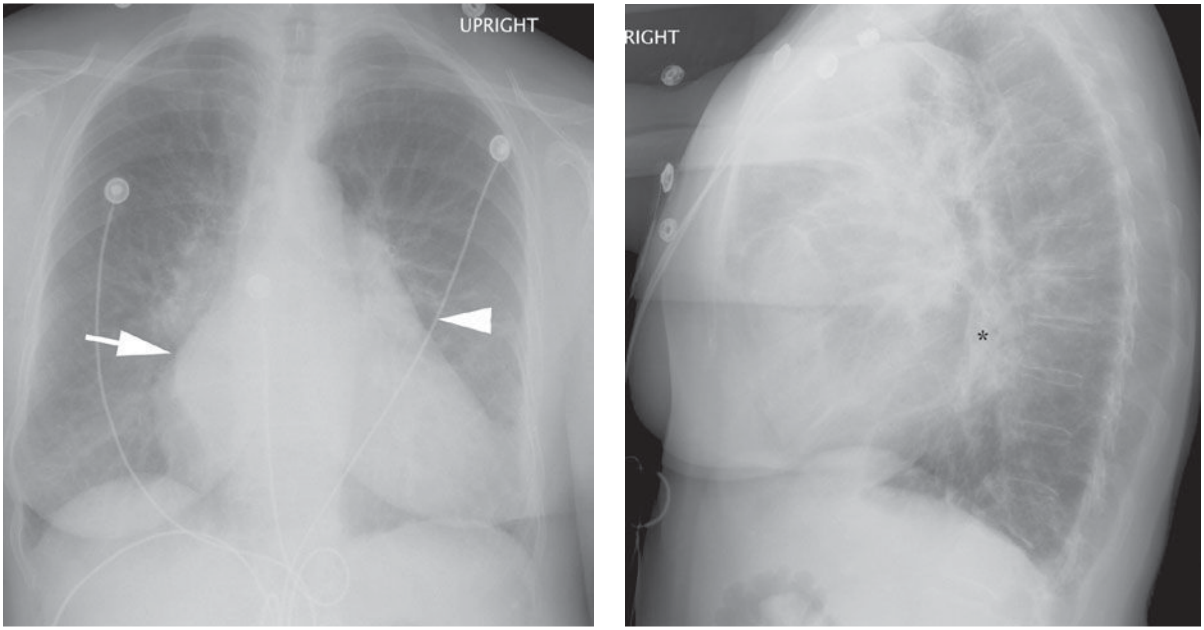

A B

▲ **Figure 3-33.** Case 3-7: 77-year-old woman with systolic and diastolic murmurs and a history of rheumatic fever as a child.

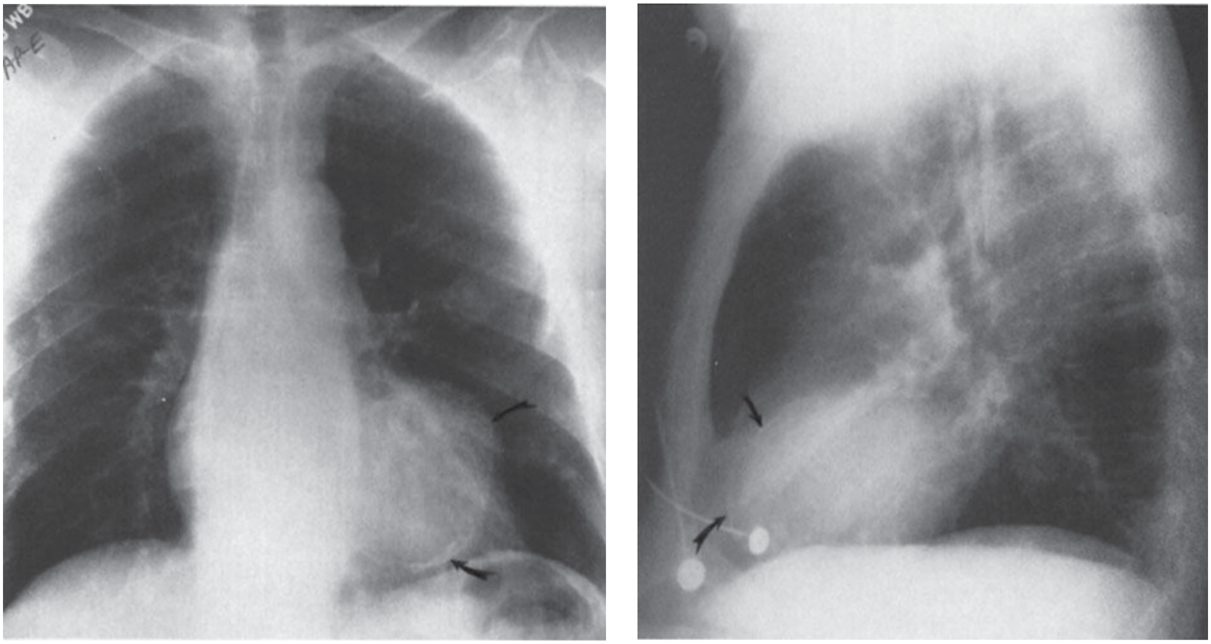

A B

▲ **Figure 3-34.** Case 3-8: 75-year-old man with a history of a myocardial infarction 10 years earlier had this study done as a routine screening examination.

▲ **Figure 3-35.** Case 3-9: 24-year-old man with recurrent pulmonary infections.

Radiographic Findings

3-6. In this case (Figure 3-32), the classical findings of enlargement of the left ventricle, characteristic of left ventricular hypertrophy, are seen on both the PA and the lateral radiograph as well as deviation of the ascending aorta contour to the right. This pattern is often the result of long-standing aortic stenosis (C is the correct answer to Question 3-6).

3-7. In this case (Figure 3-33), a double density to the right side of the heart is seen on the PA radiograph (arrow). There is also an enlarged left atrial appendage (arrowhead). The lateral radiograph shows enlargement of the left atrial shadow, the superior and posterior region of the cardiac contour (*), and posterior displacement of the left main bronchus and enlargement of the right ventricle (A is the correct answer to Question 3-7). Along with increased pulmonary vascularity, the constellation of findings is characteristic of left atrial enlargement due to mitral valve insufficiency.

3-8. The PA and lateral radiographs in this case (Figure 3-34) show an enlargement of the left ventricular contour with a focal bulge containing calcification within its wall (arrows). The lateral radiograph confirms the calcification (curved arrows). Given the history of myocardial infarction 10 years earlier, the most likely diagnosis is a left ventricular aneurysm (D is the correct answer to Question 3-8).

3-9. The patient in this case (Figure 3-35) shows the apex of the heart to be on the right side of the chest and the descending aorta to be in its correct position on the left. These findings are diagnostic of dextrocardia, which in this case is secondary to Kartagener syndrome (B is the correct answer to Question 3-9).

3-10. In this case (Figure 3-36), tetralogy of Fallot, the apex of the left ventricle is elevated by right ventricular hypertrophy. These findings are sometimes referred to as a boot-shaped heart (A is the correct answer to Question 3-10).

▲ **Figure 3-36.** Case 3-10: 3-year-old child with a history of cardiac complications since birth.

Discussion

Alterations of the normal cardiac contour are common clinical scenarios. The most common contour abnormality is probably enlargement of the left ventricle from long-standing hypertension, as exhibited by the 68-year-old man in Case 3-6 (Figure 3-32). Cardiac enlargement is first suggested on the PA view by an increase in the CT ratio to over 50%. Left ventricular enlargement is suggested by prominence of the apex of the cardiac contour. On the lateral projection, the left ventricle should not project more than 2 cm posterior to the IVC measured 2 cm above the diaphragm. If the left ventricle projects more than 2 cm behind this landmark, left ventricular enlargement should be suspected. The configuration of the left ventricle and ascending aorta has been likened to the Schmoo from Al Capp's Li'l Abner.

Left atrial enlargement (LAE), as shown in Case 3-7 (Figure 3-33), occurs mainly with left-sided obstructive lesions such as mitral stenosis or mitral regurgitation, often the result of rheumatic heart disease. The major sign of LAE on the PA view is a double density centrally caused by the dilated left atrium extending to the right of the spine projected behind the right atrium (Figure 3-33A, arrow). Another sign of LAE is enlargement of the left atrial appendage. The left atrial appendage is immediately adjacent and inferior to the left main bronchus.

When enlarged, there is an extra bump along the left heart border, the so-called third mogul of the left cardiac border (Figure 3-33A, arrowhead). LAE also causes a separation and widening of the carinal angle that can be seen on the PA chest radiograph, although this is a late sign of LAE. The carinal angle normally measures between 60 and 120 degrees. Widening of this angle may occasionally be caused by subcarinal adenopathy and therefore should be correlated with other signs of LAE.

The left atrium makes up the posterior cardiac shadow just above the left ventricle (LA in Figure 3-1). Left atrial enlargement is recognized on the lateral film by enlargement and posterior displacement of the left atrial shadow (Figure 3-33B, *). As further enlargement occurs, the left atrium displaces the left main and left lower lobe bronchus posteriorly. Ultimately the elevated left heart pressures can be transmitted back across the pulmonary circulation, leading to pulmonary arterial hypertension and subsequent right heart enlargement (see later discussion).

Right ventricular enlargement (RVE) or hypertrophy (RVH) results most commonly from right-sided heart failure from a variety of disorders resulting in pulmonary hypertension (Table 3-5). In this cardiac contour abnormality there is an increase in the soft-tissue density within the retrosternal clear space that is best seen on the lateral radiograph (Figure 3-37). On the PA film, uplifting of the cardiac apex may be also seen. Anterior mediastinal masses may also cause retrosternal soft tissue density and should be included in the differential diagnosis (Figure 3-38); however, the majority of anterior mediastinal masses fill the RSS from superior to inferior and may not obscure right sided cardiac structures. When the cause is not clear from the conventional radiograph, CT is the next most appropriate test to differentiate between these two considerations.

Cardiac aneurysms, as shown in the patient in Case 3-8 (Figure 3-34), are almost always the sequelae of myocardial

Table 3-5. Causes of Pulmonary Hypertension

Pulmonary arterial hypertension
Idiopathic
Familial
Associated
Collagen vascular disease
Congenital systemic-pulmonary shunt
Portal hypertension
HIV
Drugs and toxins
Associated with venous or capillary involvement
Persistent pulmonary hypertension of newborn
Pulmonary hypertension with left heart disease
Pulmonary hypertension with lung disease or hypoxemia
Pulmonary hypertension due to chronic thrombotic/embolic disease
Miscellaneous

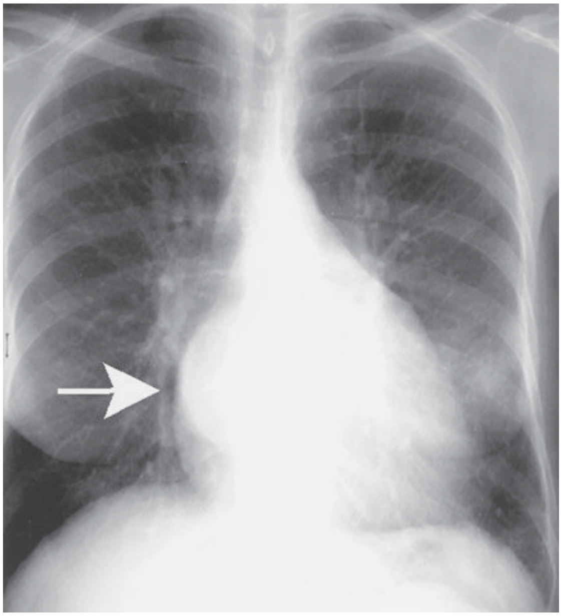

A

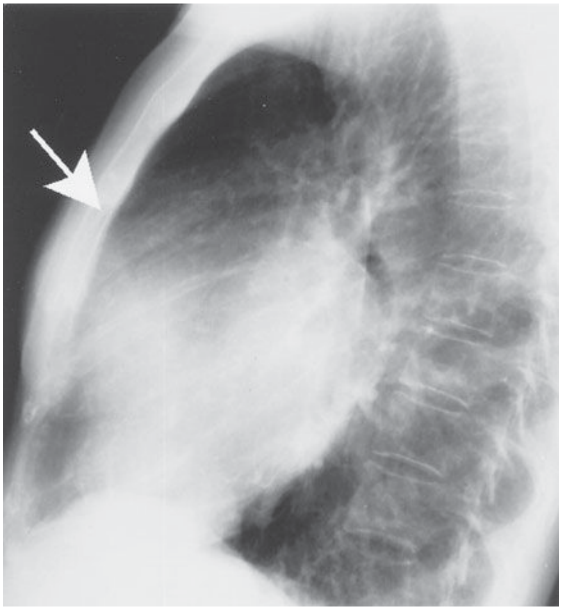

B

▲ **Figure 3-37.** PA (**A**) and lateral (**B**) views of patient with long-standing mitral stenosis show the double contour (arrow) on the PA view and filling in of the retrosternal space (arrow) on the lateral view. Right ventricular hypertrophy will be manifested as soft-tissue density in the retrosternal space on the lateral view.

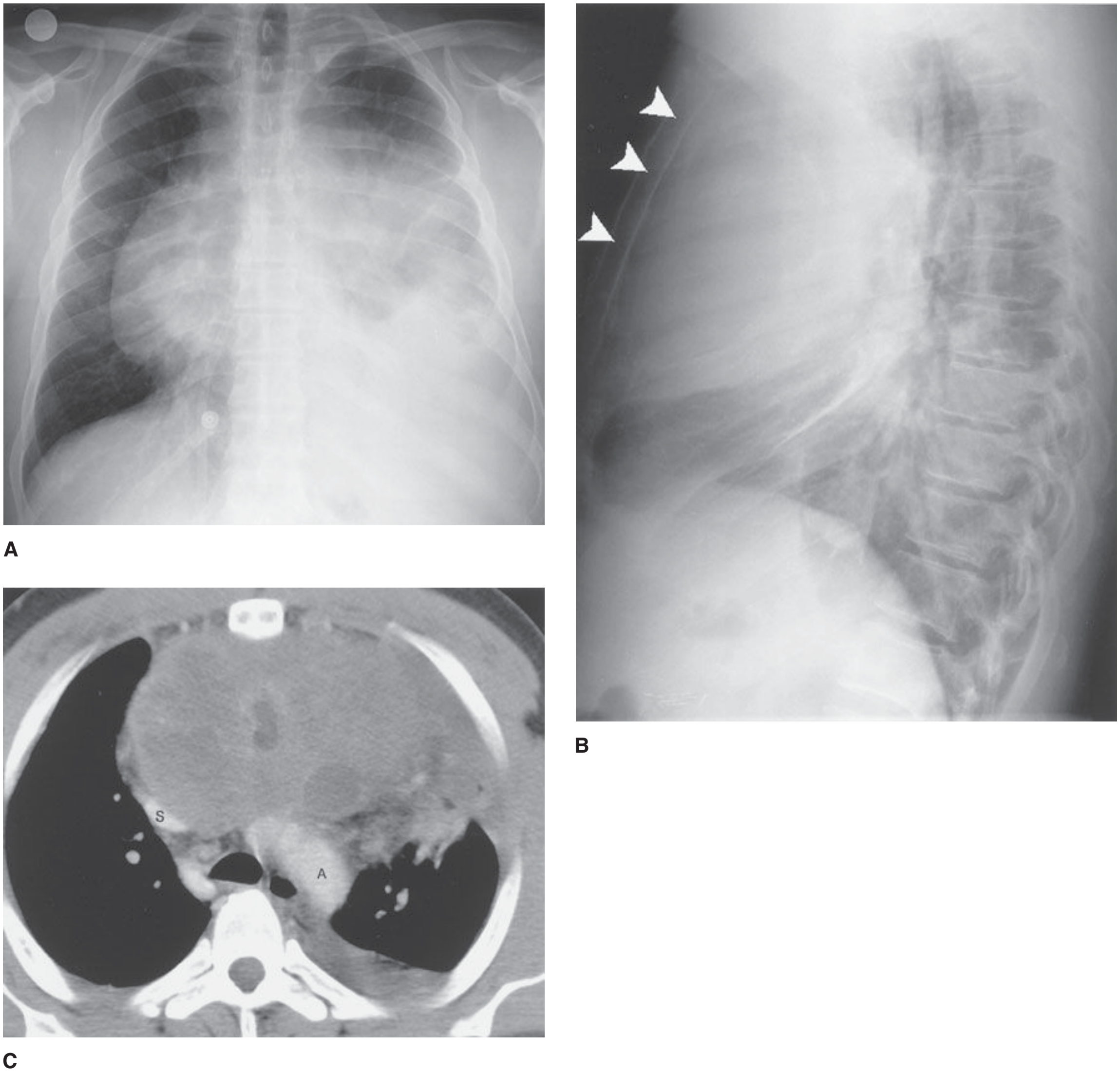

▲ Figure 3-38. PA (**A**) and lateral (**B**) views of patient with night sweats show an anterior mediastinal mass, which fills in the retrosternal space on the lateral view (arrowheads). A CT scan (**C**) in the same patient shows the location of the anterior mediastinal mass adjacent to the aortic arch (A). S, superior vena cava. Biopsy of the mass revealed germ-cell neoplasm.

infarction. There are two types of cardiac aneurysms: true and false aneurysms. True aneurysms most frequently occur at the cardiac apex and contain all three layers of myocardium. False aneurysms or pseudoaneurysms occur with disruption of the endocardium, with dissection of blood into the cardiac wall. Pseudoaneurysms, therefore, are not bound by all three layers of the heart wall. Pseudoaneurysms most frequently occur along the free walls of the heart (inferior and lateral walls). Aneurysms are usually diagnosed on the PA chest radiograph as localized soft-tissue outpouchings or irregularities at the apical or anterolateral segments of the left ventricular cardiac contour. A linear rim of dystrophic calcification may develop within the nonviable myocardium after the infarction. With echocardiography, aneurysms show paradoxical enlargement during systole. Because there is stasis of blood in the aneurysm, blood clots can develop and may be a source of distal systemic arterial emboli. Echocardiography, CT, and MR imaging can all be used to make the diagnosis of cardiac aneurysm and distinguish between true and false aneurysms. The distinction is important because false aneurysms are at higher risk for rupture and require surgical repair.

Dextrocardia, as shown in Case 3-9 (Figure 3-35), is usually recognized easily on the PA chest radiograph. However, this finding may be overlooked if the left and right designations on the film are marked incorrectly or are misinterpreted. In most cases of dextrocardia, the aorta descends on the left side and the patient is asymptomatic. If the aorta descends on the right side, a number of other abnormalities should be considered. The references provide more in-depth discussion of this topic.

The boot shape of the cardiac shadow in Case 3-10 (Figure 3-36) is secondary to tetralogy of Fallot. The four components of this congenital cardiac anomaly are an overriding aorta, ventricular septal defect, pulmonic stenosis, and right ventricular hypertrophy. It is the right heart enlargement that results in the upturned cardiac apex. The degree of shunt and pulmonary stenosis dictate the presentation. In cases where the stenosis is severe, infants are cyanotic and there is generalized decrease in pulmonary vasculature. If the pulmonary stenosis and degree of left-to-right shunt is mild, the abnormality may not manifest itself until childhood (Figure 3-39).

EXERCISE 3-3. PULMONARY VASCULARITY

3-11. The most likely cause of the patient's symptoms in Case 3-11 (Figure 3-40) is
A. pneumonia.
B. pulmonary edema.
C. interstitial lung disease.
D. panic attack.
E. pneumothorax.

3-12. The curved arrow in Case 3-12 (Figure 3-41A) is directed to the
A. right atrium.
B. ascending aorta.
C. right descending pulmonary artery.
D. main pulmonary artery.
E. pneumonia.

3-13. The most likely diagnosis in Case 3-13 (Figure 3-42) is
A. aortic stenosis.
B. pulmonic stenosis.
C. VSD.
D. pulmonary edema.
E. normal chest radiograph.

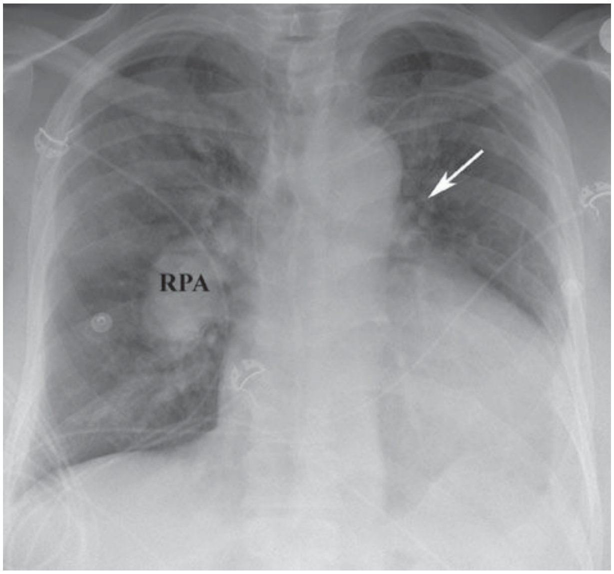

A

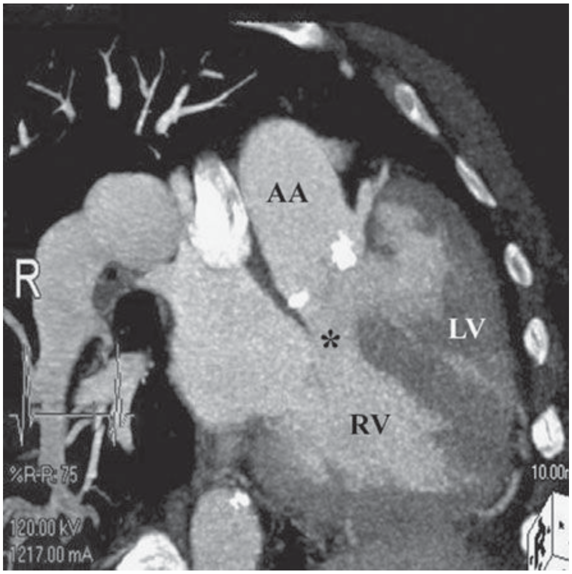

B

▲ **Figure 3-39.** Frontal radiograph (**A**) and oblique coronal reformatted CT (**B**) of an adult patient with uncorrected tetralogy of Fallot. On chest radiograph, note enlarged right pulmonary artery (RPA). Left pulmonary artery is diminutive because of long-standing stenosis (arrow). CT image reveals characteristic features including ventricular septal defect (*), overriding aorta, and right ventricular hypertrophy secondary to pulmonary stenosis. AA, ascending aorta; LV, left ventricle; RV, right ventricle.

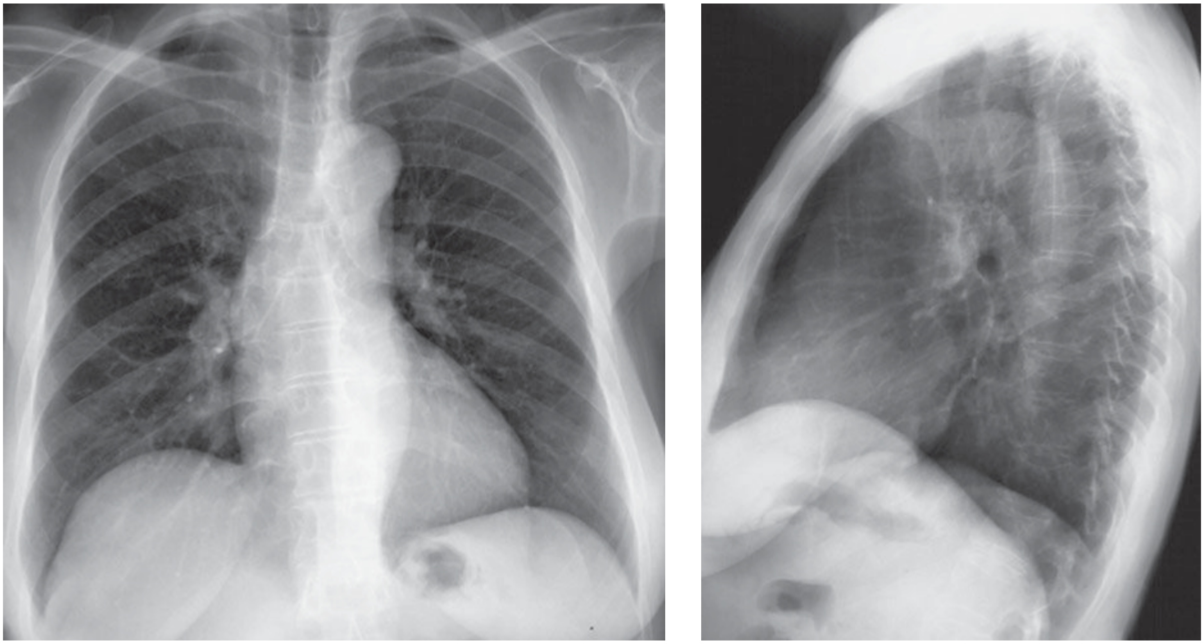

A B

▲ **Figure 3-40.** Case 3-11: 53-year-old woman examined in the emergency department for chest pain, tachycardia, and shortness of breath with normal ECG.

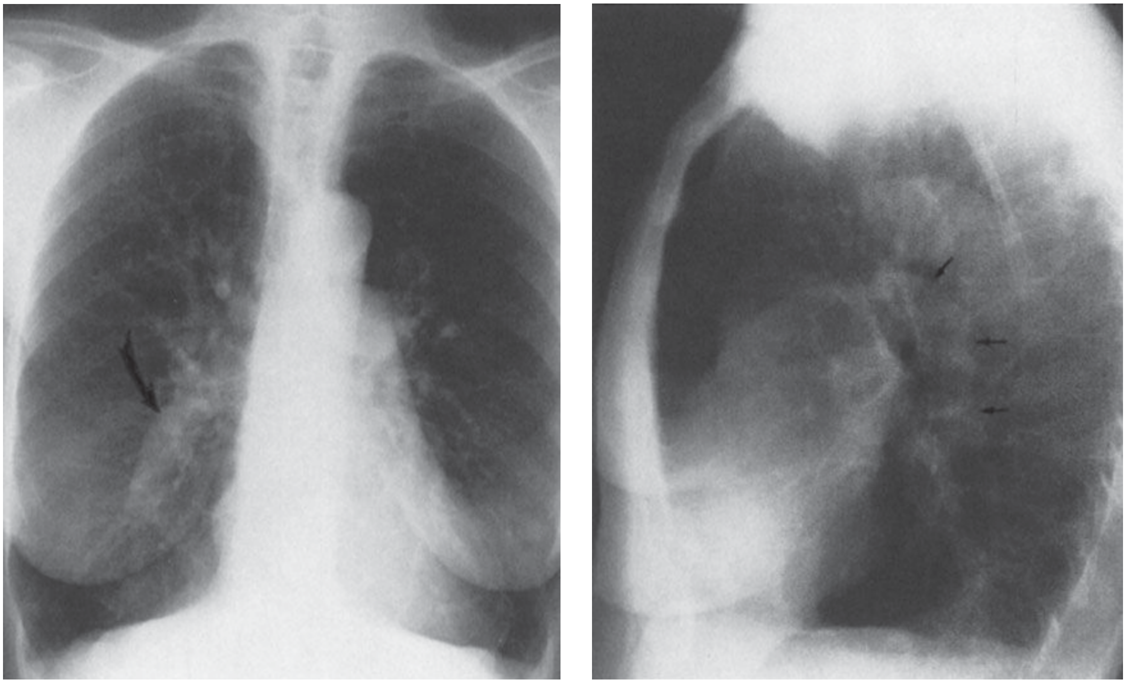

A B

▲ **Figure 3-41.** Case 3-12: 65-year-old woman with a 100-pack-a-year history of smoking.

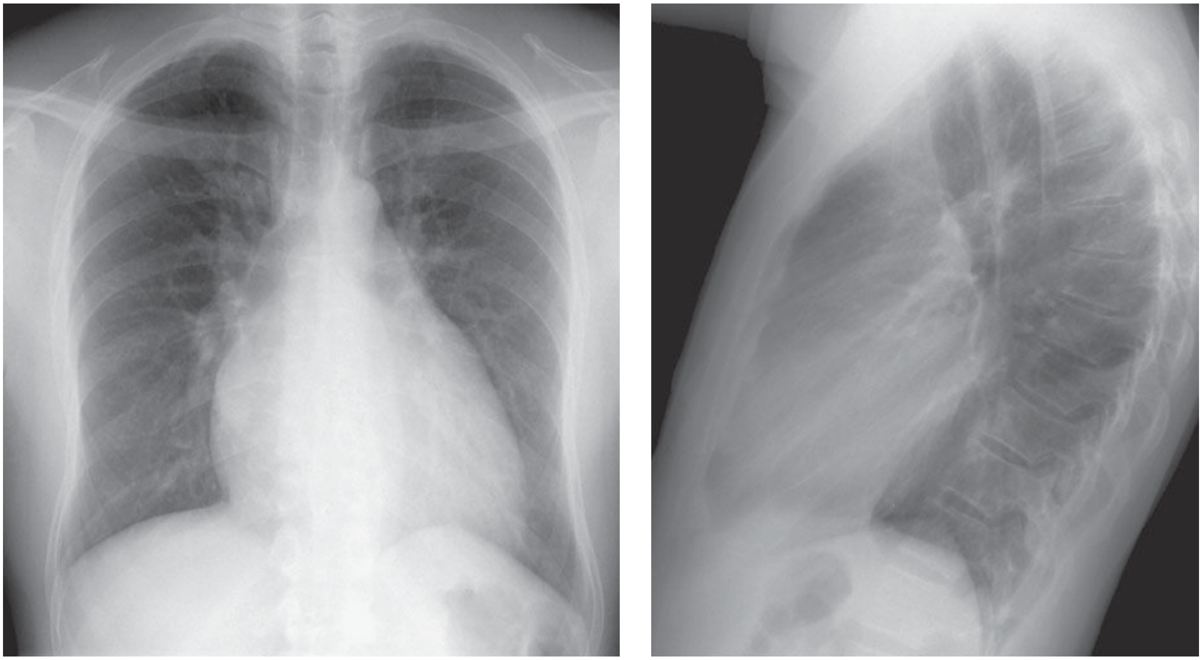

▲ **Figure 3-42.** **A,B**. Case 3-13: An acyanotic 40-year-old man with a systolic murmur.

3-14. The appearance of the pulmonary vasculature indicates that the diagnosis in Case 3-14 (Figure 3-43) is

▲ **Figure 3-43.** Case 3-14: 36-year-old man with asthma.

A. enlarged atrial appendage.
B. partial anomalous pulmonary venous return.
C. right ventricular hypertrophy.
D. left atrial enlargement.
E. pulmonary arteriovenous malformation.

3-15. The most likely etiology of the radiographic findings in Case 3-15 (Figure 3-44) is
A. cardiac failure with pulmonary edema.
B. pulmonic stenosis with pneumonia.
C. pulmonary embolism.
D. pneumomediastinum.
E. pneumothorax.

Radiologic Findings

3-11. In this case (Figure 3-40), the chest radiograph was normal in a 53-year-old woman seen in the emergency department for left-sided chest pain. The electrocardiogram was also normal, and there was no obvious cause for the patient's pain. (D is the correct answer to Question 3-11). Note the well-defined pulmonary vessels in the perihilar region and normal branching of these vessels into the lungs. There is a gradient of pulmonary vascular markings from the bases to the apices on an upright radiograph due to the increased perfusion to the lower lobes. No

▲ **Figure 3-44.** Case 3-15: 50-year-old woman with acute shortness of breath.

pulmonary parenchymal abnormalities are present to support the other diagnoses. It should be noted that the chest radiograph is often normal in myocardial infarction, and a normal chest x-ray does not exclude intrinsic cardiac disease per se.

3-12. This case (Figure 3-41) is an example of chronic obstructive pulmonary disease. The large central pulmonary arteries indicate pulmonary arterial hypertension. The curved arrow in Figure 3-41A identifies the enlarged right descending pulmonary artery (C is the correct answer to Question 3-12). The generalized proximal pulmonary artery enlargement is confirmed on the lateral radiograph by the large left pulmonary artery (arrows in Figure 3-41B). Note the attenuation of vessels in the periphery of the lungs. This constellation of findings is typical of emphysema. There are also large bullae, which result in an absence of pulmonary vessels and hyperlucency of the lungs.

3-13. This case (Figure 3-42) shows increased pulmonary vascularity in a 40-year-old patient with VSD (C is the correct answer to Question 3-13). Note the large central pulmonary arteries, the increased linear opacities radiating out into the lungs, and the relatively uniform distribution of the pulmonary vascular shadows. In individuals with long-standing intracardiac shunts and pulmonary hypertension, the pulmonary arterial resistance may exceed systemic pressures, resulting in Eisenmenger's physiology, a reversal of an intracardiac shunt from L > R to R > L. In these individuals, the central pulmonary arteries are quite large, but the peripheral pulmonary arteries are markedly attenuated.

3-14. This case (Figure 3-43) shows the characteristic appearance of venolobar (scimitar) syndrome (B is the correct answer to Question 3-14). The scimitar vein is the result of partial anomalous pulmonary venous return.

3-15. This case (Figure 3-44) is an example of a pulmonary edema due to fluid overload and congestive heart failure (A is the correct answer to Question 3-15). Note the increased size of the cardiac silhouette, the ill-defined reticular perihilar air-space opacities, the enlargement of the vascular pedicle, and the redistribution of blood flow to the upper lung zones.

Discussion

The main pulmonary arteries are large, the lobar arteries smaller, and each branching segment becomes progressively smaller. As the vasculature tree ramifies, the arteries are closely related to the adjacent bronchus and are approximately the same size. On the chest radiograph, this pattern is manifest by linear opacities or shadows that are much more prominent in the central portion of the chest and gradually become less prominent toward the periphery of the lung, as in the normal person in Case 3-11. The right descending pulmonary artery is one important landmark on the PA chest film (see Figure 3-1). In the normal chest, the lateral border of the RDPA is usually well demarcated, and the artery usually measures less than 15 mm in its widest diameter.

Enlargement of the pulmonary vessels is caused by a variety of abnormalities (see Table 3-5). Chronic obstructive pulmonary disease, with resultant pulmonary hypertension, is the most common cause of pulmonary arterial hypertension and is shown in the patient in Case 3-12 (Figure 3-41).

Intracardiac shunts that result in increased pulmonary arterial flow can also enlarge the pulmonary vascular system. The most common lesions causing increased vascularity without cyanosis are ASD, VSD, and patent ductus arteriosus (PDA). Case 3-13 (Figure 3-42) is an example of a VSD with increased vascularity. The main cardiac lesions with cyanosis and increased pulmonary vascularity are transposition of the great vessels, truncus arteriosus, and total anomalous pulmonary venous return (TAPVR). The standard texts listed at the end of the chapter can provide more in-depth discussions of these entities.

One other common cause of pulmonary artery enlargement is mitral disease (either stenosis or regurgitation). In this case, increasing left atrial pressures are transmitted to the pulmonary veins. In time, this raises pulmonary capillary wedge pressures and eventually right heart pressures, similar to cor pulmonale from left heart failure (see Case 3-7).

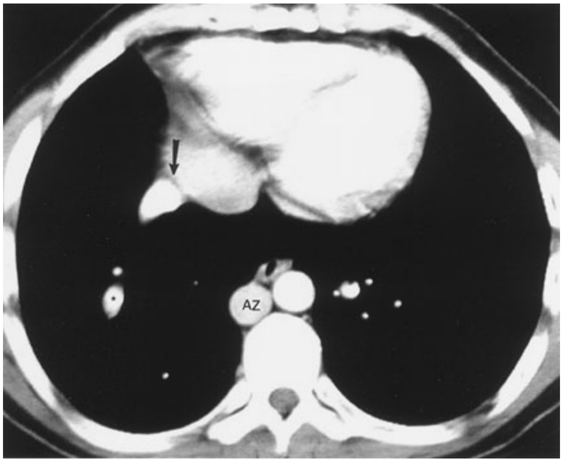

▲ **Figure 3-45.** Axial CT with contrast shows anomalous right pulmonary vein descending (*) and entering (arrow) inferior vena cava. AZ, azygous vein.

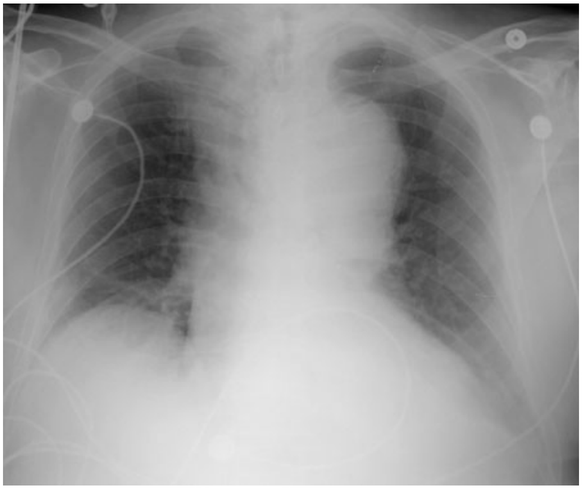

▲ **Figure 3-46.** Case 3-16: 74-year-old man with a long history of hypertension and ripping pain between the scapulae.

Venolobar syndrome is a form of partial anomalous pulmonary venous return. Note the right inferior pulmonary vein descending in a curvilinear fashion to empty into the inferior vena cava (Figures 3-43 and 3-45). Right lung hypoplasia causes the small size of the right hemithorax and results in shift of the heart and mediastinum to the right. Other congenital anomalies may be present.

Pulmonary edema, as exhibited in Case 3-15 (Figure 3-44), regardless of the cause, is another process that causes the increase in the pulmonary vascularity seen on chest radiograph (discussed further in the next chapter). Perihilar indistinctness, caused by interstitial edema, may obliterate the borders of the pulmonary vessels. Associated findings are redistribution of blood flow to the apices, engorgement of the central veins, Kerley's B-lines, and pleural effusions (see Figure 3-31).

EXERCISE 3-4. VASCULAR ABNORMALITIES

3-16. The most likely diagnosis in Case 3-16 (Figure 3-46) is
- **A.** pericardial cyst.
- **B.** adenopathy.
- **C.** aortic dissection.
- **D.** pulmonary artery aneurysm.
- **E.** enlarged azygous vein.

3-17. The abnormality outlined by arrows in Case 3-17 (Figure 3-47) is
- **A.** substernal goiter.
- **B.** innominate artery aneurysm.
- **C.** lung cancer.
- **D.** right aortic arch.
- **E.** mediastinal adenopathy.

3-18. Causes for the appearance of the chest in Case 3-18 (Figure 3-48) include all of the following except
- **A.** ascending aortic aneurysm.
- **B.** anterior mediastinal mass.
- **C.** pleural mass.
- **D.** lung cancer.
- **E.** Ewing's sarcoma of the rib.

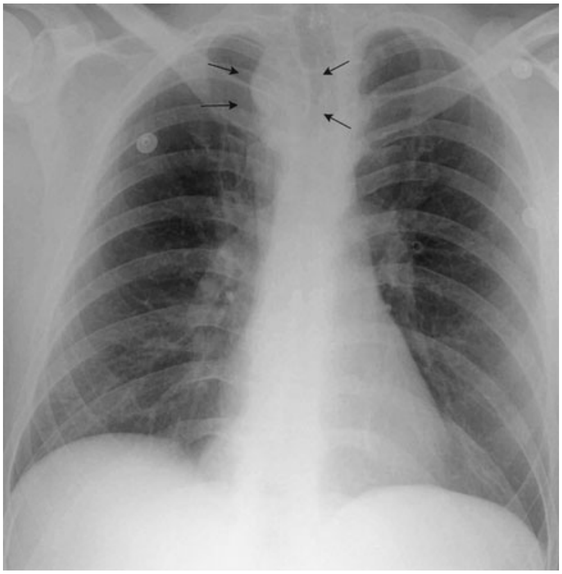

▲ **Figure 3-47.** Case 3-17: 25-year-old man with chest fullness.

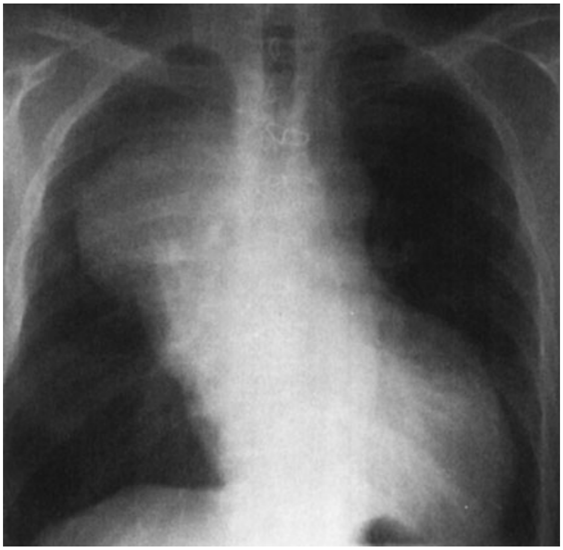

▲ **Figure 3-48.** Case 3-18: 76-year-old man with substernal chest pain.

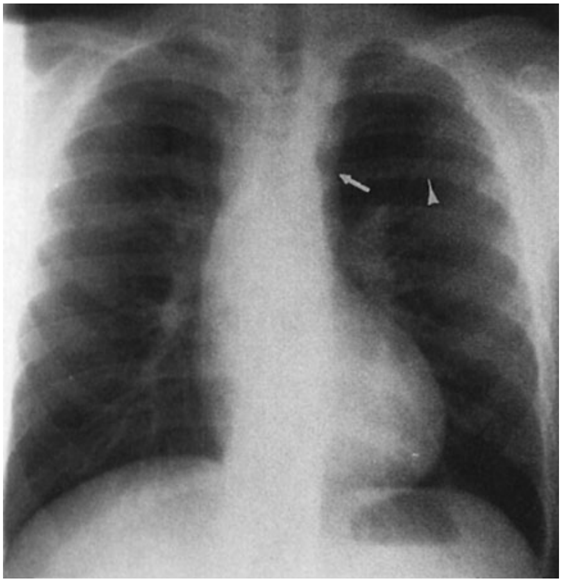

▲ **Figure 3-49.** Case 3-19: 22-year-old man with differential pulses in the legs and arms.

3-19. The arrow in Figure 3-49 is showing
- **A.** aortic ectasia.
- **B.** aortic constriction.
- **C.** pulmonary artery dilatation.
- **D.** adenopathy.
- **E.** embolic changes.

3-20. The abnormality shown by the arrow in Figure 3-50 is most likely a(n)
- **A.** enlarged main pulmonary artery.
- **B.** descending thoracic aorta aneurysm.
- **C.** patent ductus arteriosus.
- **D.** pulmonary vein stenosis.
- **E.** left superior vena cava.

Radiographic Findings

3-16. In this case (Figure 3-46), there is marked enlargement of the distal ascending and transverse thoracic aorta with shift of the trachea to the right. In association with the clinical symptoms, the most worrisome diagnosis is dissection of the aorta (C is the correct answer to Question 3-16).

3-17. This case (Figure 3-47) is an example of a right-sided aortic arch in an asymptomatic individual (D is the correct answer to Question 3-17).

3-18. This case (Figure 3-48) is a radiograph of the patient in Case 3-16 (Figure 3-46) 9 years later and shows a localized mass in the region of the ascending aorta. The CT image (Figure 3-51) confirmed the large ascending aorta aneurysm (E is correct answer to Question 3-18).

3-19. This case (Figure 3-49) shows rib notching (arrowhead) and a localized constriction of the proximal descending aorta (arrow) (B is the correct answer to Question 3-19). These findings are diagnostic of coarctation of the aorta.

3-20. This case (Figure 3-50) is an example of a chronic pseudoaneurysm of the proximal descending aorta (arrow) in a patient with remote major trauma (B is the correct answer to Question 3-20).

Discussion

Anomalies of the major vessels are commonly encountered on the chest radiograph. The aortic arch is an easily recognized shadow. On the PA projection, the aorta originates in the middle of the chest and then arches superiorly and slightly to the left (hence the term *aortic arch*), then curves, crosses the mediastinum at an oblique angle, and continues as the descending thoracic aorta (see Figure 3-1). The configuration of the aorta changes during life. In the young person, the aortic arch is narrow and smooth and the descending thoracic segment very straight. In the older individual with atherosclerotic disease or aortic stenosis, the ascending aorta becomes more prominent along the right heart border and may have an undulating pattern in the descending thoracic portion.

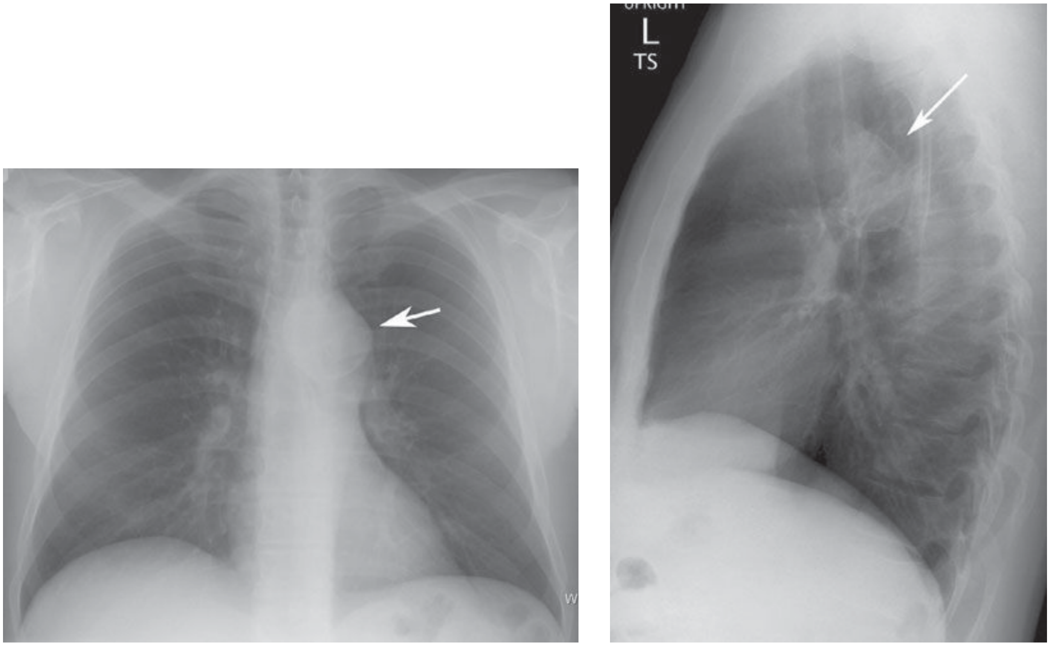

A B

▲ **Figure 3-50.** Case 3-20: 38-year-old man with atypical chest pain.

Aortic dissection as seen in Case 3-16 (Figure 3-46) can be a life-threatening diagnosis. This is often the result of atherosclerosis and/or medial layer necrosis. In this disorder, blood dissects into the aortic wall through a tear of the intima. This process may begin anywhere along the course of the thoracic aorta, but the exact location is very important because it has therapeutic implications. Aortic dissection is most easily classified by the Stanford system. This divides dissections into type A, those involving the ascending aorta, and type B, those that begin distal to the left subclavian. When associated with symptoms, type A dissections are considered surgical emergencies, whereas symptomatic

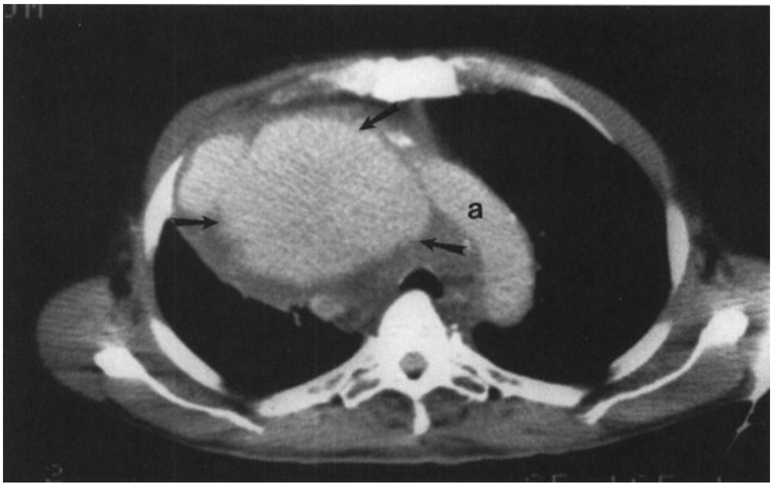

▲ **Figure 3-51.** Axial CT image shows large aortic aneurysm (arrows) originating from the proximal ascending portion of the aortic arch (a).

type B dissections often can be managed medically. In the acute setting, the diagnosis is best established by CT because it can rapidly define the entire scope of the dissection as well as show the relationship to other major vessels (see Figure 3-15). Echocardiography can also rapidly detect dissection but provides less anatomic detail. MR imaging is often not used in the acute setting because of time and availability issues. The role of angiography as a diagnostic procedure for dissection has virtually disappeared; however, intravascular therapy including placement of stent-grafts and fenestration of the dissection flap can be performed for treatment in many instances, including medically inoperable individuals.

Other abnormalities of the aortic arch are uncommon. Congenital aortic anomalies include left aortic arch with aberrant branching, right aortic arch, and double aortic arch. The most prominent of these aberrations is the right aortic arch, which occurs in 1 in 2500 people. It can be diagnosed on the conventional radiograph by noting an indentation to and slight deviation of the right side of the trachea and displacement of the SVC shadow, as shown in Case 3-17 (Figure 3-47, arrows). In many individuals, the right arch is discovered incidentally and in these cases, is usually associated with an aberrant left subclavian artery (Figure 3-52). The barium swallow can also demonstrate mass effect on the esophagus by the aberrant subclavian and aorta as it crosses from right to left in the chest. When associated with congenital anomalies (tetralogy of Fallot, truncus arteriosus, etc), the great vessel branching pattern is a mirror image of that seen in a normal left aortic arch.

▲ **Figure 3-52.** Axial CT shows aberrant left subclavian artery coursing posterior to the esophagus (e).

Aneurysms of the aorta, shown in Cases 3-18 and 3-20 (Figure 3-48 and 3-50), are most often caused by atherosclerosis. Trauma, infection, and connective tissue disorders such as Marfan and Ehlers-Danlos syndrome are other causes. Aneurysms may be saccular or fusiform in shape, and symptoms include chest pain, hoarseness from compression of the recurrent laryngeal nerve, postobstructive atelectasis from compression of a bronchus, and dysphagia from esophageal compression. However, aneurysms are most commonly discovered as an incidental finding on an imaging study done for other reasons. An aneurysm of the ascending or transverse aortic segments shows a focal enlargement of the aortic shadow, usually with curvilinear calcification in its wall. A saccular aneurysm of the descending aorta may be misdiagnosed as a lung, mediastinal, or pleural mass, especially if it does not contain linear calcification. In these cases, as mentioned previously, CT is the next best imaging modality to perform (see Figure 3-51). The lack of rib destruction in Case 3-18 strongly argues against a chest wall sarcoma.

The abnormality in Case 3-19 (Figure 3-49) is coarctation of the aorta. This congenital anomaly results in partial or complete obstruction of the aorta at the junction of the aortic arch and descending aorta near the ligamentum arteriosum (the in utero connection between the aorta and pulmonary arteries). About one half of these individuals also have a bicuspid aortic valve. The obstruction to flow due to the coarctation results in elevated upper-extremity blood pressure and decreased lower-extremity blood pressure. A systolic ejection murmur may also be heard. Because of the partial aortic obstruction, collateral flow through the intercostal arteries results in the rib notching seen (Figure 3-53).

EXERCISE 3-5. HEART AND GREAT VESSEL CALCIFICATIONS

3-21. In Case 3-21 (Figure 3-54) the calcific density (straight arrow) is due to calcification of the
- **A.** mitral annulus.
- **B.** tricuspid valve.
- **C.** aortic valve.
- **D.** pulmonary embolus.
- **E.** pericardium.

3-22. In Case 3-22 (Figure 3-55) the calcifications are related to
- **A.** pulmonary arteries.
- **B.** pericardium.
- **C.** myocardium.
- **D.** ascending aorta.
- **E.** descending thoracic aorta.

3-23. In Case 3-23 (Figure 3-56) the calcifications on the chest radiograph are related to which structure?
- **A.** Pericardium
- **B.** Mitral valve
- **C.** Aortic valve

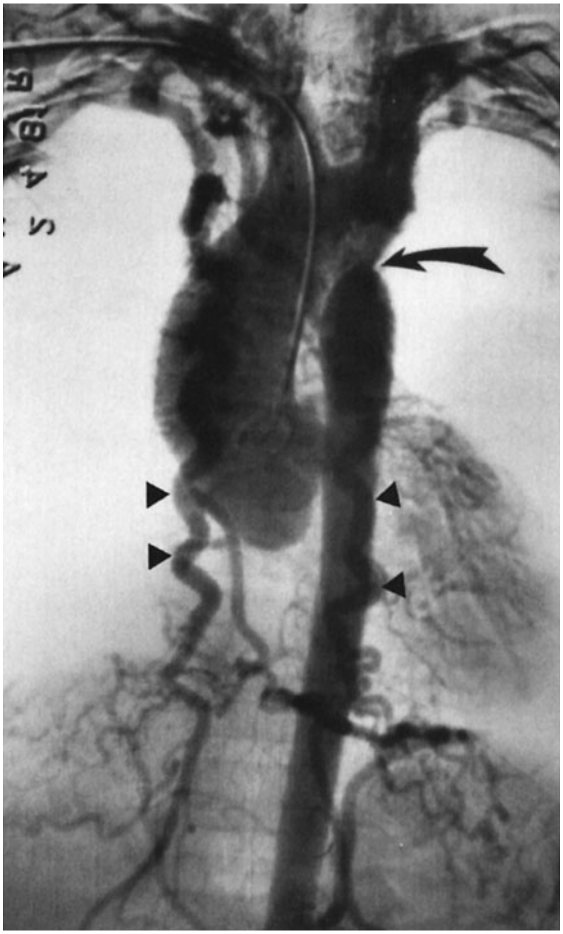

▲ **Figure 3-53.** Aortogram of the patient in Case 3-19 shows the characteristic constriction in the descending aorta (curved arrow) and the dilated intercostal veins (arrowheads).

D. Descending aorta
E. Left ventricle

3-24. In Case 3-24 (Figure 3-57) the curved arrows point to calcification within the region of which cardiac structure?
A. Aortic valve
B. Mitral valve
C. Pericardium
D. Coronary artery
E. Aortic aneurysm

3-25. In Case 3-25 (Figure 3-58) the arrows and arrowheads point to a(n)
A. calcified mediastinal mass.
B. calcified left atrial myxoma.

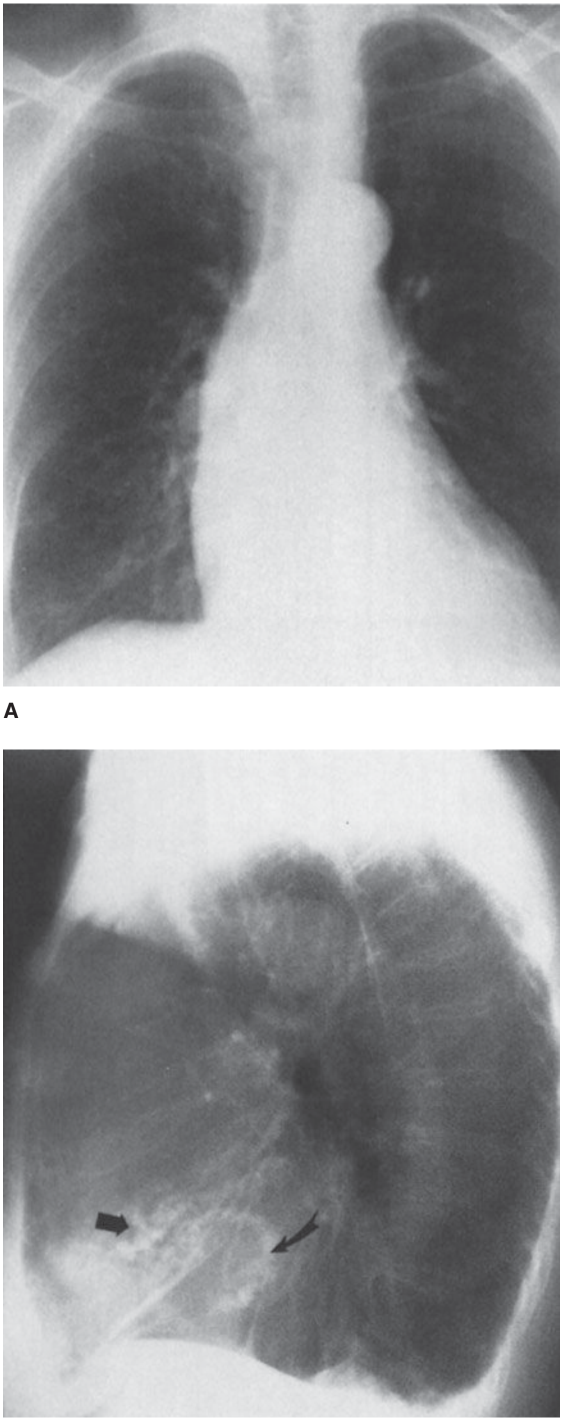

A

B

▲ **Figure 3-54.** Case 3-21: 75-year-old woman with rheumatic fever as a young adult.

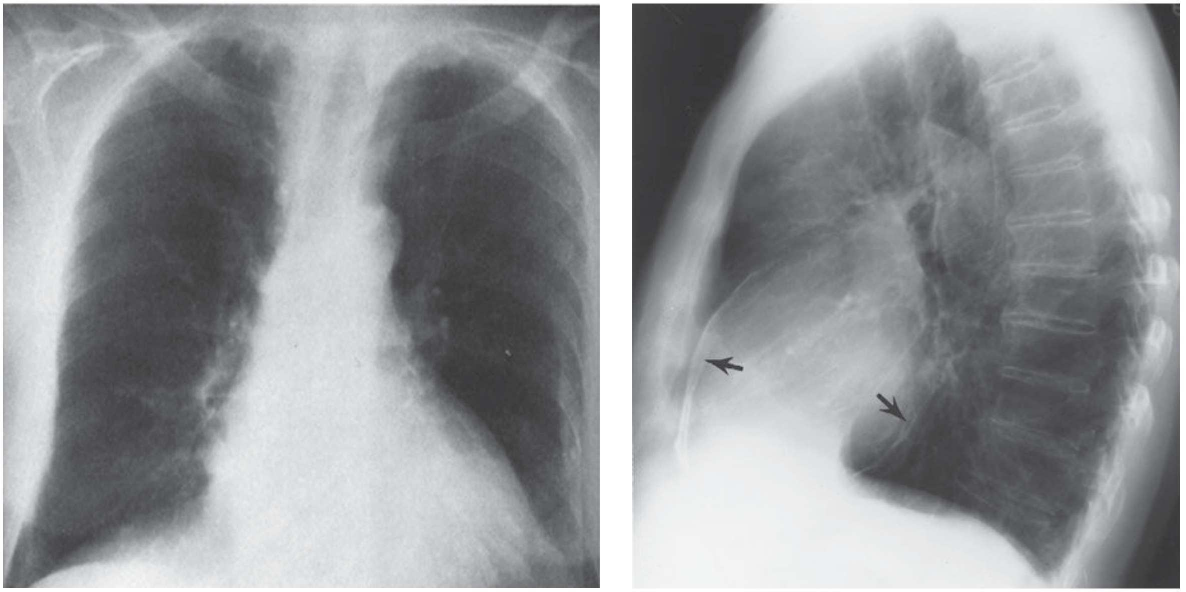

A B

▲ **Figure 3-55.** Case 3-22: 70-year-old woman who has peripheral edema and jugular venous distention.

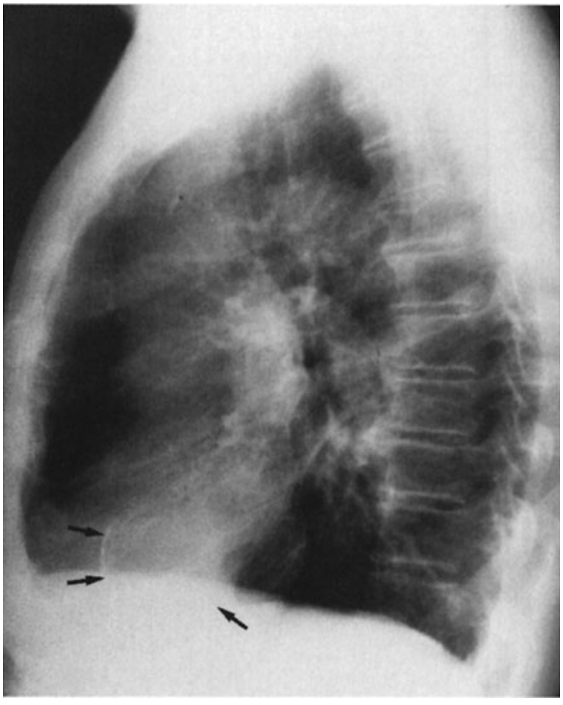

▲ **Figure 3-56.** Case 3-23: Lateral chest radiograph in a 65-year-old man with a long history of hypertension hospitalized 6 years ago with an acute illness.

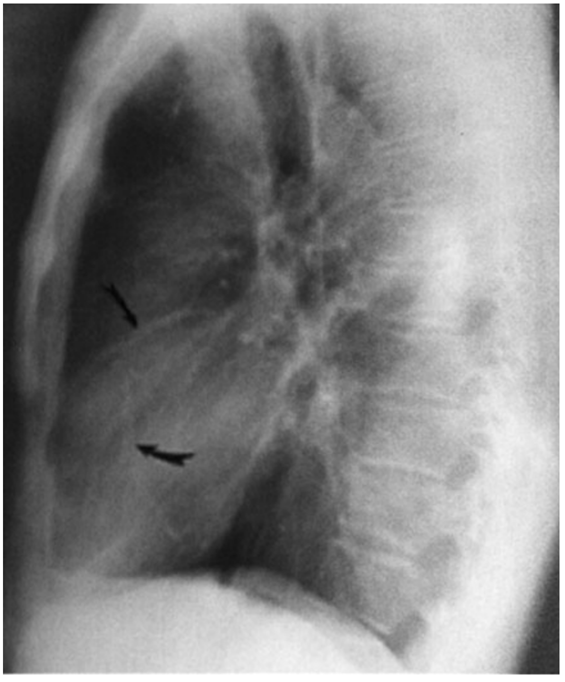

▲ **Figure 3-57.** Case 3-24: Lateral chest radiograph in a 66-year-old man with long-standing diabetes mellitus.

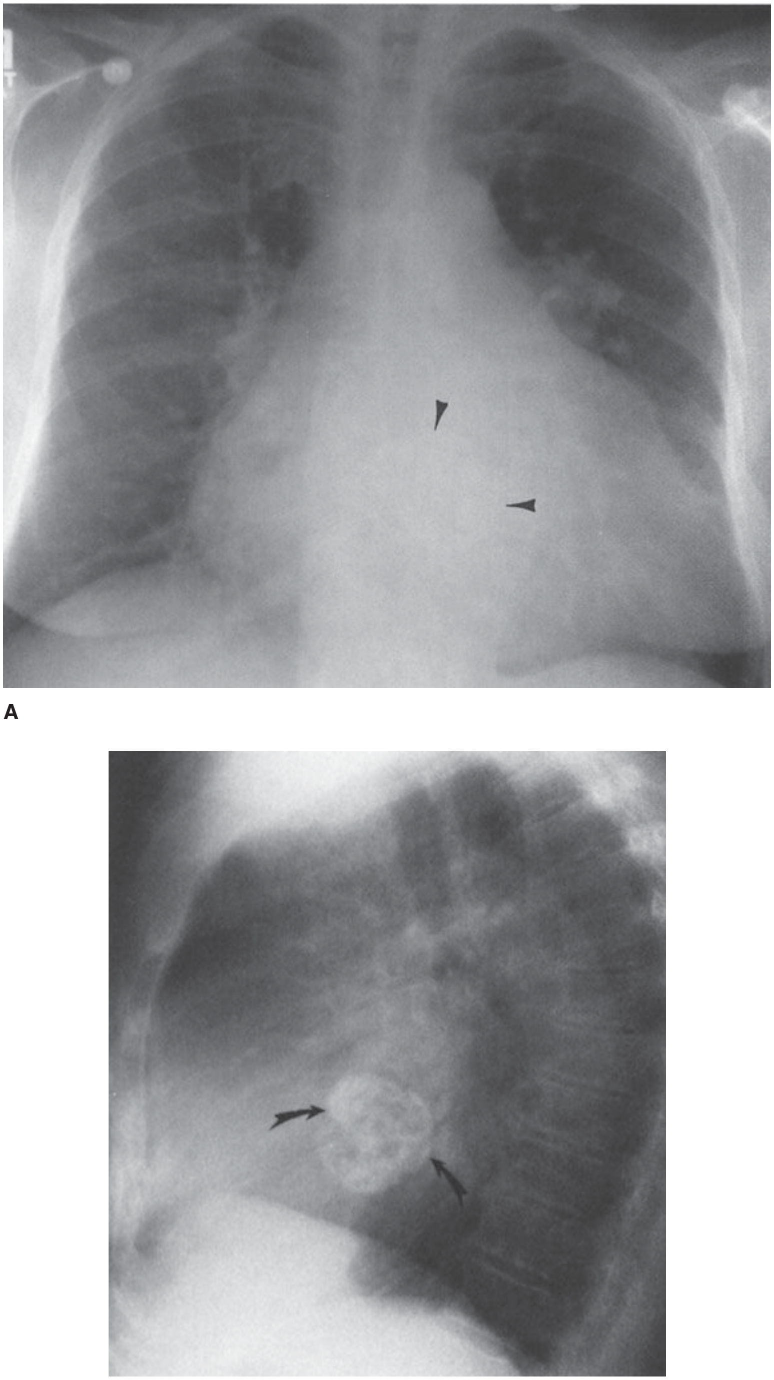

A

B

▲ **Figure 3-58.** Case 3-25. PA and lateral chest radiographs in a woman with shortness of breath and decreased exercise tolerance.

C. pulmonary embolus calcification.
D. aortic valve calcification.
E. mitral valve calcification.

Radiographic Findings

3-21. The PA and lateral chest radiographs (Figure 3-54) show curvilinear coarse calcifications in the mitral annulus (curve arrow) and linear calcification (straight arrow) reside in the aortic value, best seen on the lateral projection (C is the correct answer to Question 3-21).

3-22. This case (Figure 3-55) shows pericardial calcification in a woman who had viral pericarditis as a young child (B is the correct answer to Question 3-22). Note that the calcification is seen much better on the lateral view.

3-23. The chest radiograph in this case (Figure 3-56) shows linear calcification (arrows) in a focal area overlying the left ventricle. This calcification resides in a left ventricular aneurysm that this man developed after a myocardial infarction 6 years earlier (E is the correct answer to Question 3-23).

3-24. The lateral chest radiograph in this case (Figure 3-57) shows linear tram-track calcifications overlying the course of the coronary arteries. These calcifications represent coronary artery atherosclerosis in a patient with long-standing diabetes (D is the correct answer to Question 3-24).

3-25. In this case (Figure 3-58), a circular, heavily calcified area overlying the left atrium is seen in both the PA (arrowheads) and lateral (curved arrows) projections. These calcifications resided within a left atrial myxoma that was causing the patient's symptoms of shortness of breath and decreased exercise tolerance (B is the correct answer to Question 3-25).

Discussion

Calcifications, present in almost any area of the cardiovascular system, may be either metastatic or dystrophic in origin. Metastatic calcifications are usually caused by soft-tissue deposition of calcium due to hypercalcemia of any cause. Dystrophic soft-tissue calcifications are responses to tissue injury or degeneration and have no metabolic cause. They can be seen in practically any of the soft-tissue components of the cardiovascular system. We concentrate here on calcifications that can be seen on the conventional radiograph, although CT is a more sensitive test for detecting calcium. Calcium scoring has become an accepted way of assessing the degree of atherosclerosis in the coronary arteries, but provides mainly risk stratification rather than site-specific information on stenosis. This technique has been shown to provide risk stratification data that are additive to traditional clinical data. The most common site of calcification seen on the conventional chest radiograph is within the aorta, usually in elderly patients with long-standing atherosclerotic disease or diabetes. In this instance, the calcification is linear and is associated with the aortic wall. These calcifications may also be present in aneurysms (see Figure 3-34).

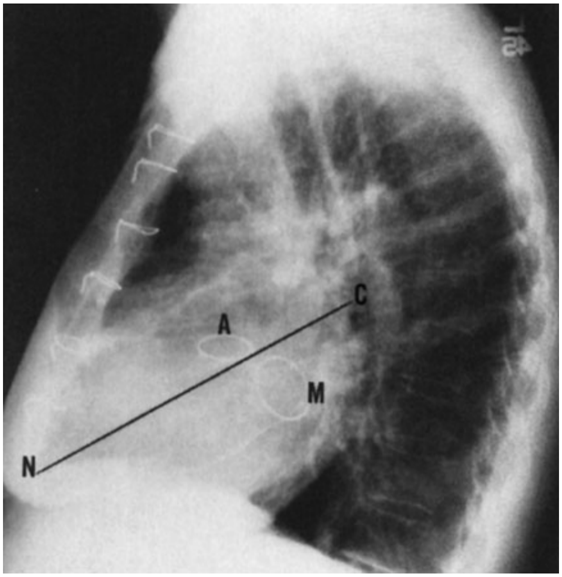

▲ **Figure 3-59.** Lateral view of a patient who had undergone replacement of the aortic (A) and mitral (M) valves. The line C to N connects the carina and the anterior cardiophrenic angle. Aortic valves usually lie above this line and mitral valves below it.

The aortic valve and mitral valve annulus are the most common intracardiac regions to demonstrate dystrophic calcification, usually secondary to long-standing stenosis or insufficiency from rheumatic fever. Bicuspid valves may also show this type of calcification. The lateral film is best for deciding which valve is calcified. A line drawn from the hilum (C) obliquely and downward to intersect the anterior cardiophrenic angle (N) will project behind aortic calcifications (A) (Figure 3-59). Calcifications that lie in back of this line are usually mitral annulus calcifications (M) (Figure 3-59). The presence of mitral annular calcification has been shown to predict the presence of carotid atherosclerosis and therefore may be associated with stroke.

Pericardial calcification as in Case 3-22 (Figure 3-55) is seen in approximately 50% of patients with constrictive pericarditis. It has a characteristic curvilinear appearance outlining the location of the pericardium and is most often seen along the right heart border (Figure 3-55).

Myocardial calcification, as is seen in left ventricular aneurysms, was discussed in the exercise on altered cardiac contour and is shown in a slightly different form in Case 3-23 (Figure 3-56). Thin, focal, linear calcifications overlying the left ventricle should be considered as aneurysms, and echocardiography, CT, and MR imaging are all useful examinations to confirm this diagnosis.

Calcifications within the wall of the coronary arteries, as exhibited in Case 3-24 (Figure 3-57), are recognized on conventional radiographs as thin, linear, calcific deposits corresponding to the course of the coronary arteries. When discovered by conventional radiographs, it is a late finding of atherosclerosis, and these patients have a high incidence of obstructive coronary artery disease.

Case 3-25 (Figure 3-58) is an example of the rare primary cardiac neoplasm that may calcify and be detected initially on the plain film. The cardiac tumor that most commonly calcifies is the left atrial myxoma, and calcification occurs in about 10% of these lesions (Figure 3-58). Rarely, myocardial metastatic disease (such as osteosarcoma) or other primary cardiac tumors may calcify. Finally, primary mediastinal neoplasms such as teratomas may rarely show calcification. In these patients, CT should be performed for diagnosis.

EXERCISE 3-6. MONITORING DEVICES

3-26. The complication of Swan-Ganz catheter placement in Case 3-26 (Figure 3-60) is
- **A.** malposition of the tip.
- **B.** pneumothorax.
- **C.** perforation.
- **D.** catheter coiling.
- **E.** catheter thrombosis.

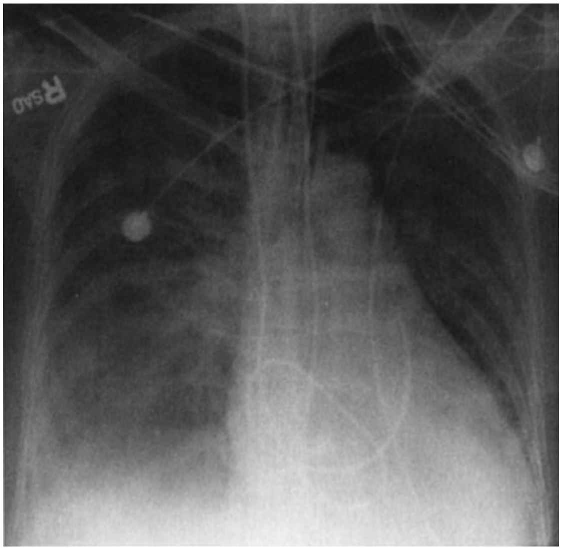

▲ **Figure 3-60.** Case 3-26: Routine supine portable chest radiograph obtained after SG catheter placement.

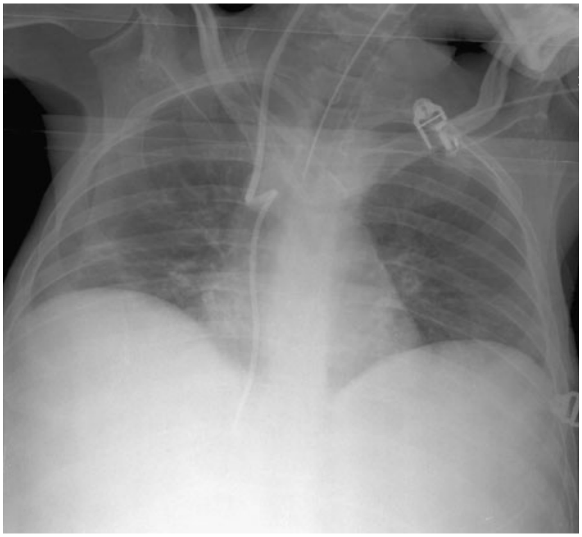

▲ **Figure 3-61.** Case 3-27: Supine chest radiograph obtained after difficult CVP placement.

3-27. The tip of the central venous catheter in Case 3-27 (Figure 3-61) is in the
- **A.** inferior vena cava.
- **B.** right ventricle.
- **C.** azygous vein.
- **D.** hemiazygous vein.
- **E.** middle hepatic vein.

3-28. The malpositioned catheter in Case 3-28 (Figure 3-62) is a(n)
- **A.** tracheostomy tube.
- **B.** intraaortic balloon pump.
- **C.** Swan-Ganz catheter.
- **D.** nasogastric tube.
- **E.** Blakemore tube.

3-29. The complication with the pacemaker shown in Case 3-29 (Figure 3-63) is
- **A.** right atrial lead dislodgement.
- **B.** right ventricular perforation.
- **C.** pneumothorax.
- **D.** right ventricular lead dislodgement.
- **E.** diaphragmatic pacing.

3-30. The catheter in Case 3-30 (Figure 3-64, arrow) is in the
- **A.** lung parenchyma.
- **B.** left superior vena cava.
- **C.** left upper lobe pulmonary vein.
- **D.** descending thoracic aorta.
- **E.** left pulmonary artery.

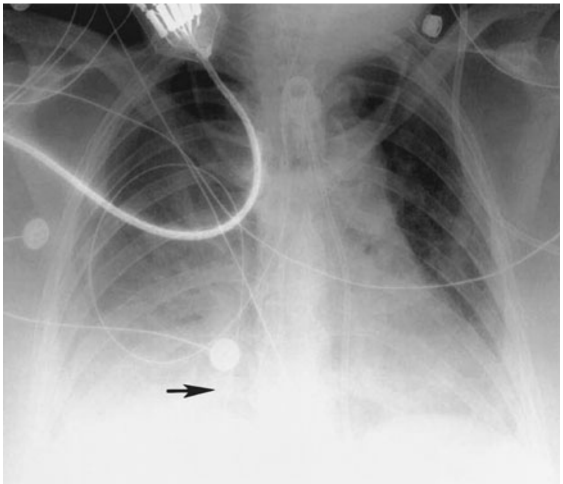

▲ **Figure 3-62.** Case 3-28: Routine supine chest radiograph in ICU patient after placement of several lines and tubes.

Radiographic Findings

3-26. The supine portable chest radiograph obtained after SG catheter placement in this case (Figure 3-60) is coiled within the right ventricle before it terminates in the proximal main pulmonary artery (D is the correct answer to Question 3-26). This coiling of the catheter in the right ventricle may cause thrombosis or arrhythmia, and it is necessary to reposition this catheter.

3-27. The supine chest radiograph in this case (Figure 3-61) shows two turns in the course of the catheter after a difficult CVP placement. The catheter turns posteriorly into the azygous vein and then descends on the right in the hemiazygous system (D is the correct answer to Question 3-27).

3-28. In this case (Figure 3-62), the chest radiograph obtained shows a nasogastric tube extending down the right main bronchus into the right lung (Figure 3-62, arrow) (D is the correct answer to Question 3-28).

3-29. In this case (Figure 3-63), the tip of the right ventricular pacemaker lead does not extend to the expected border of the myocardium. Usually a slight shouldering is encountered as the lead crosses the tricuspid valve. In some cases, the right ventricular lead may be positioned higher along the interventricular septum and may take a more horizontal course. A vertical course, as in this case, indicates the tip is not lodged in the myocardium. This positioning results in a lack of normal pacing function. The right atrial lead is in an appropriate position. (D is the correct answer to Question 3-29.)

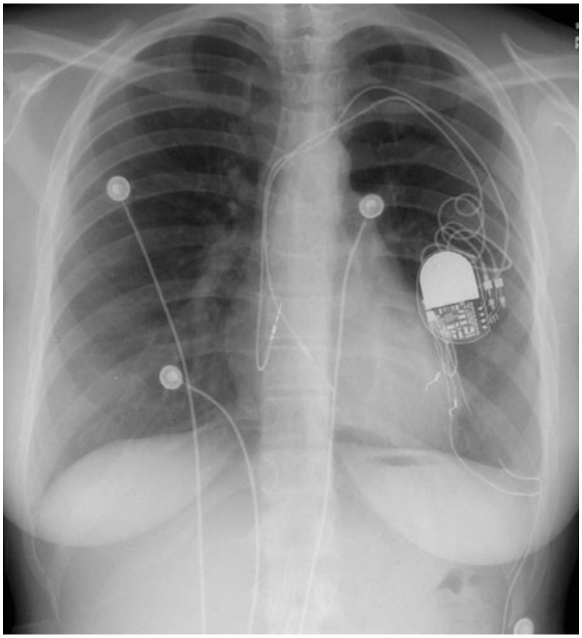

▲ **Figure 3-63.** Case 3-29: Chest radiograph obtained following pacemaker insertion.

3-30. This case (Figure 3-64) is a patient who has anomalous venous return from the upper lobe. The catheter placed in the left internal jugular vein courses into the left brachiocephalic vein and, rather than crossing the

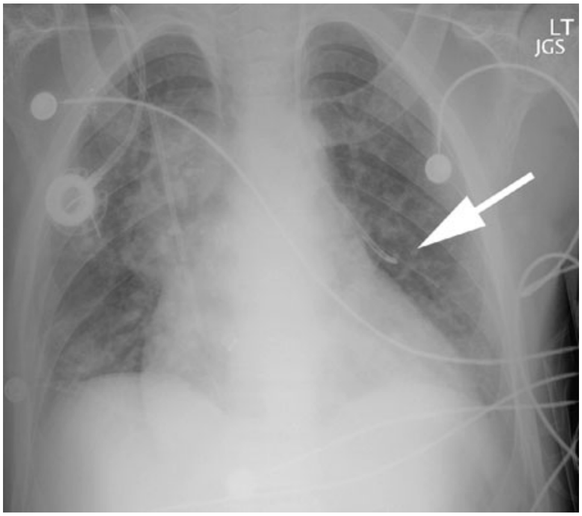

▲ **Figure 3-64.** Case 3-30: Chest radiograph obtained following central venous catheter placement with return of low-pressure oxygenated blood.

midline to the superior vena cava, extends into the left superior pulmonary vein (C is the correct answer to Question 3-30). Because it is carrying blood returning from the pulmonary capillary bed, it is oxygenated like systemic arterial blood, but comes from a low-pressure system.

Discussion

As mentioned in the subsection on monitoring devices within the chapter, a variety of catheters can be inserted into the heart and great vessels to monitor various hemodynamic parameters, particularly in the ICU setting. Table 3-3 lists the most common monitoring devices, and Table 3-4 shows the most common complications from placement of these devices. It is important to trace out and account for each catheter individually. For instance, the nasogastric tube might have initially been mistaken for an ECG lead. The result of instilling fluid through this tube could have been disastrous. Even so, the result of this placement was a pneumothorax. We have reviewed the normal placement of catheters and some of the more common related complications. The student should be familiar with this aspect of radiography in the ICU setting, and the references cited at the end of the chapter will provide further in-depth learning.

CONCLUSION

The heart and great vessels present an interesting and demanding diagnostic challenge to the physician. A thorough history and physical examination are the initial steps to generate a differential diagnosis and to decide which imaging tests are necessary to limit these possibilities. The choice of imaging tests should ideally be made in consultation with the radiologist, taking into consideration potential morbidity, cost, availability of the technology, and the interest and expertise of the radiologist. Students should be aware that careful decision making has the potential to decrease the cost of medical care in the United States.

Acknowledgments *Special thanks to my colleague Gregory Braden, MD, for providing Figure 3-12 for use in this chapter.*

SUGGESTED READING

1. Bastarrika G, Lee YS, Huda W, Ruzsics B, Costello P, Schoepf UJ. CT of coronary artery disease. *Radiology.* 2009;253:317-338.
2. Bengel FM, Takahiro H, Javadi MS, Lautamaki R. Cardiac positron emission tomography. *J Am Coll Cardiol.* 2009;54:1-15.
3. Chen JT: *Essentials of Cardiac Imaging*. Philadelphia: Lippincott-Raven; 1997.
4. Finn JP, Nael K, Deshpande V, Ratib O, Laub G. Cardiac MR imaging: state of the art technology. *Radiology.* 2006;241:338-354.
5. Higgins CB: *Essentials of Cardiac Radiology and Imaging*. Philadelphia: Lippincott; 1992.
6. Lee VS: *Cardiovascular MR Imaging: Physical Principles to Practical Protocols*. Philadelphia: Lippincott Williams & Wilkins; 2005.
7. Miller SW, Abbara S, Boxt L: *Cardiac Radiology: The Requisites*. 3rd ed. St. Louis, Mo: Mosby; 2009.
8. Remy-Jardin M, Remy J, Baert AL: *Integrated Cardiothoracic Imaging with MDCT*. New York: Springer; 2008.
9. Vitola JV, Delbeke D: *Nuclear Cardiology and Correlative Imaging: A Teaching File*. New York: Springer; 2004.
10. Warnes CA: *Adult Congenital Heart Disease*. Hoboken, NJ: Wiley-Blackwell; 2009.

Radiology of the Chest

4

Caroline Chiles, MD
Shannon M. Gulla, MD

INTRODUCTION

The chest radiograph is the most frequently performed radiographic study in the United States. It should almost always be the first radiologic study ordered for evaluation of diseases of the thorax. The natural contrast of the aerated lungs provides a window into the body to evaluate the patient for diseases involving the heart, lungs, pleurae, tracheobronchial tree, esophagus, thoracic lymph nodes, thoracic skeleton, chest wall, and upper abdomen. In both acute and chronic illnesses, the chest radiograph allows one to detect a disease and monitor its response to therapy. For many disease processes (eg, pneumonia and congestive heart failure) the diagnosis can be established and the disease followed to resolution with no further imaging studies. There are limitations to the chest radiograph, and diseases may not be sufficiently advanced to be detected or may not result in detectable abnormalities. Other imaging methods are needed to complement the conventional chest radiograph. These imaging methods include computed tomography (CT), positron emission tomography/computed tomography (PET/CT) and other radionuclide studies, magnetic resonance (MR) imaging, and ultrasound (US). These techniques, their clinical uses, and case studies are included in this chapter.

TECHNIQUES

Conventional Radiography

The Posteroanterior and Lateral Chest Radiograph

The simplest conventional study of the chest is a posteroanterior and lateral chest radiograph taken in a radiographic unit specially designed for these studies. The x-rays travel through the patient and expose a receptor from which the image is recorded. Most commonly, digital receptors are used, although a receptor utilizing an intensifying screen and radiographic film remains in some use as well. Computed radiography and large field-of-view image intensifiers are two types of digital receptors. The digital images may be printed on film by laser printers but are generally viewed on monitors. The two views of a chest radiograph are taken in projections at 90 degrees to each other with the patient's breath held at the end of a maximum inspiration. The first view is obtained as the patient faces the receptor with the x-ray beam source positioned 6 feet behind him. Because the x-ray beam travels in a posterior-to-anterior direction, this view is called a posteroanterior (PA) chest radiograph. Another view is then obtained with the patient turned 90 degrees and the left side against the receptor and arms overhead. The x-ray beam travels from right to left through the patient, and this is called a left lateral view. Anatomic features of the chest that are readily identifiable on conventional radiographs are shown in Figures 4-1 and 4-2.

Other Radiographic Projections

In some clinical situations, patients may not be able to stand or sit upright for the conventional PA and lateral radiographs, and an image must be taken with the patient's back turned to the receptor and the x-ray beam traversing the patient in an anterior-to-posterior direction. These radiographs are called anteroposterior (AP) radiographs. They may be taken in the x-ray department but are more commonly obtained as portable studies at the patient's bedside.

Images may also be obtained with the patient lying on one side in a decubitus position with the x-ray beam traversing the patient either PA or AP along a horizontal plane. These images are designated as lateral decubitus images (see Figure 4-63c). A left lateral decubitus radiograph indicates that the left side of the patient is dependent against the table. A right lateral decubitus radiograph indicates that the right side of the patient is dependent against the table.

The Portable Chest Radiograph

If the clinical situation prevents the patient from coming to the radiology department, a chest radiograph may be obtained at the patient's bedside, and these are almost always AP radiographs. The AP portable radiograph does not provide as much information as PA and lateral chest radiographs for a number of reasons. Because it is a single view, lesions are not as easily or accurately localized along the AP axis of the thorax. The patients for whom these images are obtained are usually quite ill and cannot be positioned as well as patients traveling to the x-ray department. An ill patient may not be able to cooperate by holding his breath at full inspiration. A mobile x-ray generator is typically not as powerful as a fixed x-ray generator, and longer exposure times therefore are necessary to obtain sufficient exposure. The quality of portable chest radiographs, therefore, is often inferior to that of PA and lateral radiographs, as a result of both respiratory and cardiac motion. X-ray grids are used to reduce scatter radiation and improve image quality. Grids are used for most conventional chest radiographs done in radiology departments where fixed equipment is present. Grids are not usually used for portable radiographs, and the result is a high proportion of scattered x-rays, which degrade the image. Paradoxically, the portable radiograph may be more expensive than a conventional PA and lateral chest radiograph, owing to extra labor and equipment costs in obtaining a bedside radiograph.

Computed Tomography of the Chest

Computed tomography is described in detail in Chapter 1. For CT examinations of the chest, intravenous contrast material is frequently administered for opacification of arteries and veins within the mediastinum and hila to facilitate the recognition of abnormal masses or lymph nodes. Anatomic features of the chest that are readily identifiable on CT scans are shown in Figures 4-3 and 4-4.

Nuclear Medicine Perfusion Imaging of the Chest

Nuclear medicine techniques used in evaluating diseases of the thorax include ventilation-perfusion (V/Q) scanning and scanning with tumor-seeking radiopharmaceuticals for tumor staging. The V/Q scan may be used for patients with suspected pulmonary thromboembolism and who have contrast allergy or renal failure. The V/Q scan is noninvasive, and when results are negative, fewer than 10% of patients have pulmonary thromboembolism. The ventilation study is typically performed with the patient inhaling 10 to 30 mCi of xenon-133 while images are obtained with a scintillation camera (Figure 4-5A). Wash-in images are obtained for two consecutive 120-second periods, an equilibrium image is obtained, and then wash-out images are obtained over 30- to 60-second periods in posterior and left and right posterior oblique projections. This portion of the study takes about 15 minutes. The perfusion scan is obtained by intravenously injecting 2 to 4 mCi of technetium-99m-labeled macroaggregated albumin containing 200,000 to 700,000 particles. The particles range in size from 10 to 100 μm, and they lodge in capillaries and capillary arterioles, accurately reflecting pulmonary blood flow (Figure 4-5B). The scintillation camera is

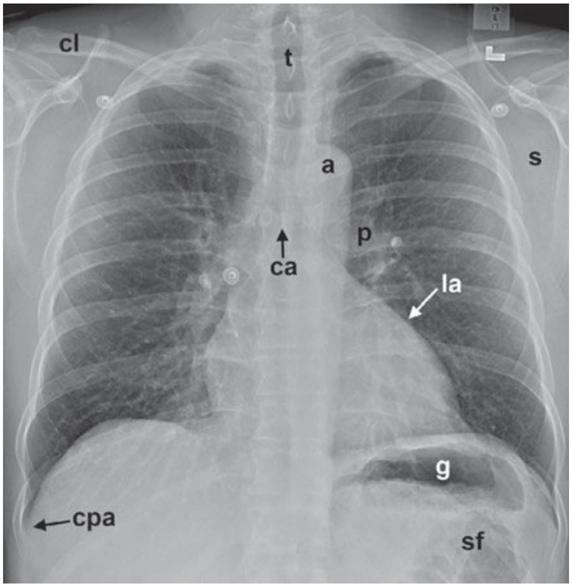

A

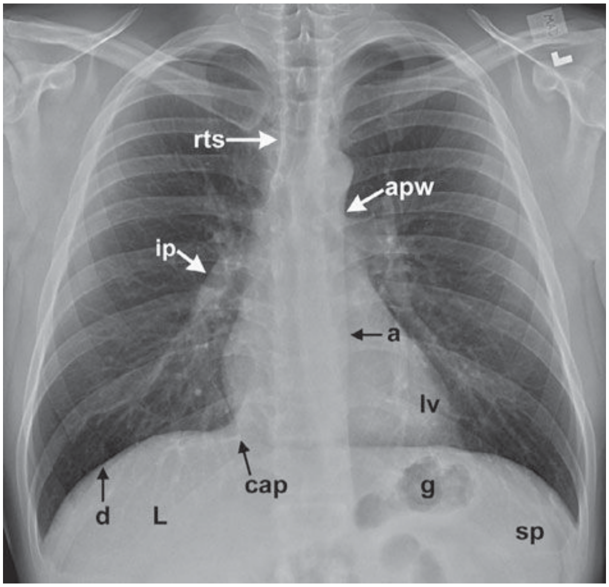

B

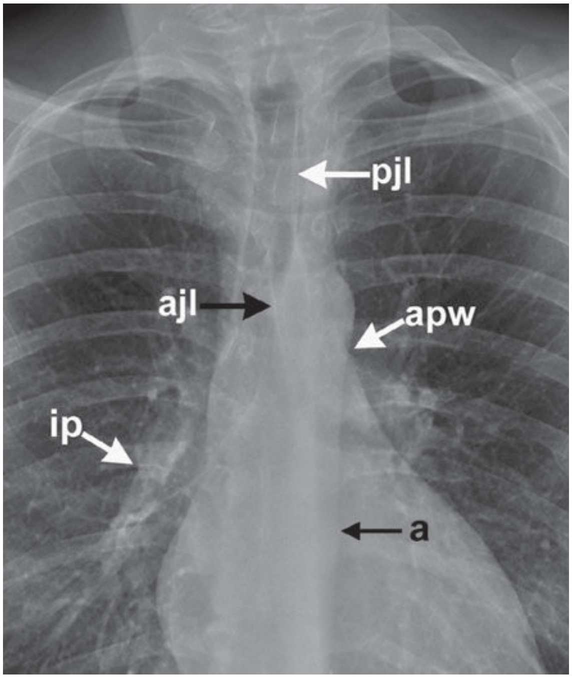

C

▲ **Figure 4-1.** (**A–C**) Normal radiographic anatomy. Posteroanterior chest radiographs. a, aorta; ajl, anterior junction line; apw, aortopulmonary window; ca, carina; cap, cardiophrenic angle; cl, clavicle; cpa, costophrenic angle; d, diaphragm; g, gastric air bubble; ip, interlobar (or descending) pulmonary artery; L, liver; la, left atrium; lv, left ventricle; p, main pulmonary artery; pjl, posterior junction line; rts, right tracheal (or paratracheal) stripe; s, scapula; sf, splenic flexure of colon; sp, spleen; t, trachea.

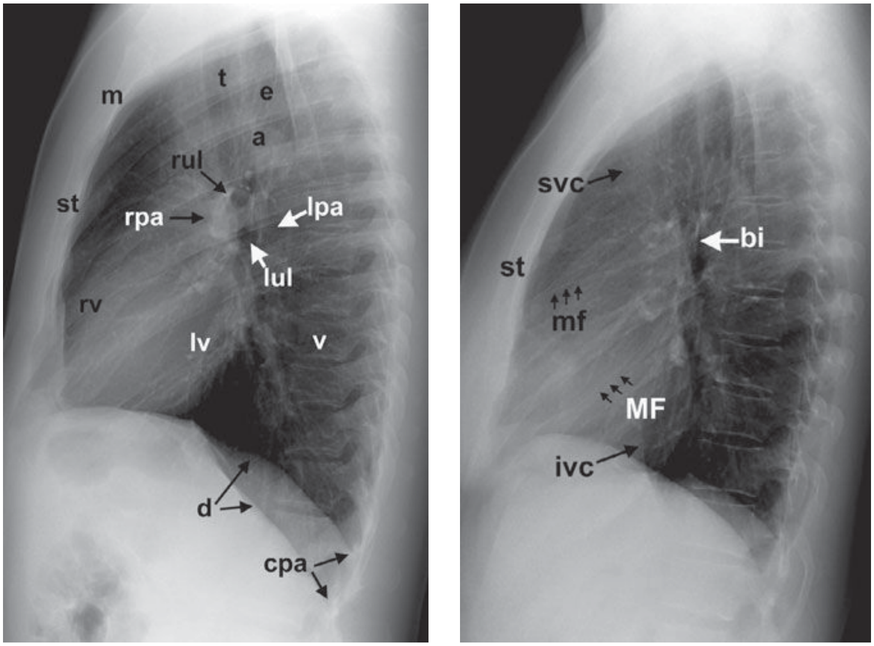

A B

▲ **Figure 4-2.** (**A,B**) Normal radiographic anatomy. Lateral chest radiographs. a, aorta; bi, bronchus intermedius; cpa, costophrenic angle; d, diaphragm; e, esophagus; ivc, inferior vena cava; lpa, left pulmonary artery; lul, left upper lobe bronchus; lv, left ventricle; m, manubrium; mf, minor fissure; MF, major fissure; rpa, right pulmonary artery; rul, right upper lobe bronchus; rv, right ventricle; st, sternum; svc, superior vena cava; t, trachea; v, vertebral body.

set so that it obtains anterior, posterior, both posterior oblique, and both anterior oblique projections for 750,000 counts per image. The perfusion study takes about 30 minutes to perform.

Positron Emission Tomography/Computed Tomography Imaging of the Chest

Tomography is also available for radionuclide imaging. A PET scanner resembles a CT scanner and uses positron emitters (fluorine-18 [F-18] or carbon-11 [C-11]). Today, the most widely used positron emitter is F-18-fluorodeoxyglucose (FDG), which is used as a metabolic tracer. The raised metabolic rate can be used to distinguish neoplasm and inflammation from normal tissue. Although PET provides tomographic images, the spatial resolution (0.7 to 1.0 cm) is somewhat inferior to that of CT. This spatial resolution is improved by utilizing PET/CT fusion imaging in which a patient receives both a PET scan with F-18 FDG as well as a CT with or without contrast. These images can then be overlaid, or fused (Figure 4-6), to combine the spatial resolution of CT with the localization power of radionuclide imaging.

Magnetic Resonance Imaging of the Chest

The principles and applications of MR are described in Chapter 1. Anatomic features of the chest that are readily identifiable on MR images are shown in Figures 4-7 and 4-8.

Ultrasonography of the Chest

Ultrasound is described in detail in Chapter 1. Ultrasound of the chest is typically performed to evaluate fluid collections within the pleural space. Ultrasound may be used to guide thoracentesis, especially when the fluid collection is small or loculated. Less frequently, ultrasound is utilized to guide percutaneous biopsy of mediastinal or peripleural lung lesions. Advances in image fusion also allow fusion of ultrasound images with a separately performed CT examination, which can be useful for ultrasound-guided biopsies in the thorax.

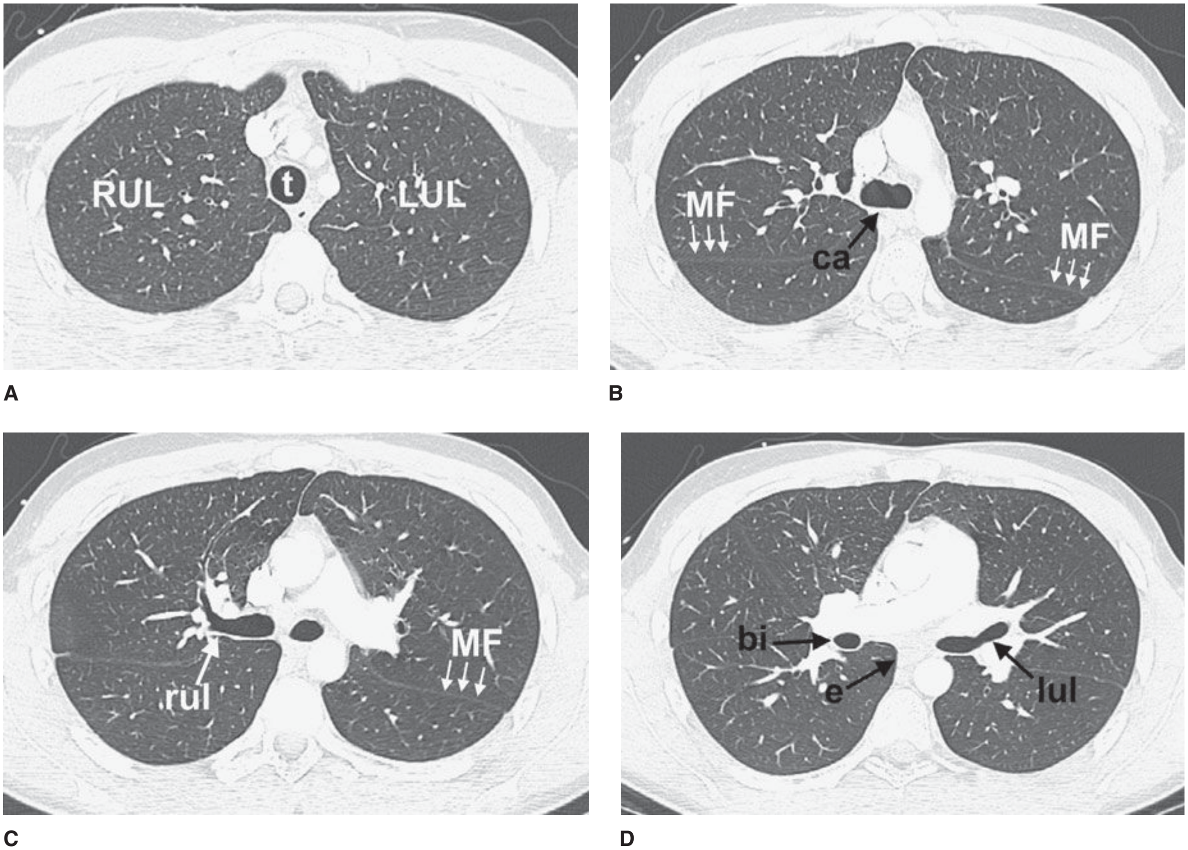

▲ **Figure 4-3.** (**A–H**) Normal CT anatomy. Axial scans of the chest, contiguous slices at approximately 1 cm collimation, lung window settings. bb, basilar segmental bronchi of lower lobes; bi, bronchus intermedius; ca, carina; e, esophagus; Li, lingula segment of the left upper lobe; LLL, left lower lobe; lul, left upper lobe bronchus; LUL, left upper lobe; MF, major fissure; RLL, right lower lobe; RML, right middle lobe; rml, right middle lobe bronchus; RUL, right upper lobe; rul, right upper lobe bronchus; ss, bronchus to superior segment of lower lobe; t, trachea.

TECHNIQUE SELECTION

The number of diseases and clinical situations for which a chest radiograph may be indicated is so large that an exhaustive listing of individual indications is prohibitive. As a general rule, however, conventional radiographs should be obtained for any patient with symptoms suggesting disease of the heart, lungs, mediastinum, or chest wall. In addition, a chest radiograph is indicated for patients with systemic diseases that have a high likelihood of secondary involvement of those structures. Examples of the former are pneumonia and congestive heart failure and of the latter are a primary extrathoracic neoplasm and connective tissue disease.

In an acutely ill patient, the portable chest radiograph is an invaluable tool for monitoring the patient's cardiopulmonary status. These radiographs are also used for monitoring of life-support hardware, such as central venous access catheters, nasogastric tubes, and endotracheal tubes.

Fluoroscopy provides real-time imaging of the chest. Fluoroscopy may be used to evaluate the motion of the diaphragm in a patient with suspected diaphragmatic paralysis. A paralyzed hemidiaphragm has sluggish motion as the patient breathes, and as the patient takes in a quick breath of air, it moves paradoxically upward as the normal hemidiaphragm moves downward ("sniff test"). Fluoroscopy and fluoroscopically positioned spot images are also useful for

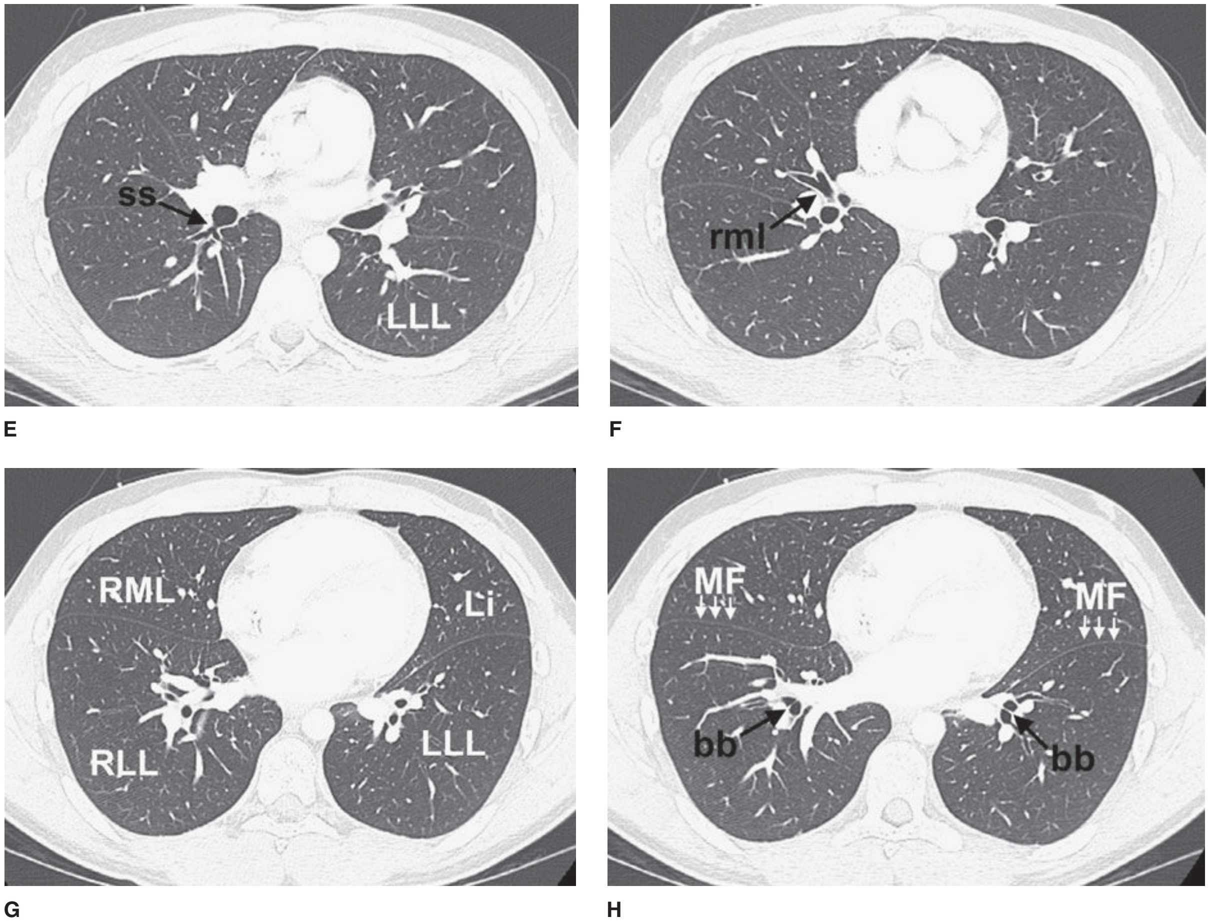

▲ **Figure 4-3.** *(Continued)*

identification of calcification within a pulmonary nodule, within coronary arteries, or within cardiac valves. Fluoroscopic guidance can also be used for percutaneous transthoracic needle biopsy of lung masses.

Because the three dimensions of the thorax are captured on a single two-dimensional chest radiograph, superimposition of structures within the thorax may result in confusing shadows. Because CT provides images without this overlap, it is frequently used to clarify confusing shadows identified on conventional radiographs (Table 4-1). These examinations are also used to detect disease that is occult because of small size or a hidden position. Because of its wider range of density discrimination, CT can demonstrate mediastinal and chest wall abnormalities earlier than is possible with conventional chest radiography. Abnormalities of hilar structures can be identified on CT scans because of the decreased overlap of the complex structures of the hilum. CT scans of the chest are routinely ordered for oncology patients, both for evaluation of the extent of disease at presentation and for monitoring response to therapy or progression of disease. CT is useful for evaluation of the lung

Table 4-1. Major Indications for CT of the Chest

Clarification of abnormal chest radiograph findings
Staging of lung cancer and esophageal cancer
Detecting metastatic disease from extrathoracic malignancy
Evaluation of a solitary pulmonary nodule
Suspected mediastinal or hilar mass
Suspected pleural tumor or empyema
Determining source of hemoptysis (eg, bronchiectasis)
CT-guided percutaneous needle aspiration of lung and mediastinal masses
CT-guided pleural drainage

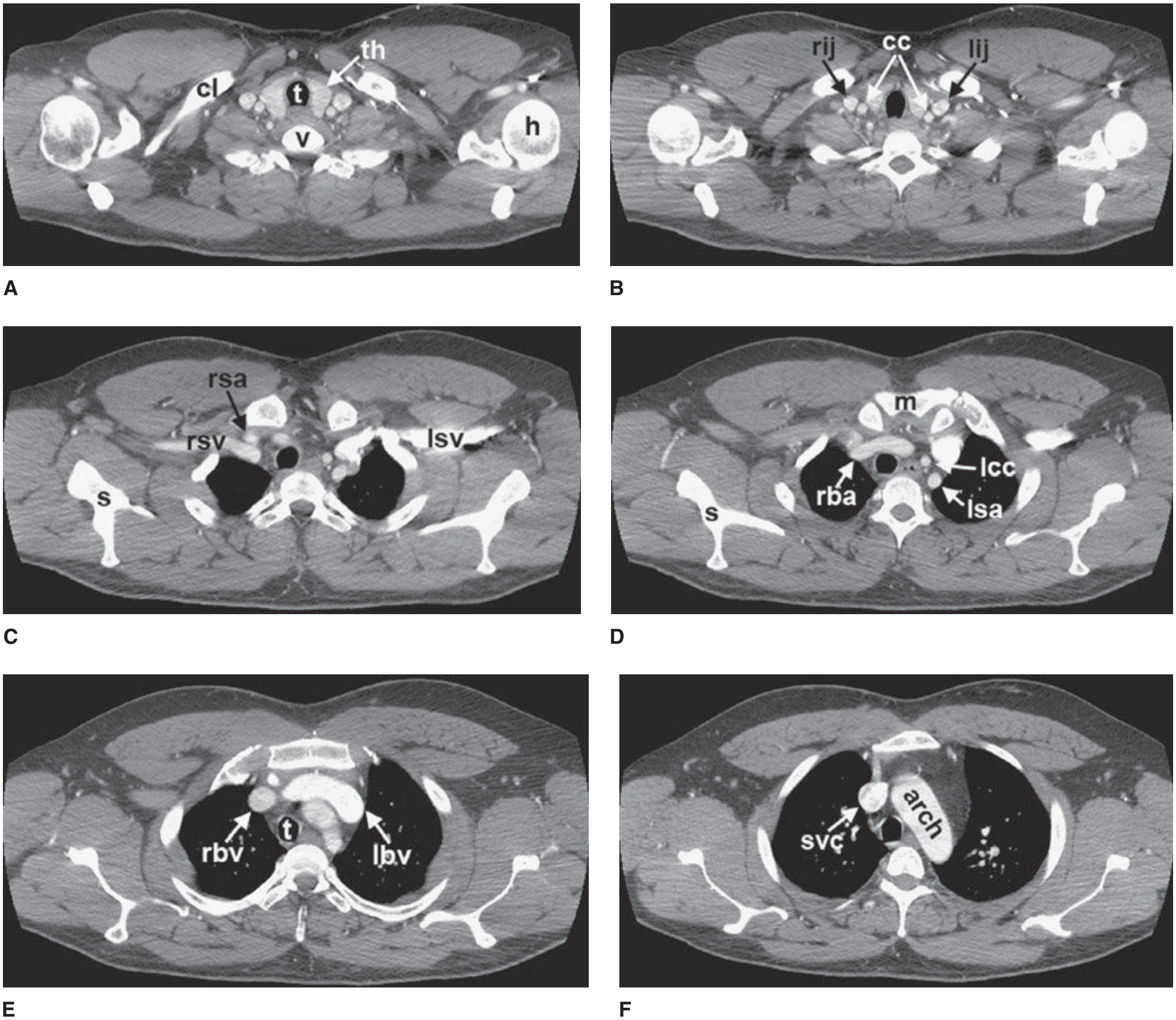

▲ **Figure 4-4.** (**A–N**) Normal CT anatomy. Axial scans of the chest, contiguous slices at approximately 1 cm collimation, soft-tissue (mediastinal) window settings. aa, ascending aorta; arch, transverse section of the aortic arch; azv, azygos vein; cc, common carotid artery; cl, clavicle; cs, coronary sinus; da, descending aorta; e, esophagus; hazv, hemiazygos vein; h, humerus; im, internal mammary artery and vein; ip, interlobar (or descending) pulmonary artery; ipv, inferior pulmonary vein; ivc, inferior vena cava; ivs, interventricular septum; L, liver; la, left atrium; LAD, left anterior descending coronary artery; lbv, left brachiocephalic vein; lcc, left common carotid artery; lij, left internal jugular vein; lpa, left pulmonary artery; lsa, left subclavian artery; lsv, left subclavian vein; lv, left ventricle; lvot, left ventricular outflow tract; m, manubrium; mpa, main pulmonary artery; pc, pericardium; r, rib; ra, right atrium; rba, right brachiocephalic artery; rbv, right bronchiocephalic vein; rij, right internal jugular vein; rpa, right pulmonary artery; rsa, right subclavian artery; rsv, right subclavian vein; rv, right ventricle; rvot, right ventricular outflow tract; s, scapula; sp, spleen; st, sternum; svc, superior vena cava; t, trachea; th, thyroid; v, vertebral body.

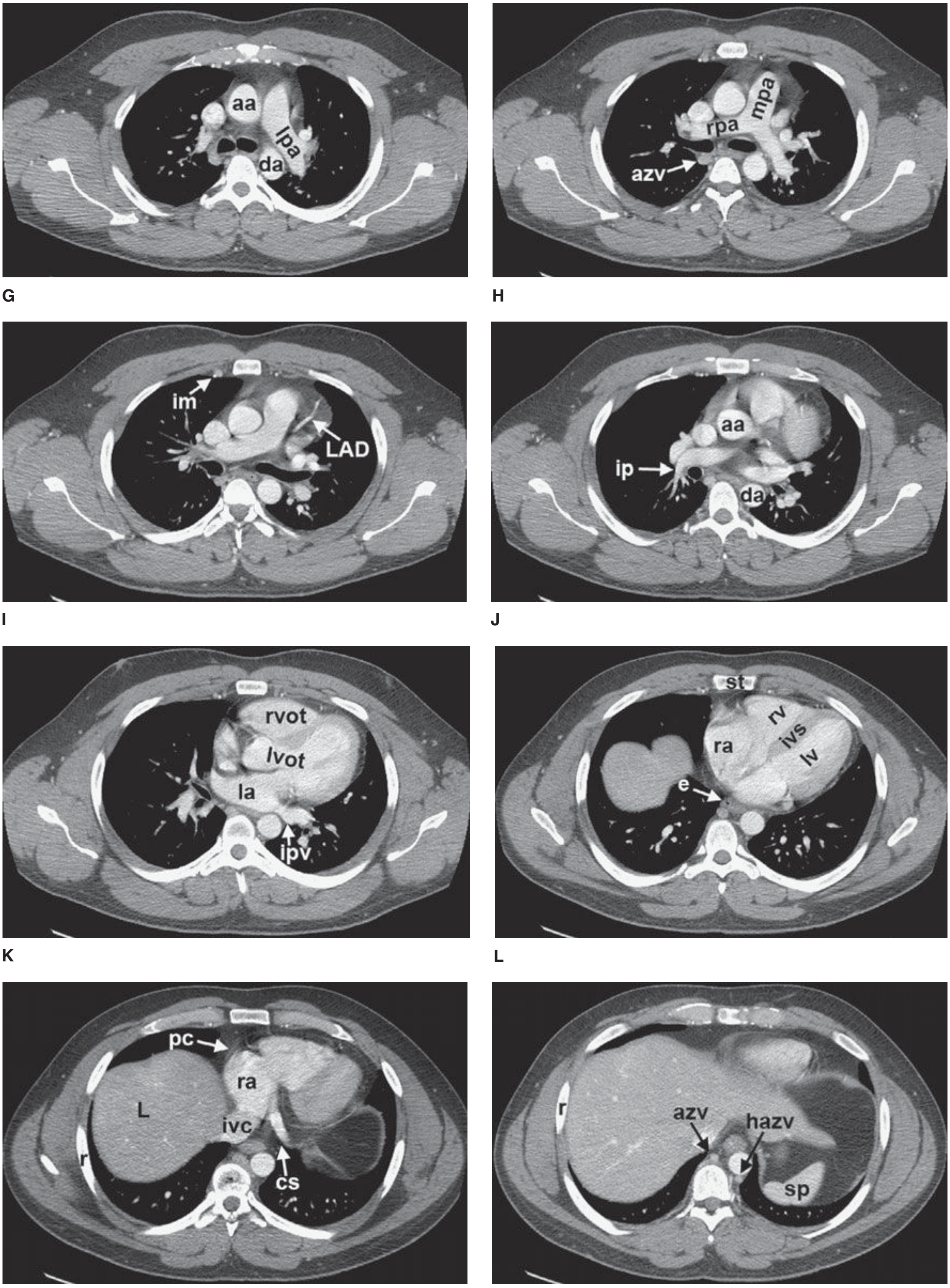

▲ **Figure 4-4.** *(Continued)*

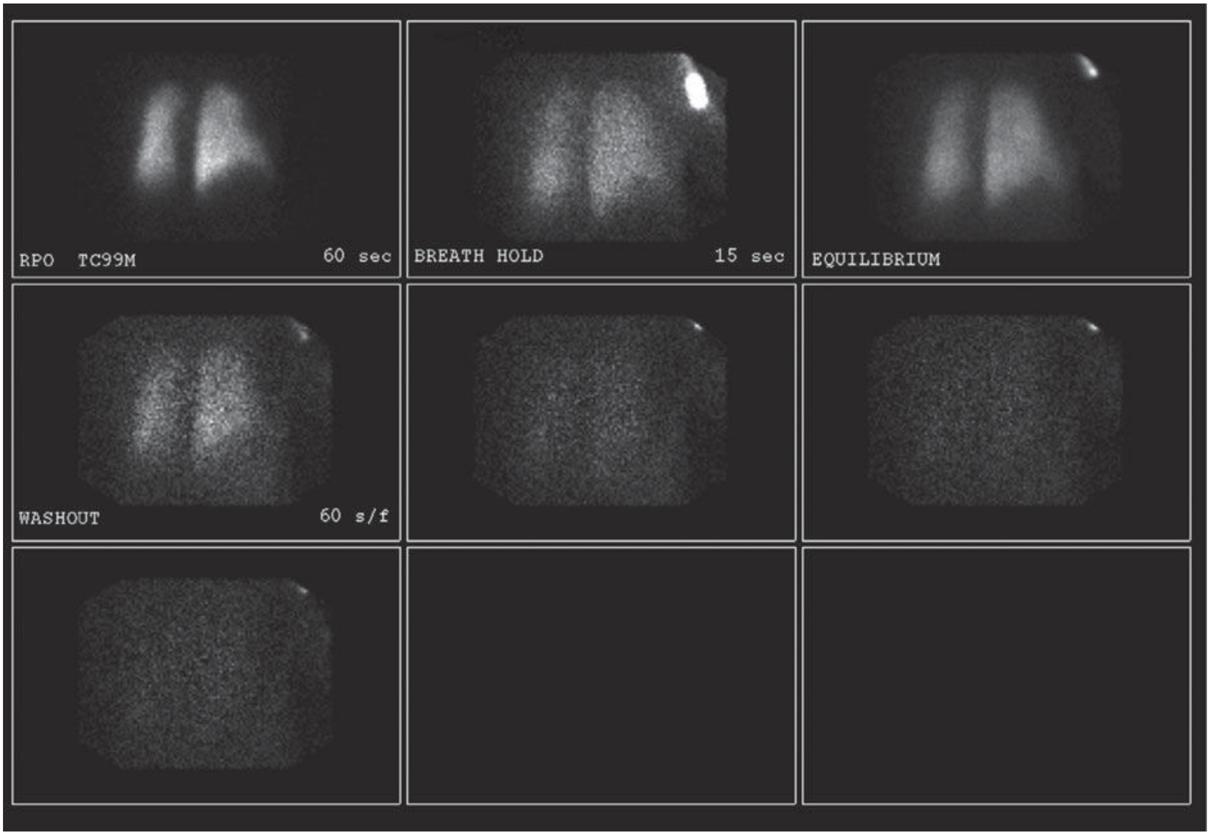

A

▲ **Figure 4-5.** (**A**) Ventilation scan performed in the right posterior oblique projection shows normal wash-in of the xenon-133 gas and no retention of gas in any regions on the wash-out views.

parenchyma, as thin sections (1 to 2 mm thick) reveal great anatomic detail. Thin-section CT (or high-resolution CT [HRCT]) may enable detection of occult pulmonary parenchymal disease and may be used for following the course of known pulmonary disease (Table 4-2). HRCT is especially useful in the diagnosis of interstitial lung diseases. Additionally, CT angiography (CTA) of the chest is particularly useful for the evaluation of vascular pathology as well as pulmonary embolus (Table 4-3). Because intravenous contrast material can be administered, vascular structures may be evaluated and the technique may be useful in patients with aortic dissection, aortic aneurysm, and superior vena caval obstruction. Because the cost of CT is approximately 10 to 20 times that of a PA and lateral chest radiograph, CT is not practical for monitoring the course of diseases on a daily basis.

The diseases and situations for which nuclear medicine techniques are helpful are determined for the most part by the radioactive tracer, and these have been outlined in the technique section (Table 4-4).

Table 4-2. Major Indications for High-Resolution CT of the Chest

Evaluation of acute and chronic pulmonary disease
Evaluation of occult parenchymal disease

Table 4-3. Major Indications for CTA of the Chest

Suspected pulmonary embolism
Suspected aortic dissection
Superior vena cava syndrome

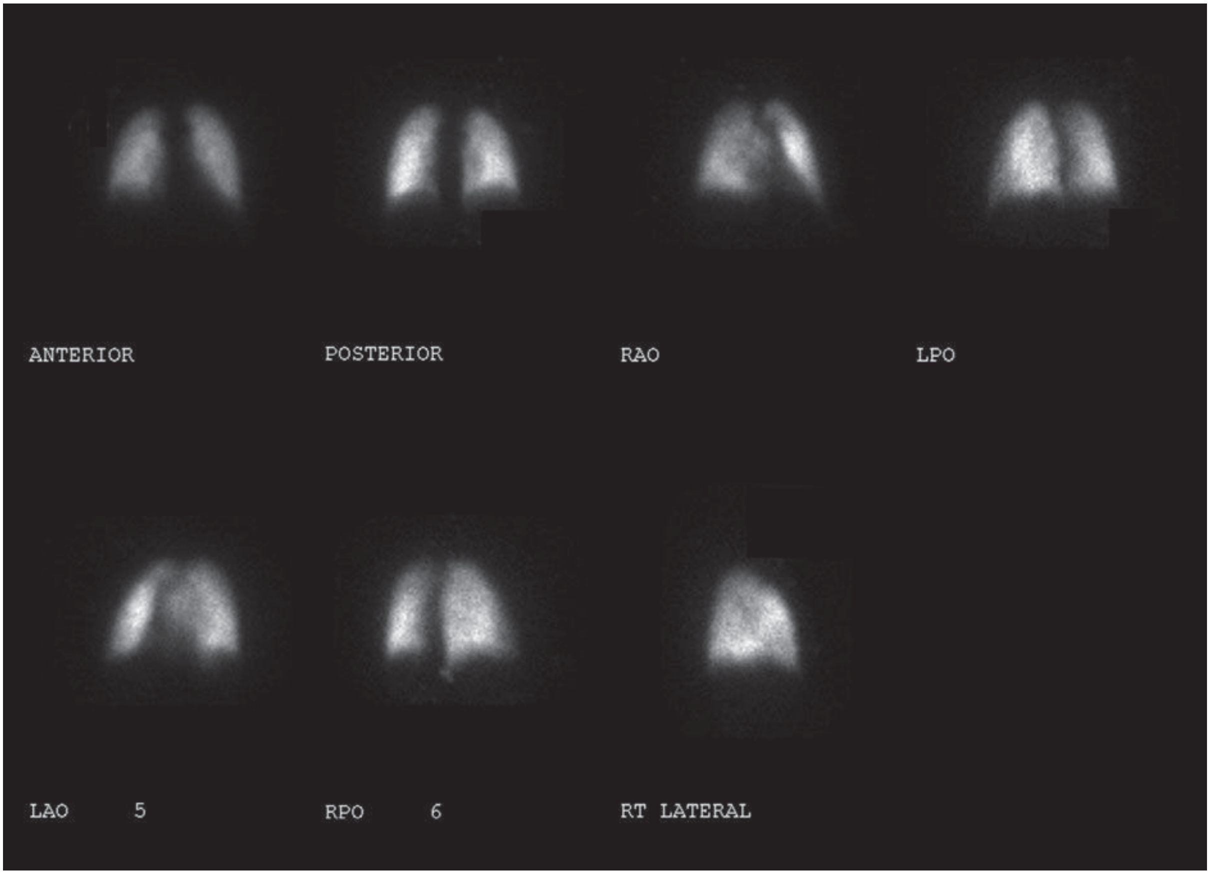

B

▲ **Figure 4-5.** *(Continued)* (**B**) Normal perfusion scan performed in seven projections, shows equal perfusion of radionuclide throughout all segments of the lungs. RAO, right anterior oblique; LAO, left anterior oblique; RPO, right posterior oblique; LPO, left posterior oblique.

MR imaging of the thorax is most commonly used for cardiovascular imaging, but there are indications for MR imaging in mediastinal and pulmonary parenchymal imaging as well (Table 4-5). MR is helpful when bronchogenic carcinoma is suspected of invading vascular structures, including the cardiac chambers, pulmonary arteries and veins, and the

Table 4-4. Major Indications for Nuclear Medicine Imaging of the Chest

Suspected pulmonary thromboembolism (V/Q scan)
Differentiation of benign and malignant pulmonary nodule (PET)
Staging of thoracic malignancy (eg, lung, breast, esophagus) (PET)
Detecting recurrent or metastatic tumor (PET)

Table 4-5. Major Indications for MR Imaging of the Chest

Evaluation of a mediastinal mass
Suspected Pancoast (superior sulcus) tumor
Superior vena cava syndrome
Staging of lung cancer, when CT suggests invasion of the heart, great vessel, chest wall, diaphragm
Suspected aortic dissection
Evaluation for central pulmonary embolus in patients with allergy to iodinated contrast media or renal failure
Evaluation of the mediastinum and hilum in patients with allergy to iodinated contrast media or renal failure
Congenital and acquired heart disease

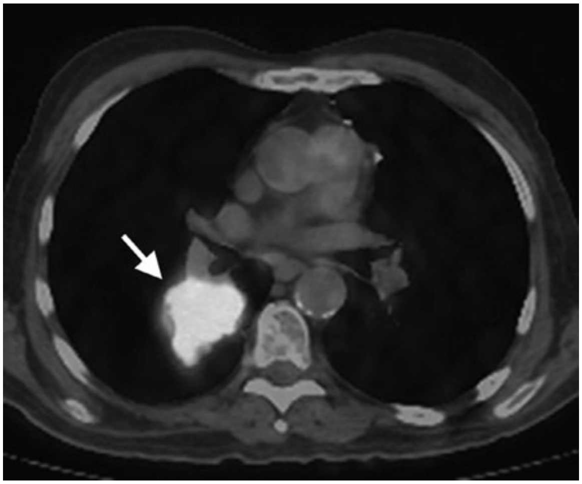

▲ **Figure 4-6.** PET-CT fused image demonstrates hypermetabolic activity in a tumor in the superior segment of the right lower lobe. Hypermetabolic activity (arrow) on fused imaging is demonstrated as a bright spot overlying the tumor.

superior vena cava. In a patient with suspected Pancoast's (superior sulcus) tumor (Figure 4-9), MR imaging is preferred to CT because of the ability to obtain images in coronal and sagittal planes. The apex of the lung can be difficult to evaluate on axial images alone because of partial-volume effects.

Ultrasonography is useful for imaging the soft tissues of the chest wall, heart, and pericardium, as well as fluid collections within the pleural space. Large, mobile pleural effusions are usually aspirated without sonographic guidance, because these collect predictably within dependent areas of the thorax. On the other hand, loculated pleural fluid collections may be difficult to aspirate without guidance, and the most appropriate entrance site may be marked with sonography for easier access. Ultrasonography has been used for guidance for biopsy of peripheral lung lesions as well.

EXERCISE 4-1. THE OPAQUE HEMITHORAX

4-1. The most likely diagnosis for Case 4-1 (Figure 4-10) is
- **A.** massive right pleural effusion.
- **B.** total atelectasis of the right lung.
- **C.** left pneumothorax.
- **D.** aplasia of the right lung.
- **E.** mediastinal hematoma.

4-2. The most likely diagnosis for Case 4-2 (Figure 4-11) is
- **A.** left pleural effusion.
- **B.** collapse of the left lung.
- **C.** right pneumothorax.
- **D.** collapse of the right lung.
- **E.** mediastinal hematoma.

Radiologic Findings

4-1. In this case, a frontal chest radiograph (Figure 4-10) shows that the right hemithorax is opaque. Signs of mass effect are present and suggest a space-occupying lesion in the right hemithorax. There is shift of the mediastinum toward the *contralateral* hemithorax, as evidenced by shift of the trachea and left heart border to the left. If a nasogastric tube were in place, esophageal shift could be inferred from the shift of the nasogastric tube. Space-occupying lesions also cause inferior displacement of the hemidiaphragm. Although the diaphragm itself is not visible, when the process is on the left, one can infer that the diaphragm is depressed by the inferior displacement of the gastric air bubble. Mass effect may also widen the distance between ribs. In this patient, the space-occupying lesion was a large right pleural effusion resulting from tuberculous empyema. A chest CT scan (Figure 4-12) in this patient shows the large pleural effusion and complete collapse of the underlying right lung against the medial aspect of the right hemithorax (A is the correct answer to Question 4-1).

4-2. In this case, a frontal chest radiograph (Figure 4-11) shows that the left hemithorax is opaque. In contrast to the patient in Figure 4-10, the patient in Figure 4-11 has signs of volume loss within the left hemithorax. There is mediastinal shift toward the *ipsilateral* hemithorax, as evidenced by shift of the trachea and the right heart border into the left hemithorax. The gastric air bubble is higher in the left upper quadrant of the abdomen than is normally seen, because of elevation of the left hemidiaphragm. The mediastinal window of the chest CT examination (Figure 4-13A) shows the mediastinal shift to the left and consolidation of the left lung. The lung window of the chest CT examination (Figure 4-13B) shows that the right lung is aerated. In this patient, the left lung collapse is due to a bronchogenic carcinoma in the left main bronchus (asterisk). This case exhibits the signs of volume loss, as opposed to mass effect (B is the correct answer to Question 4-2).

Discussion

This exercise reviews the principal signs that allow one to distinguish mass effect from volume loss. The mass effect caused by a tumor or by a large pleural effusion expands the hemithorax and displaces the trachea, mediastinum, and

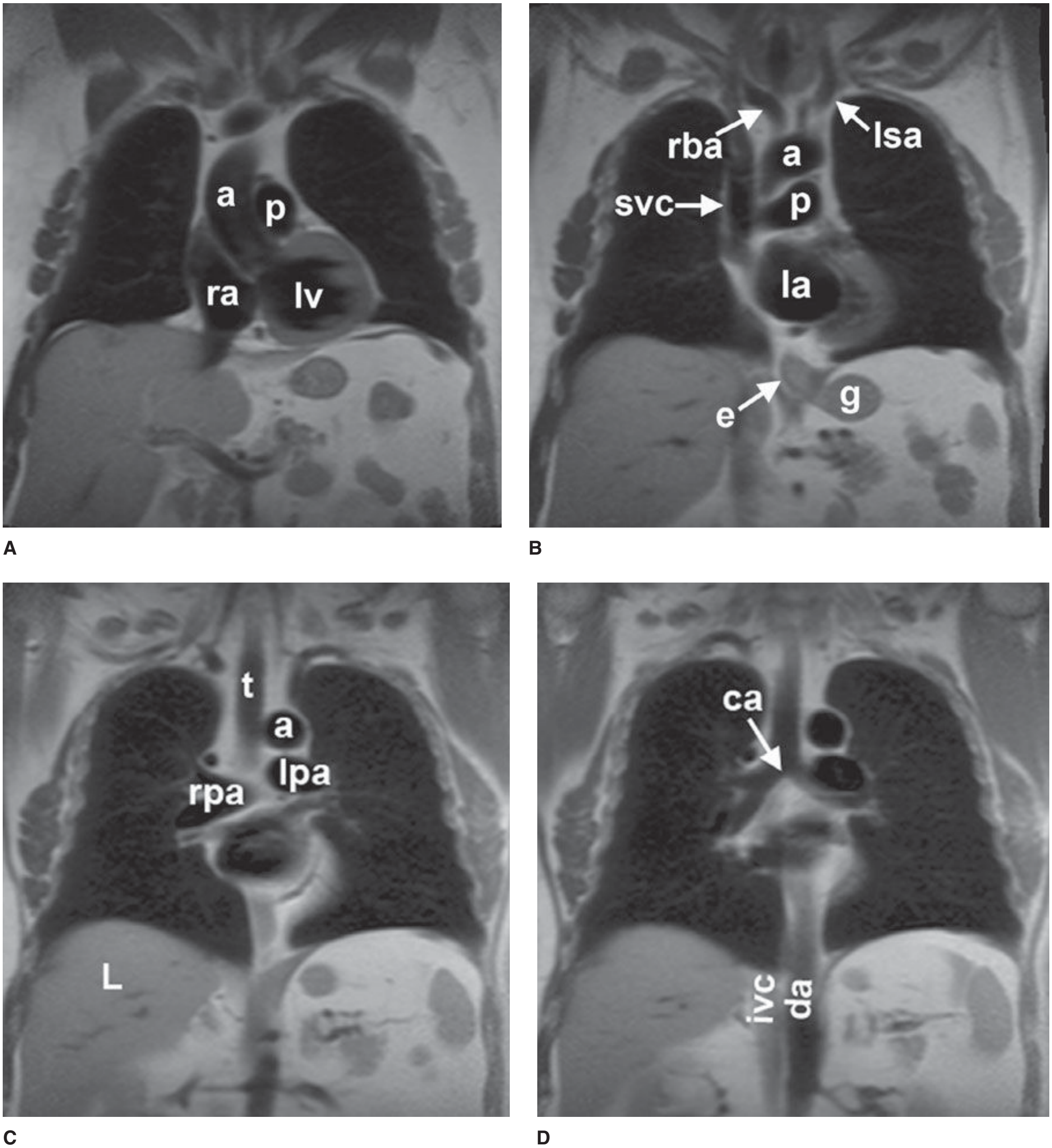

▲ **Figure 4-7.** (**A–E**) Normal MR anatomy. Coronal spin-echo images of the thorax. a, aorta; azv, azygos vein; ca, carina; da, descending aorta; e, esophagus (seen distally); g, gastric fundus; h, humerus; ivc, inferior vena cava; k, kidney; L, Liver; la, left atrium; lpa, left pulmonary artery; lsa, left subclavian artery; lv, left ventricle; p, pulmonary artery; ra, right atrium; rba, right brachiocephalic artery; rpa, right pulmonary artery; sp, spleen; svc, superior vena cava; t, trachea; v, vertebral body.

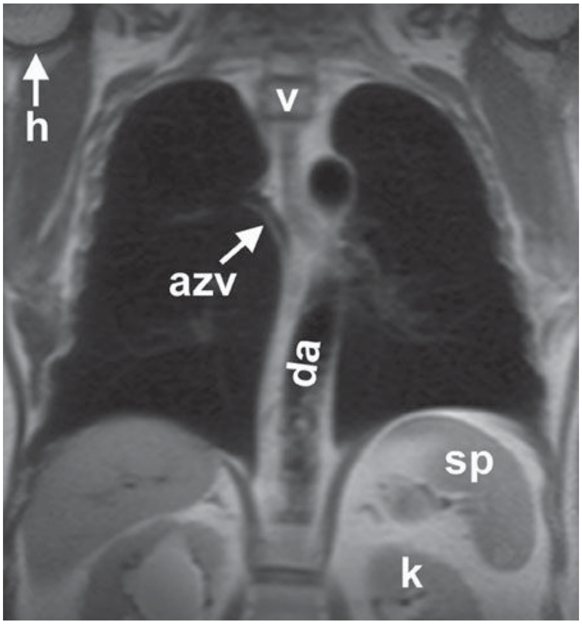

E

▲ **Figure 4-7.** *(Continued)*

diaphragm away from the mass. There may be a subtle increase in the distance between ribs. Volume loss, on the other hand, decreases the size of the hemithorax, and the trachea, mediastinum, and diaphragm move toward the involved hemithorax. The distance between the ribs on the abnormal side will be slightly decreased. In Figure 4-10, the opacification of the right hemithorax occurs as a result of massive right pleural effusion, and the right lung is collapsed as a result of both compression by the fluid present within the right pleural space and a loss of the negative intrapleural pressure that keeps the lung in close juxtaposition to the chest wall. In Figure 4-11, the collapse is due to obstruction of the left main bronchus, resulting in atelectasis (airlessness) of the left lung.

EXERCISE 4-2. LOBAR ATELECTASIS

4-3. In Figure 4-14 A,B, the inferior margin of the opacity in the right upper thorax is due to

A. the major fissure in right upper lobe (RUL) collapse without a hilar mass.
B. the minor fissure in RUL collapse with a hilar mass.
C. the minor fissure in RUL collapse without a hilar mass.
D. the major fissure in RUL collapse with a hilar mass.

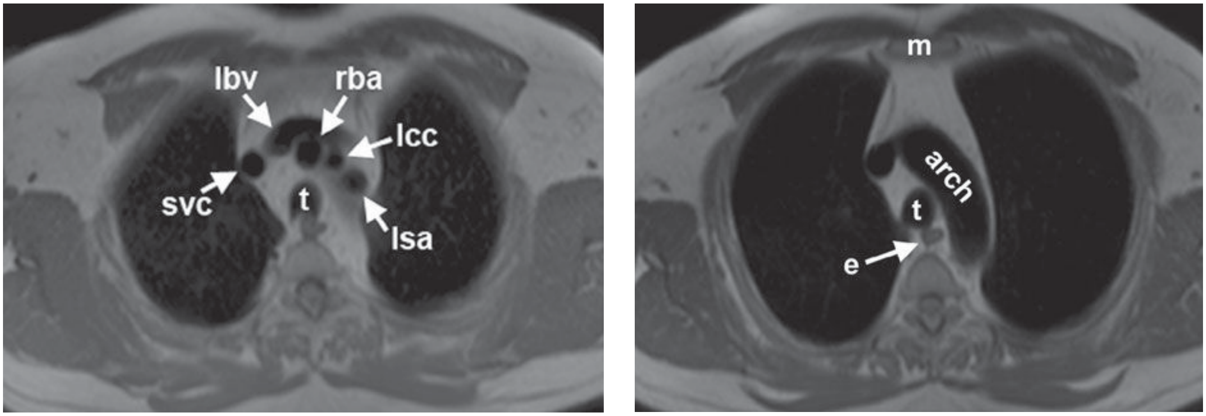

A B

▲ **Figure 4-8.** (**A–L**) Normal MR anatomy. Axial spin-echo images of the thorax. aa, ascending aorta; arch, transverse section of the aortic arch; azv, azygos vein; bi, bronchus intermedius; ca, carina; cs, coronary sinus; da, descending aorta; e, esophagus; g, gastric fundus; hazv, hemiazygos vein; im, internal mammary artery and vein; ip, interlobar (or descending) pulmonary artery; ipv, inferior pulmonary vein; ivc, inferior vena cava; ivs, interventricular septum; L, Liver; la, left atrium; laa, left atrial appendage; lbv, left brachiocephalic vein; lcc, left common carotid artery; LM, left main coronary artery; lpa, left pulmonary artery; lsa, left subclavian artery; lv, left ventricle; m, manubrium; pc, pericardium; ra, right atrium; rba, right brachiocephalic artery; rpa, right pulmonary artery; rv, right ventricle; rvot, right ventricular outflow tract; spv, superior pulmonary vein; st, sternum; svc, superior vena cava; t, trachea; v, vertebral body.

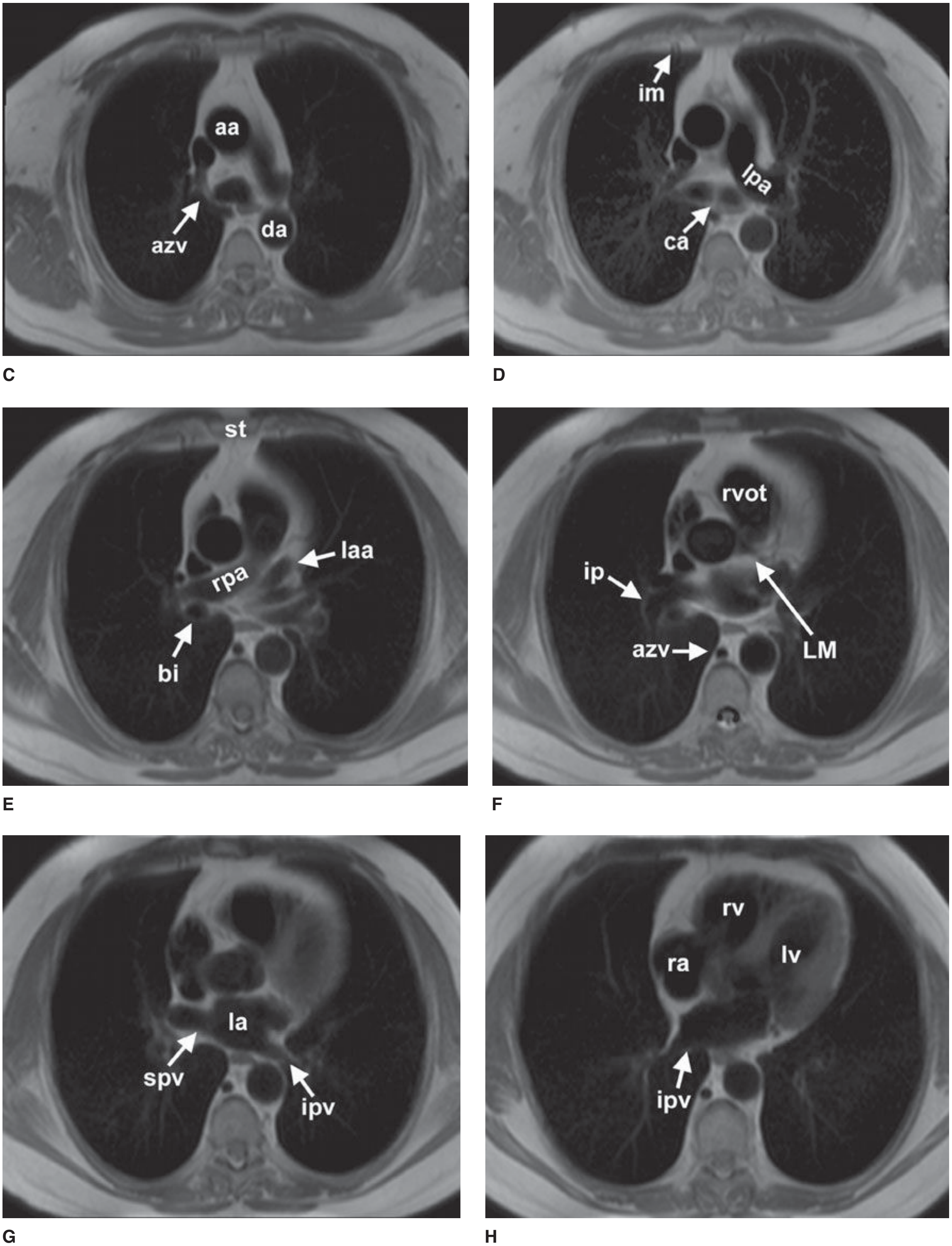

▲ **Figure 4-8.** *(Continued)*

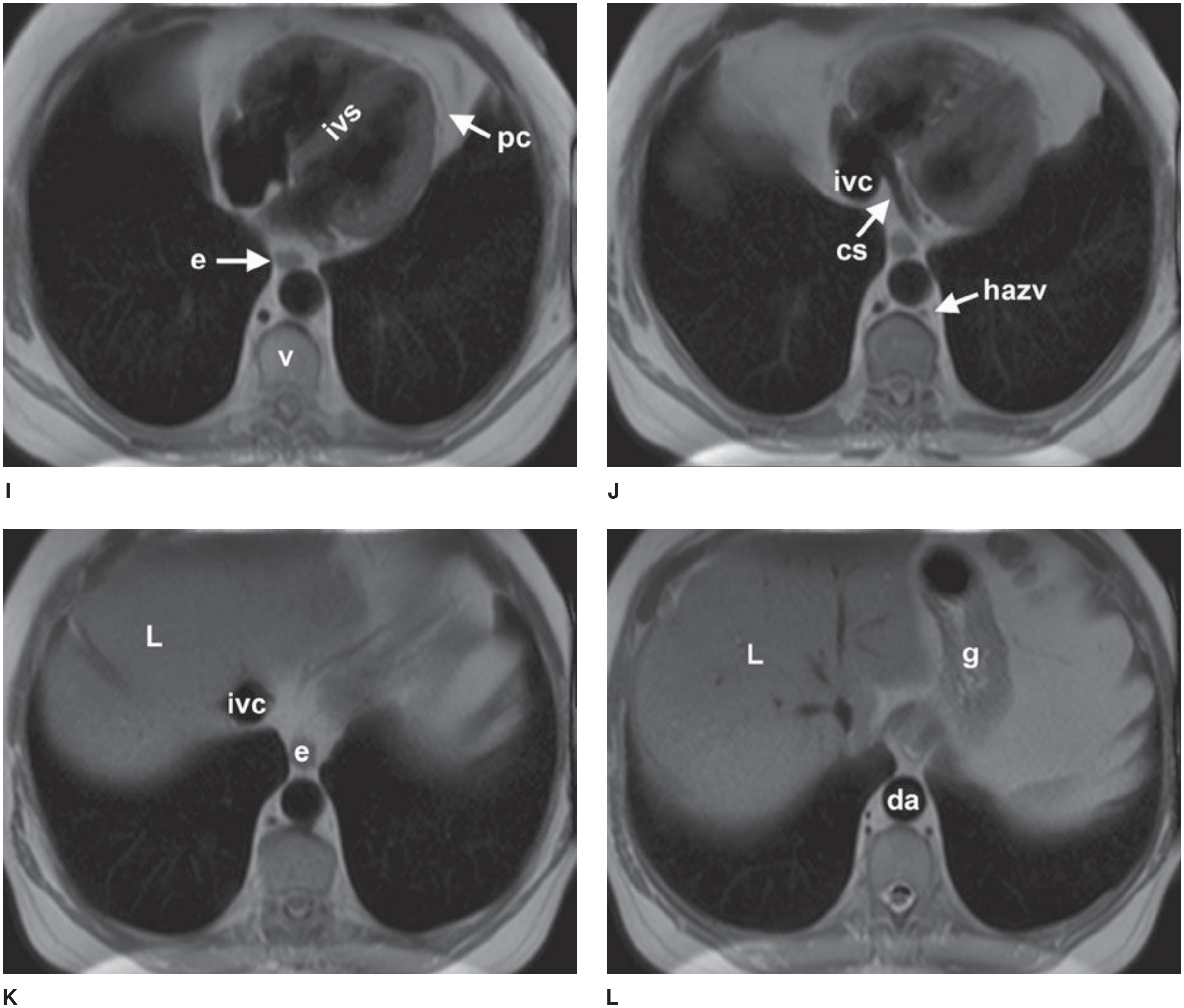

▲ **Figure 4-8.** *(Continued)*

4-4. In Figure 4-15 A,B, which of the following is true regarding right middle lobe collapse?
- **A.** A triangular opacity is superimposed on the heart on the frontal radiograph.
- **B.** The right heart border is obscured.
- **C.** The minor fissure is superiorly displaced.
- **D.** The right heart border is shifted to the left.

4-5. In Figure 4-16 A,B, a sign of left lower lobe collapse in this patient is which of the following?
- **A.** Obscuration of the lateral wall of the ascending thoracic aorta
- **B.** Superior displacement of the left hilum
- **C.** Obliteration of the anterior aspect of the left hemidiaphragm on the lateral view
- **D.** Triangular opacity in the left retrocardiac area on the frontal view
- **E.** Shift of the major fissure toward the anterior chest wall on the lateral view

4-6. In Figure 4-17 A,B, signs of left upper lobe collapse seen in this patient include which of the following?
- **A.** Crescent of air around the transverse section of the aortic arch resulting from hyperexpansion of the superior segment of the left lower lobe
- **B.** Posterior displacement of the left major fissure on the lateral view
- **C.** Obscuration of the right heart border
- **D.** Tracheal deviation to the right
- **E.** Inferior displacement of the left hilum

▲ **Figure 4-9.** Coronal post-gadolinium MRI image demonstrates an enhancing mass (arrow) in the right lung apex extending superiorly into the soft tissues of the chest wall.

▲ **Figure 4-10.** Case 4-1: 40-year-old man with fever and dyspnea.

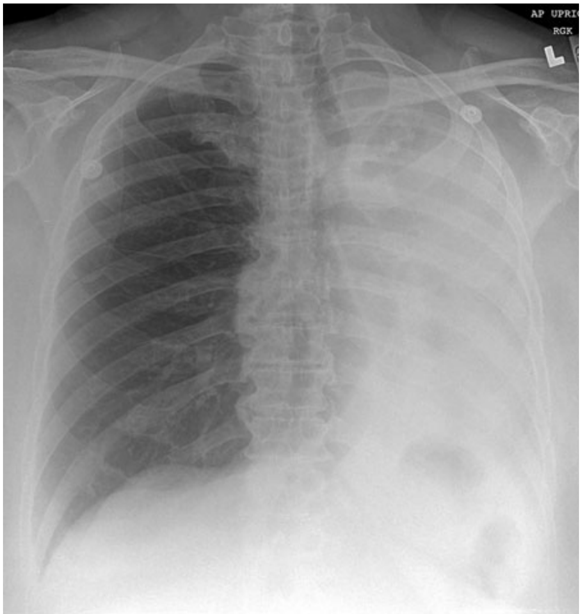

▲ **Figure 4-11.** Case 4-2: 62-year-old man with dyspnea, increased over the past several months.

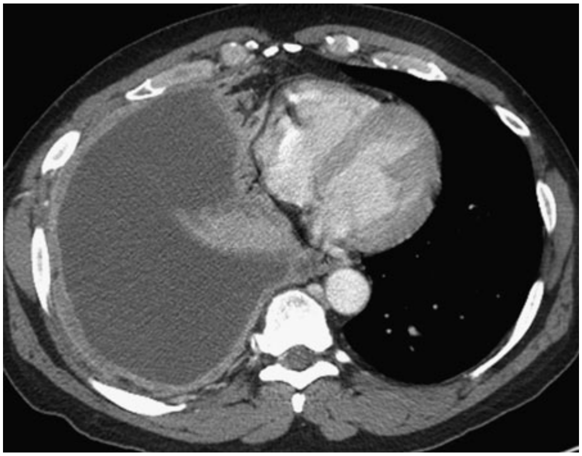

▲ **Figure 4-12.** Axial CT scan of the chest of the same patient as in Figure 4-10 shows filling of the right pleural space by fluid, with compression of the right lung and displacement of the mediastinal contents into the left hemithorax. The pleural fluid in this case represented tuberculous empyema.